DETERMINATION OF GROWTH INHIBITORY EFFECT OF IMINODIBENZYL AGAINST BREAST CANCER

A Dissertation
Submitted to the Graduate Faculty
of the
North Dakota State University
of Agriculture and Applied Science

By

Harshit Pareshbhai Shah

In Partial Fulfillment of the Requirements
for the Degree of
DOCTOR OF PHILOSOPHY

Major Department:
Pharmaceutical Sciences

September 2021

Fargo, North Dakota

North Dakota State University
Graduate School

Title

DETERMINATION OF GROWTH INHIBITORY EFFECT OF IMINODIBENZYL AGAINST BREAST CANCER

By

Harshit Pareshbhai Shah

The Supervisory Committee certifies that this ***disquisition*** complies with North Dakota State University's regulations and meets the accepted standards for the degree of

DOCTOR OF PHILOSOPHY

SUPERVISORY COMMITTEE:

Dr. Sathish Venkatachalem
Chair

Dr. Sanku Mallik

Dr. Sijo Mathew

Dr. Mohiuddin Quadir

Approved:

September 29, 2021
Date

Dr. Jagdish Singh
Department Chair

ABSTRACT

Breast cancer arises from the culmination of complex process enclosing multiple gene modifications such as cyclooxygenase-2 (COX-2). It catalyzes arachidonic acid (AA, downstream ω-6 polyunsaturated fatty acid (ω-6 PUFA)) metabolism to cancer-promoting prostaglandin E_2 (PGE_2). Hence, COX-2 inhibition was considered an ideal strategy to inhibit the cancer progression. However, COX-2 inhibitors are no longer advised for cancer management due to life threatening cardiovascular adverse events. Recently, we found that inhibition of delta-5-desaturase (D5D, enzyme catalyzing di homo-gamma-linolenic acid (DGLA) metabolism to AA) in breast cancer cells by siRNA/shRNA caused the diversion of DGLA metabolism from PGE_2 to anti-cancer metabolite 8-hydroxyoctanoic acid (8-HOA). But, the approach of using siRNA/shRNA was limited by endonucleases mediated physiological degradation and inability to cross the cell membrane. Therefore, to overcome the limitation and to stimulate DGLA metabolism towards anti-cancer activity, small molecule D5D activity inhibitor Iminodibenzyl was identified. Here, we have hypothesized that Iminodibenzyl could inhibit the DGLA metabolism by inhibiting the D5D activity, and simultaneously overexpressed COX-2 in breast cancer cells would peroxidize the accumulated DGLA to an anti-cancer metabolite 8-HOA. To achieve the research goal, we have performed various *in vitro* and *in vivo* studies (orthotopic breast cancer model). From these studies, we noted that Iminodibenzyl could alter DGLA metabolism to anti-cancer metabolite 8-HOA in 4T1 and MDA-MB-231 breast cancer cells. After treating cancer cells with the combination of Iminodibenzyl and DGLA, a significant increase in apoptosis was observed through the caspase-dependent mechanism, which was validated by pretreating cells with nonspecific caspase inhibitor Z-VAD-FMK. Additionally, a significant reduction in HDAC activity and β-Catenin was observed, which might have reduced cancer cell survival fraction and proliferation. We believe

that all the above mechanisms affected by the combination might have reduced the cancer growth resulting in significant reduction in tumor size. Additionally, combination treatment also reduced lamellipodia and filopodia, and EMT markers resulting in reduction in cancer cell migration as visible from larger wound size and less number of metastatic nodules. Hence, all the above findings provide evidence about the efficacy of Iminodibenzyl to shift the DGLA metabolism producing anti-cancer activity in breast cancer cells.

ACKNOWLEDGMENTS

There are many people whom I would like to thank for their direct and indirect contribution to the thesis. First, I would like to thank my first supervisor Dr. Steven Qian, for giving me an opportunity to work in his lab as a graduate student. I would like to thank my current supervisor, Dr. Sathish Venkatachalem, who took me under his supervision after Dr. Qian's sad demise and allowed me to work in his lab and simultaneously guided me in both graduate research work and professional development, few lines would not be sufficient to thank him.

I would like to acknowledge my thesis committee members, Dr. Sanku Mallik, Dr. Sijo Mathew, and Dr. Mohiuddin Quadir, for their valuable comments and concerns, which greatly improved my thesis work. I am also very grateful to Dr. Jagadish Singh, who has provided an excellent work environment in the department to conduct the research work. I would also like to thank the animal house scientist, Dr. Jodie Haring and Megan, for providing me training and providing me guidance when required. To the pharmaceutical science admin staff, Janet, Diana, and Tiffany, for helping me out in all the administrative tasks and ordering the research materials.

To my lab partner and friend, Lizhi Pang, I would like to thank him for all the help in professional as well as in personal life. To my best friend, Shrinidh Joshi, I would like to thank him for all the support he has provided till date in my professional career growth. I would also like to thank my previous and current lab members, Yi, Peter, Nilesh, Ram, Prem, Ashish, Sangeeta, Priyanka, and Niyati for all the direct and indirect help.

In the end, I would like to thank my parents, my wife, and my brother for all the support in good and worse times during the PhD. This achievement would not have been possible without their support. To them I dedicate this thesis.

TABLE OF CONTENTS

LIST OF TABLES

LIST OF FIGURES

LIST OF SCHEMES

LIST OF ABBREVIATIONS

8-HOA ..... 8-Hydroxy Octanoic Acid

AA ..... Arachidonic Acid

ANOVA ..... Analysis of Variance

APS ..... Ammonium Persulfate

BSA ..... Bovine serum albumin

C.Caspase-3 ..... Cleaved Caspase-3

COX-2 ..... Cyclooxygenase-2

DAPI ..... 4′,6-diamidino-2-phenylindole

DCM ..... Dichloromethane

DGLA ..... Dihomo-Gamma-Linolenic Acid

DI ..... Deionized

DMSO ..... Dimethyl Sulfoxide

FADS1 ..... Fatty Acid Desaturase 1

FAK ..... Focal Adhesion Kinase

FBS ..... Fetal Bovine Serum

GC/MS ..... Gas Chromatography / Mass Spectrometry

H&E ..... Hematoxylin and Eosin

HCl ..... Hydrochloric Acid

HDAC ..... Histone Deacetylase

HPLC ..... High-Performance Liquid Chromatography

I.P ..... Intraperitoneal

IACUC ..... Institutional Animal Care and Use Committee

Iminodibenzyl ..... 10,11-Dihydro-5H-dibenz[b,f] azepine

LC/MS ..... Liquid Chromatography / Mass Spectrometry

MMP-2	Matrix Metalloproteinases-2
MMP-9	Matrix Metalloproteinases-9
MTT	3-(4,5-Dimethylthiazol-2-yl)-2,5-Diphenyltetrazolium Bromide
NaCl	Sodium Chloride
P.O	Per Oral
PARP	Poly-ADP-ribose polymerase
PBS	Phosphate Buffered Saline
PFB-bromide	Pentafluorobenzyl-bromide
PFB	Pentafluorobenzyl Bromide
PG	Prostaglandin
PGE_1	Prostaglandin E_1
PGE_2	Prostaglandin E_2
PI	Propidium Iodide
pSIVA	Polarity Sensitive Indicator of Viability & Apoptosis
PVDF	Polyvinylidene Fluoride
RIPA	Radioimmunoprecipitation Assay
SDS	Sodium Dodecyl Sulfate
SEM	Standard Error of the Mean
TBS	Tris-buffered saline
TBST	TBS-Tween 20
TEMED	Tetramethyl Ethylenediamine
TGF-β	Tissue growth factor- β

1. INTRODUCTION

Despite the availability of a variety of effective therapeutic approaches like chemotherapy, targeted therapy, radiotherapy, and gene therapy, breast cancer is the most significant health concern among the female population throughout the world. As per the American Cancer Society factsheet, 1 in 8 females develops breast cancer in their lifetime[1,2]. For decades, researchers have studied various dietary manipulations in attenuating the severity of different types of cancers. Out of all the analyzed dietary manipulations, polyunsaturated fatty acids (PUFAs) are considerable because of their significant capability to combat various diseases and as well as their availability in large amounts in the daily diet[3-5].

PUFAs mainly include two types, omega-6 (ω-6) and omega-3 (ω-3) fatty acids. The ω-3, such as eicosapentaenoic acid (EPA) and docosahexaenoic acid (DHA) are available in great quantity in seafood and have been rigorously studied for their beneficial effects in treatments of inflammation, inflammatory bowel disease, asthma severity, cardiovascular disease, cognitive improvement ability and cancer[6-9]. The dietary sources of ω-6 are different than ω-3. ω-6 fatty acid such as Linolenic acid (LA), gamma-linolenic acid (GLA) can be obtained from vegetable oils including sunflower, corn and soybean oil, primrose oil, borage oil, black currant oil, and hemp seed oil, and a very small amount of arachidonic acid (AA) found from egg yolk [10-12]. In the typical western diet, the ratio of daily intake of ω-6 to ω-3 is around 10:1 to 30:1 [10-12].

As per the recent data from various research groups, breast cancer is associated with overexpression of lipid peroxidizing enzyme, cyclooxygenase-2, commonly referred to as COX-2[13-20]. COX-2 catalyzes the rate-limiting step of prostaglandin (PG) synthesis from arachidonic acid (AA)[21-24]. As per the research findings, COX-2 may play a role in different steps in cancer progression, which are through increased proliferation and metastasis of mutated cells or by

resisting apoptosis[25-27]. These effects are due to the conversion of AA to the prostaglandin E_2 (PGE_2), which is known to modulate cell proliferation, cell death, and metastasis and invasion in many types of cancer by activating various molecular cancer-promoting pathways[27-30] (Scheme 1 in Introduction). Hence, researchers have considered COX-2 inhibition for breast cancer management. However, the strategy of inhibition of COX-2 by various selective and non-selective COX-2 inhibitors to halt the cancer progression was inconclusive and contrary resulted in serious cardiovascular adverse events causing clinical patients' death[26,31-36]. Therefore, in 2005, FDA has barred the use of COX-2 inhibitors for cancer management[37].

Many research groups have gathered evidence suggesting a prominent association between dietary fatty acid consumption and cancer incidences. For example, ω-3 fatty acids have been reported to have an anti-cancer effect in colon cancer and beneficial effect in overcoming drug resistance[38-40], while ω-6 fatty acids are reported to have a role in cancer progression[41-43]. This effect of ω-6 fatty acid may be due to its metabolic pathway. ω-6 fatty acid, such as linolenic acid (LA) gets converted to gamma-linolenic acid (GLA) by delta-6-desaturase (D6D), which further undergoes two carbon chain elongation in the presence of elongase to form Dihomo-γ-linolenic acid (DGLA). The produced DGLA further undergoes metabolic reaction in presence of the delta-5-desaturase (D5D) enzyme to produce AA. The produced AA in the presence of the COX-2 enzyme generates PGE_2, which is reported to cause cancer progression and metastasis[3,10,44-46]. However, as per the increasing evidence from the various studies, DGLA (precursor of AA) can be considered as an exceptional omega-6 fatty acid due to its anti-inflammatory and anti-cancer effect[47,48]. There were several assumptions about the anti-cancer activity of DGLA, which might be due to the DGLA itself, or through prostaglandin series 1 (PGE_1) or due to the generation of free radical metabolites (produced by COX catalyzed peroxidation of DGLA)[47,48].

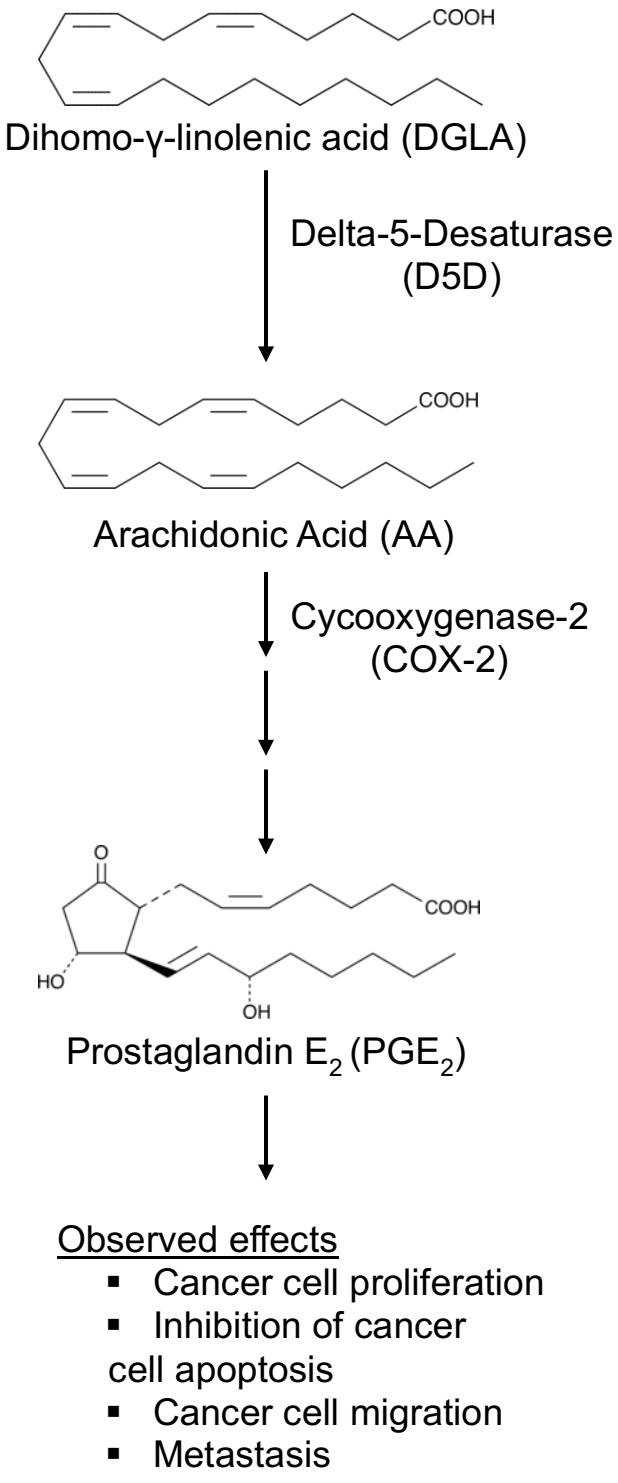

Scheme 1. Role of ω-6 polyunsaturated fatty acids in cancer. Upon uptake Linolenic acid is metabolized by delta-6-desaturase (D6D) and elongase sequentially to dihomo-gamma-linolenic acid (DGLA). The produced DGLA is further metabolized by D5D to Arachidonic acid (AA). In cancer cells, the produced AA is further peroxidized to Prostaglandin E_2, which activates various pathways leading to cancer growth and cancer cell migration.

Hence, considering the therapeutic effectiveness and inevitability in daily diet, DGLA may be an effective and safe nutritional approach for cancer prevention and treatment. Previously, Xiao et al., have shown that DGLA on peroxidation by COX-2 produced hexanol (HEX), heptanoic acid (HET), and 8-hydroxy octanoic acid (8-HOA)[49]. Later, Yu et al. provided evidence about the anti-cancer effect of 8-HOA on colon cancer cells[50].

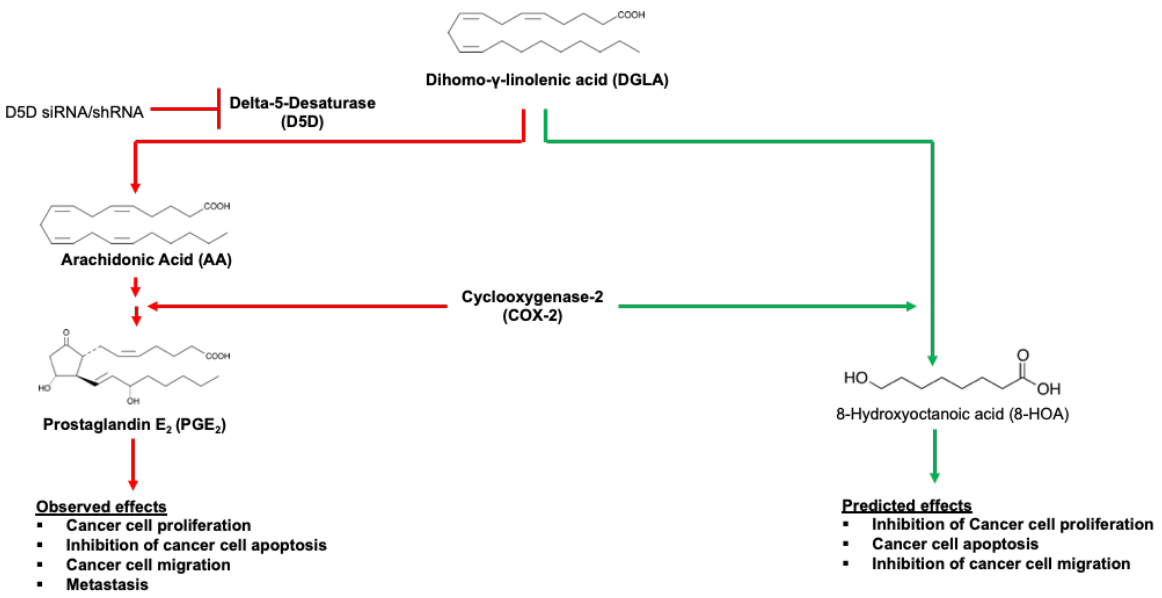

Scheme 2. The COX-2 paradigm shift in cancer therapeutics. DGLA upon metabolism by D5D produces AA, which further upon metabolism by COX-2 result in precancerous PGE_2 causing cell proliferation, inhibition of cell apoptosis, cell migration, and metastasis. Inhibition of D5D by D5D siRNA/shRNA will inhibit the precancerous pathway (on the left in red arrows) and stimulate an alternate pathway where DGLA is peroxidized to anti-cancer metabolite 8-HOA causing inhibition of cancer cell proliferation, cancer cell apoptosis, and inhibition of cancer cell migration (on right side in green arrow).

In the natural DGLA metabolism pathway, DGLA metabolizes to AA through D5D, which further translates to PGE_2. Contrary, inhibition of D5D fueled the conversion of DGLA to 8-HOA by COX-2 induced peroxidation in HCA-7 colony 29 cells, BxPC-3, 4T1, and MDA-MB-231[51-53]. Additionally, treatment with DGLA in D5D-KD cancer cells showed a significant increase in 8-HOA and percentage apoptotic cells compared to *wt*-type cells[52-54]. Moreover, after exogenous 8-HOA or 8-HOA from COX-2 stimulated DGLA peroxidation treatment, p53 level was found

upregulated in HCA-7 cell lines (p53 dependent mechanism). Cancer suppression was also achieved by p53 independent mechanism as cancer cell apoptosis was observed in p53 mutated BxPC3 cell lines[55]. This result suggested that 8-HOA can cause apoptosis through p53 dependent as well as p53 independent pathway[55]. In line with the colon and pancreatic cancer cell lines, the breast cancer cell line (MDA-MB-231) also exhibited similar results[51,56]. Moreover, the 8-HOA (direct as well as COX-2 stimulated) also reduced the cancer cell migration and reduced the epithelial-mesenchymal transition (EMT) markers[56,57].

In cancer therapeutics, drug resistance is a well-studied phenomenon, which is due to the insensitivity of the cancer cells to the treatment modalities[58-60]. The insensitivity to chemotherapy is by DNA mutation or metabolic changes, which cause drug degradation and/or inhibition of drug permeation across the cell membrane, drug target alteration, efflux of the drug, and other unknown mechanisms[58,60]. These results in failure of chemotherapy and/or less therapeutic outcome and cancer progression. To solve this concern, there is a need to develop a supportive therapeutic or nutritional regimen. On analysis of 8-HOA (direct as well as produced from COX-2 catalyzed peroxidation) with gemcitabine (BxPC-3 cells) or 5-fluorouracil (5-FU), a significant increase in the effect of a chemotherapeutic agent was observed[51,55].

Despite the efficiency, the use of D5D siRNA or shRNA to exert COX-2 paradigm shift to exert cancer growth inhibitory effect is limited by endonuclease mediated degradation, off-target side effects, and limited availability at the site of action, which makes it difficult to execute the research strategy, a COX-2 paradigm shift for anti-cancer effect[61]. Hence, to overcome the limitations and to achieve constant 8-HOA in the tumor microenvironment, different naturally occurring / chemically synthesized small molecule D5D inhibitors were identified. These inhibitors were Curcumin, Sesame, CP-24879, and Iminodibenzyl[62-65].

Previously, other researchers attempted to analyze the comparative IC_{50} for D5D inhibition for Curcumin and Sesame, and the observed findings suggested that curcumin is more potent than Sesame to inhibit D5D activity[62]. However, the attempt was not made to compare sesame, curcumin, CP-24879, and Iminodibenzyl. To screen out the potent D5D inhibitor, the rat liver microsome was used as a tool. From this experiment, Iminodibenzyl was identified as the most potent D5D inhibitor having the lowest IC_{50} (104nM) compared to CP-24879 (144nM), Curcumin (148nM), and Sesame (346nM) (Table 1)[63].

Table 1. Therapeutic properties of different identified D5D inhibitors

D5D Inhibitor	IC50 (nM)	8-HOA (μM)	% Survival fraction	
			D5D Inhibitor	D5D Inhibitor + DGLA
Sesame	346	0.33	100	107.65 ± 6.48
Curcumin	148	0.43	----	----
CP-24879	144	0.42	92.94 ± 6.14	85.55 ± 8.48
Iminodibenzyl	**104**	**0.65**	**101.03 ± 2.92**	**68.05 ± 7.28**

According to the COX-2 paradigm shift, D5D inhibition should result in the diversion of DGLA metabolism to an alternative metabolism pathway producing 8-HOA. On quantifying 8-HOA (produced from a combination of DGLA and different D5D activity inhibitors in colon cancer cell line), only Iminodibenzyl was able to produce 8-HOA above the threshold value (>0.5μM, required to exert therapeutic effects) (Table 1). Additionally, percentage survival fraction analysis after treatment with different D5D inhibitors +/- DGLA treatment showed a significant reduction in survival fraction with the treatment with Iminodibenzyl and DGLA compared to Sesame (+/- DGLA) or CP-24879 (+/- DGLA) treatment in colon cancer cells (Table 1)[63]. From the preliminary reported studies, we find Iminodibenzyl as the most potent D5D activity inhibitor among identified ones.

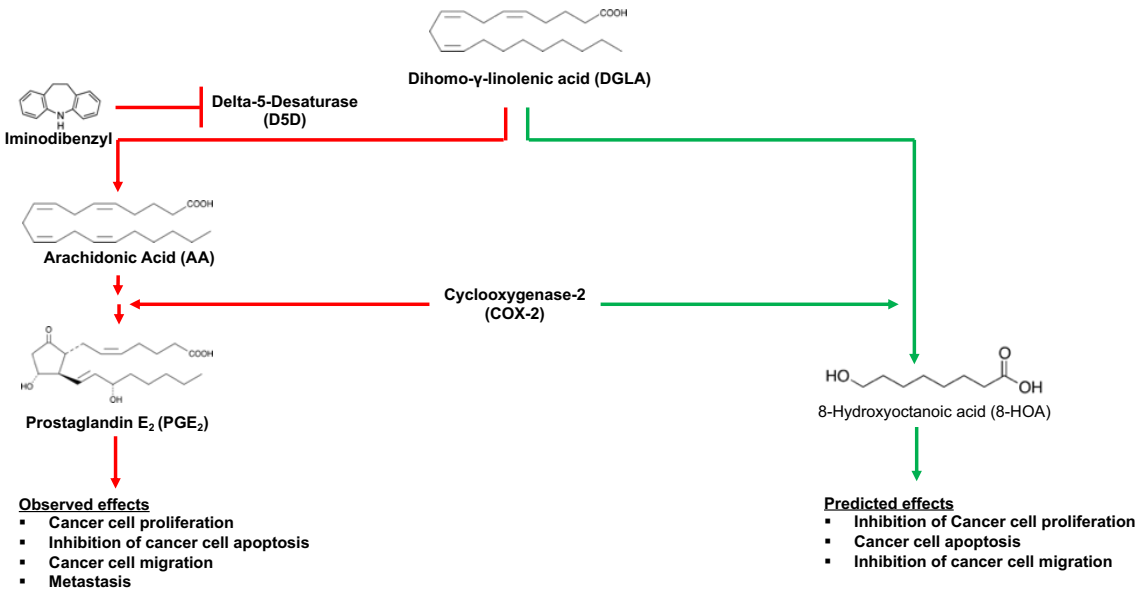

Scheme 3. Iminodibenzyl mediated COX-2 paradigm shift in cancer therapeutics. Inhibition of D5D activity by Iminodibenzyl would cause inhibition of precancerous pathway (highlighted on left side in red arrows) and simultaneously caused elevation of DGLA/AA ratio in cancer cells. The accumulated DGLA further metabolizes to cancer cell growth-inhibiting unique free radical metabolite 8-HOA, which exercises an inhibitory effect on cancer cell growth and migration (highlighted on right side in green arrows).

Iminodibenzyl (10,11-Dihydro-5H-dibenzo[b,f]azepine) is an impurity in commercial Carbamazepine preparations. Iminodibenzyl is a building block of many antipsychotic drugs. Additionally, Iminodibenzyl analogs such as clocapramine, carpipramine, Desipramine, and Imipramine are widely used anti-psychotics acting as potent dopaminergic antagonists exert an effect by blocking alpha 1- and alpha 2-adrenoceptors in the brain[66]. Additionally, Iminodibenzyl derivatives demonstrated anti-leishmanial activity[66]. However, the role of Iminodibenzyl as a D5D inhibitor in cancer therapeutics was unexplored. Hence, based on the role of a COX-2 paradigm shift in cancer therapeutics and potency of Iminodibenzyl to inhibit D5D activity, in this research work, we have hypothesized that treatment with Iminodibenzyl would exert inhibition of DGLA metabolism producing a high DGLA/AA ratio in breast cancer cells. The accumulated DGLA would undergo C-8 oxygenation by the COX-2 in the cancer cells to produce consistent 8-HOA,

which would exert cancer growth inhibitory effect on breast cancer cells (Scheme 3 in Introduction).

This research work would provide the first evidence regarding the anti-cancer activity of Iminodibenzyl in Breast Cancer. Previously, researchers have targeted COX-2 inhibition to achieve cancer growth inhibition. However, the concept of COX-2 inhibition as an anti-cancer strategy has failed significantly in clinics with serious adverse effects. Recent evidence exploring the role of D5D inhibition in DGLA (ω-6 PUFA) metabolism and cancer growth inhibitory effect by 8-HOA, as a unique free radicle metabolite, by COX-2 peroxidation has provided a new therapeutic strategy. To execute this approach physiologically, the D5D enzyme or its activity inhibition is essential, which can be achieved by either delivering siRNA *in vivo* or delivering a small molecule inhibitor having the property to inhibit D5D activity. However, the approach of delivering RNA interference (RNAi) molecules is restricted due to endonucleases, the inability of RNAi to cross the cell membrane, and dissociation at ultra-low concentrations. However, another approach of using a small molecule D5D activity inhibitor is more convenient due to high penetrant effects across whole cell populations, ability to conduct large-scale biochemical experiments, added advantage towrads combination with other treatments, and easy titration of dose. Hence, in this study, we identified the potent D5D inhibitor Iminodibenzyl and explored its potential as a therapeutic approach against breast cancer.

2. METHODS AND MATERIALS

2.1. Chemicals and reagents

2.1.1. Chemicals

Pure DGLA for cell culture treatment was purchased from Nu-Check-Prep (MN, USA). Iminodibenzyl (10,11-Dihydro-5H-dibenz[b,f]azepine) for cell culture and animal study dosing was obtained from Millipore Sigma (MO, USA). 3-(4,5-Dimethylthiazol-2-yl)-2,5-Diphenyltetrazolium Bromide (MTT) was purchased from alfa aesar (MA, USA). Analytical standard solutions (AA, DGLA, PGE_1, PGE_2) and internal standards (AA-d_8, DGLA-d_6, PGE1-d_4, PGE2-d_9) were acquired from Cayman chemicals (MI, USA). Pure DGLA for the animal study was acquired from Cayman Chemicals. Crystal violet, diisopropylethylamine, pentafluorobenzyl bromide (PFB), sodium dodecyl sulfate (SDS), tetramethyl ethylenediamine (TEMED), ammonium persulfate (APS), tris base, acrylamide/bis acrylamide, sodium chloride (NaCl), glycine, HPLC grade water, HPLC grade methanol, acetonitrile, and acetic acid were purchased from VWR (PA, USA). SampliQ Silica C18 ODS reverse phase SPE cartridges were acquired from Agilent (CA, USA). Dimethyl sulfoxide (DMSO) and ethanol for cell culture were bought from Santacruz Biotechnology (TX, USA). Radioimmunoprecipitation (RIPA) lysis buffer, and protease and phosphatase inhibitor cocktail were acquired from Thermo Fisher scientific (CA, USA).

2.1.2. Biological reagents

DMEM cell culture medium was obtained from Santa Cruz Biotechnology. F-12K cell culture medium was acquired from American Type Culture Connection (ATCC) (VA, USA). Fetal bovine serum (FBS) and Trypsin were obtained from Gibco (MA, USA). PI Annexin V FITC kit was purchased from BD Pharmingen™ (NJ, USA). The kinetic Apoptosis kit was bought from

Abcam (ab129817) (MA, USA). HDAC activity colorimetry kit was bought from BioVision (CA, USA). Primary antibodies for Western blot and Immunocytochemistry study were acquired from Cell Signaling Technology (AcH3 (9649S), BCl2 (2872S), β-Actin (4970S), PARP (9542S), MMP-9 (2270S), FAK (3285S), β-Catenin (8480S), Paxillin (12065S)), Abcam (C.PARP (ab32064), C.Caspase-3 (ab2302), MMP-2 (ab37150), E-Cadherin (ab1416), FADS1 (D5D) (ab126706), Vimentin (ab8978), Ki-67 (16667)), Santacruz biotechnology (Vinculin (SC-73614), Snai (SC-271977), Total H3 (SC517576), MMP-2 (SC13594)), and Abm (β-Actin (G043)). Secondary antibodies against rabbit species (800 channel) and mouse species (680 channel) were acquired from LiCor Biosciences (NE, USA). Precast 4-20% gels were acquired from Bio-Rad laboratories (CA, USA). Gelatin zymography gel was acquired from Thermo Fisher Scientific.

2.2. Cell lines

The breast cancer cell line derived from mouse mammary gland tissue 4T1 and epithelial human breast cancer cell line MDA-MB-231 were a kind gift by Dr. Keith Miskimins (Center for Cancer Biology Research, Sanford Research). The non-tumorigenic human mammary epithelial cell line MCF-12a was acquired from ATCC (lot number 70010185). All the cell lines were cultured as per the standard conditions mentioned on ATCC.

2.3. Cell viability analysis

In the initial analysis, to determine the dose of the Iminodibenzyl and/or DGLA to be used for the *in vitro* studies, cell viability analysis by MTT assay was performed. MTT assay is a widely used cytotoxicity or viability assay to determine the cytotoxic effect of drugs on immortalized or primary cells. MTT assay is based on the principle of transformation of MTT to formazan crystals by live cells representing the mitochondrial activity[67].

For the MTT assay, approximately 5 x 10^3 4T1, MDA-MB-231, and MCF-12a cells (in 100µl medium) were seeded in a 96-well culture plate. After overnight incubation, cells were treated with DGLA (1µM to 500µM), Iminodibenzyl (0.1µM to 50µM), and a combination of Iminodibenzyl and DGLA (1:10 ratio from 0.1µM Iminodibenzyl + 1µM DGLA to 50µM Iminodibenzyl + 500µM DGLA) for 48 hours. At the end of the treatment, MTT (5mg/ml) was added to the cells and the plate was incubated at 37℃. After 3 hours of incubation, the medium containing MTT was discarded and the formed formazan crystals were dissolved by adding DMSO with continuous shaking for 30 minutes, and absorbance was measured at 570nm[67] with a plate reader (SpectraMax M5; Molecular Devices). Cells treated with vehicle served as control. Cell viability in different treatment groups was calculated as the percentage change compared to the Vehicle treated group.

2.4. *In vitro* treatment

Based on the finding from cell viability assay, 4T1 and MDA-MB-231 cells were provided 100µM DGLA, 10µM Iminodibenzyl, or a combination of 10µM Iminodibenzyl and 100µM DGLA for 48 hours.

2.5. Proliferation analysis

Cancer cell proliferation under the influence of various treatments was assessed by colony formation assay. In this assay, cancer cells' ability to proliferate and form colonies from a single cell was assessed[68]. Briefly, 1000-1500 4T1 and MDA-MB-231 cancer cells were seeded in the 6-well culture plates and incubated overnight. After overnight incubation, cells were provided different treatments as mentioned in 2.4. for 48 hours. After treatment, the cells were washed twice with the sterile Phosphate Buffered Saline (PBS) and incubated with the fresh DMEM media containing 10% FBS until the single-cell forms colonies (group of 50 or more cells). At the end

of incubation, the cells were washed with PBS and fixed with 2ml of 10% Paraformaldehyde solution for 30 minutes, followed by staining with 2ml of 0.5% w/v crystal violet solution for another 30 minutes. After colony staining, the cells were washed multiple times with PBS, and images were taken and ImageJ software (NIH, Bethesda, MD, USA) was used to calculate colonies in each treatment group. After data analysis, it was reported in terms of percentage reduction of survival fraction compared to vehicle treatment group[51,55].

$$\text{Survival fraction} = \frac{Number\ of\ colonies\ in\ treatment\ group}{Number\ of\ colonies\ in\ vehicle\ group}$$

2.6. Apoptosis analysis

The PI-Annexin V approach is the most used approach to determine cell apoptosis. The approach is based on the differential ability of the dye to bind to the cells. Staining with Annexin V labeled with FITC is typically used in conjunction with PI to distinguish early apoptotic cells from dead or damaged cells. The ability of the PI to stain the cells depends upon the permeability of the membrane as PI is not able to enter live or early apoptotic cells[69]. While, Annexin V, a Ca^{+2} dependent phospholipid-binding protein, can only bind to phosphatidylserine, which externalizes upon apoptosis stimulation[70]. Therefore, cells that are both FITC Annexin V and PI negative are considered viable; cells that are Annexin V FITC positive and PI negative are considered in early apoptosis, and cells that are both Annexin V FITC and PI-positive are considered in late apoptosis or already dead.

The PI-Annexin V staining was performed as per the standard procedure provided with the kit (BD Pharmingen, Catalog number: 556547). Briefly, 0.25 x 10^6 4T1 and MDA-MB-231 cells were seeded and incubated overnight. The next day, the cells were provided the treatment mentioned in 2.4. for 48 hours. After treatment, the cells were collected by trypsinization. The cells were washed twice with ice-cold PBS buffer, followed by mixing with 100µl 1x binding

buffer at a concentration of 1 x 10^6 cells/ml. The cells were then stained with 5µl PI and 5µl Annexin V FITC for 30 minutes in dark at room temperature. After incubation with dye, the volume was made to 500µl with 1x binding buffer, and the reading was taken by Acuri C6 flow cytometer. The data analysis was done by Acuri C6 software as described elsewhere[52,54,55].

2.7. Wound healing assay

The wound-healing assay was conducted to determine the alleviating effect of different treatments on 4T1 and MDA-MB-231 cell migration. To perform the wound healing assay, approximately 0.25 x 10^6 4T1 cells were seeded in a 6-well culture plate and incubated till a cell monolayer was formed. After that, the wound was made by gently scratching the cell monolayer with a sterile pipette tip. Followed by the cells were washed 2-3 times by sterile PBS to remove any dislodged cells and provided the treatment mentioned in 2.4. in DMEM media having 1% FBS. During the treatment time, the wound size was captured at 0, 24, and 48 hours by brightfield microscopy using a Leica Microsystem. The wound area at different time points was measured by using ImageJ software. The reduction in wound area was measured and migration rate was analyzed by comparing the wound area at 24- and 48-hour time point with the wound area of the 0-hour time point for each treatment group[52,55,56].

2.8. Transwell migration assay

The transwell migration assay is a commonly used assay to assess the migratory response of the cancer cells after various treatments. The assay was executed by using the Costar transwell chamber (6.5 mm insert, 8.0µm polycarbonate membrane). To perform the transwell assay, approximately, 25 x 10^3 4T1 cells were seeded in the insert. The next day, the media in the upper chamber was replaced with serum-free DMEM media containing different treatments mentioned in 2.4. and the 10% FBS holding media was kept at the lower chamber. After treatment, the cells

were fixed with 10% paraformaldehyde and then stained using 0.5% w/v crystal violet solution. After staining, the extra crystal violet solution was removed by washing the insert 4-5 times with deionized water. The cells on the upper side of the chamber were scraped off by a cotton stick and the images of the migrated cells across the membrane were taken by Lecia Microsystems. The migration rate was determined by using ImageJ as the area covered by the cell after the treatment. The analysis was done by comparing the migration rate in the treatment group with the Vehicle treatment group[52,55,56].

2.9. 8-HOA analysis

8-HOA is a highly unstable compound and hence it is extremely difficult to analyze it in its original form by using high-performance liquid chromatography (HPLC), liquid chromatography/mass spectrometry (LC/MS), or gas chromatography/mass spectrometry (GC/MS). Hence, 8-HOA produced from DGLA peroxidation was analyzed in its pentafluorobenzyl bromide (PFB-Br) derivatized form by using GC/MS[71].

To determine produced 8-HOA from the cell, briefly 0.25 x 10^6 4T1 and MDA-MB-231 cells were seeded and provided treatments for 48 hours as mentioned in 2.4. After treatment, the cells were scratched off and 1ml of cell suspension was taken from different treatment groups. The solution was then mixed with 500µl methanol containing hexanoic acid as an internal standard, 50µl 1N HCl, and 3ml Dichloromethane (DCM). The sample solution was then vortexed (30 seconds), centrifuged (3000 rpm for 4 minutes), and the organic DCM layer was collected. This extraction step was repeated twice. The obtained DCM layers were combined and dried in a vacuum evaporator (Vacufuge). The samples were then reconstituted in diisopropylethylamine (50µl, 1.0% v/v) and PFB-bromide (Pentafluorobenzyl-bromide) in acetonitrile (1.0% v/v) and

heated for 30 minutes at 37°C. Then, the acetonitrile was removed using a vacuum evaporator, the residue was reconstituted in 100µl of dichloromethane.

Then, 2µl Sample solution was injected into the gas chromatograph (Agilent 7890A). The GC oven temperature was set to 300°C, and the injector and transfer line were kept at 280°C. Quantitative analysis was done by a mass selective detector with a source temperature of 230°C. For quantification, an internal standard curve was developed from a gradient 8-HOA concentration, and internal standard hexanoic acid at a constant concentration. The peaks of Hexanoic acid and PFB derivatized 8-HOA were analyzed at extracted ion current with m/z 181. The concentration of 8-HOA was determined by extrapolating the value of the ratio of the area of the 8-HOA peak and hexanoic acid peak into the internal standard curve[57,72].

2.10. Western blot analysis

2.10.1. Protein extraction

For Western blot analysis approximately, 0.5 x 10^6 4T1 and MDA-MB-231 cells were seeded in a 10cm^2 plate and provided the treatment for 48 hours. After treatment, the cells are collected by trypsinization and mixed with modified radioimmunoprecipitation assay (RIPA) buffer, premixed with protease and phosphatase inhibitor cocktail. The cell solution was then sonicated (2.5sec cycle for 20 seconds) and the solution was kept on ice for 30 minutes, followed by it was centrifuged at 13000rpm for 10 minutes. After centrifugation, the clear protein solution was collected and stored at -80C until further use.

2.10.2. Protein concentration measurement

For Western blot analysis, protein concentration was measured after protein extraction. Protein concentration was measured by the Pierce™ BCA protein assay kit from Thermo Scientific (Catalog number: 23225). For determining protein concentration, 5µl of protein lysate from

different treatment groups was mixed with 195µl of a solution containing 50 parts of solution A to 1 part of solution B. The solution in the plate was mixed by shaking for ~30 seconds on a shaker and incubated for 30 minutes in dark. After incubation, the absorbance was measured at 562nm. The protein concentration was determined by extrapolating the absorbance value of the sample to the equation obtained from a standard curve developed by gradient concentration of albumin.

2.10.3. Solution preparation

10% SDS solution was prepared by dissolving 1g of SDS in 10ml DI water.

10% APS solution was prepared by dissolving 100mg of APS in 1ml DI water.

1.5 M Tris buffer (pH 8.8) was prepared by dissolving 18.2g of Tris base into a 90ml DI water and 6 N HCl was used to adjust the pH of the solution to 8.8 ± 0.05. After pH setting, the volume was made up to 100ml with DI water.

1.0 M Tris buffer (pH 6.8) was prepared by dissolving 12.1g of Tris base into 90ml DI water. 6 N HCl was used to adjust the pH to 6.8. After pH setting, the volume was made up to 100ml with DI water.

Running buffer 10× stock solution was prepared by transferring 30.3g of Tris base, 144g glycine, and 10g SDS into a 900ml DI water and stirred for 15-20 minutes to dissolve completely. The volume was made up to 1000ml with DI water and stored at 4°C. 1x running buffer was prepared by diluting 100ml of 10x running buffer to 1000ml with DI water.

Table 2. Recipe to prepare 10x running buffer

Ingredient	Quantity
Tris base	30.3g
Glycine	144g
SDS	10g
DI water	1000ml

Transfer buffer was prepared by mixing 200ml of 5x transfer buffer (Bio-Rad, Catalog number 1704272), 200ml ethanol, and 600ml of DI water. The reagent was stored at 4°C.

Tris-buffered saline (TBS) 10x stock solution was prepared by dissolving 12.1g of Tris base, 87.7g of NaCl in 900ml of DI water. The pH of the solution was adjusted to 7.6 by using 6N HCl and volume was made to 1000ml with DI water. 1x TBS-Tween 20 (TBST) solution was prepared by diluting 100ml of 10x TBS solution to 999ml with DI water followed by 1ml Tween-20 and the solution was stored at 4°C.

Table 3. Recipe to prepare 10x TBS

Ingredient	Quantity
Tris base	12.1g
NaCl	87.7g
DI water	1000ml

Blocking Solution (5% Bovine serum albumin (BSA)) was prepared by dissolving 5g of BSA to 100ml TBS with continuous stirring.

2.10.4. Gel preparation

The 10% resolving gels and 4% stacking gels were prepared using 1.5mm glass plates according to the formula mentioned in Table 3.

Table 4. Recipe to prepare 10% resolving and 4% stacking gels

Ingredient	Resolving gel	Stacking gel
H_2O	7.8ml	7.25ml
Tris buffer	2ml (1.5 M, pH 8.8)	1.25ml (1.0 M, pH 6.8)
acrylamide/bis-acrylamide (30% solution)	5ml	1.3ml
10% SDS	150µl	100µl
10% APS	150µl	100µl
TEMED	15µl	10µl
Total volume	15ml	10ml

2.10.5. Western blot procedure

The protein sample to load was prepared by taking ~50µg of protein from 2.10.2. and volume was made equal by diluting with DI water for all the employed samples. The samples were further mixed with 4x loading buffer (diluted 4 times) and heated at 70°C for 10 minutes for denaturation. The samples were then vortexed and centrifuged for 30 seconds. The gel electrophoresis was then performed by loading the protein samples in the prepared gel and running the gel at 80V constant volt for 30 minutes followed by at 120V for another 1 hour. The ran proteins were then transferred to the activated PVDF membrane (soaking of membrane for 2 minutes in methanol, 2 minutes in DI water, and then in transfer buffer) by semi-dry transfer method by using Turbo Transfer blot machine.

After transfer, the membrane was blocked by incubating with a 5 % BSA with continuous shaking for 1 hour at room temperature to prevent any non-specific binding. The blot was then incubated with primary antibody (in 5% BSA in TBST) overnight at 4°C with continuous rocking. The next day, the loosely attached antibody was removed by washing the membrane with TBST (7 minutes, x3) and then incubated with anti-mouse or anti-rabbit Licor secondary antibody for 1 hour at room temperature. Then the loosely attached secondary antibody was washed off by TBST (7 minutes, x3) washing with continuous rotation and the membrane was then exposed to the Licor odyssey system to measure the reading. Data analysis was done by using Image lite software[57,72].

2.11. HDAC analysis

HDAC activity was analyzed as per the standard procedure mentioned in the HDAC activity colorimetric assay kit from BioVision (CA, USA). Briefly, the protein was extracted from different groups received different treatments as mentioned in 2.10.1. and 2.10.2. To quantify the percentage HDAC activity reduction, ~50µg of protein was taken and diluted to 85µl with ddH2O.

The protein solution was then mixed with 10µl of 10X HDAC assay buffer and 5µl HDAC colorimetric substrate. The plate was then kept on the shaker for 1-2 minutes, and then the plate was incubated at 37°C for 1 hour to deacetylate the substrate. Followed by incubation, the deacetylation reaction was stopped by adding 10µl lysine developer (to produce chromophore), and the plate was again incubated for 30 minutes at 37°C. After 30 minutes, the reading was observed at 405nm, and calculation was done by considering the Vehicle group has 100% HDAC activity[57,72].

2.12. Immunocytochemistry

Immunocytochemistry or immunofluorescence method to detect protein level is a widely used technique by using primary and corresponding fluorescence secondary antibody. For this analysis, ~1500-2000 cells were seeded in ibidi 8 well µ-slides (Catalog number: 80826) and incubated until the colonies are formed. The cells were provided different treatments as mentioned in 2.4. After treatment, the cells were fixed by using 4% Paraformaldehyde for 10 minutes at room temperature and then washed with ice-cold PBS (x3). Followed by cell permeabilization was performed by incubating the cells for 7 minutes with 0.25% Triton X-100 (detergent, which improves antibody penetration) in PBS. Then, the cells were washed 3 times for 5 minutes with PBS. Then, the cells were blocked with 10% goat serum for 30 minutes at room temperature followed by incubated with primary antibody for 1 hour at room temperature in 10% goat serum. The cells were washed 3 times with PBS for 5 minutes. It was then incubated with a corresponding secondary antibody for 1 hour at room temperature in 10% goat serum and then again washed 3 times with PBS for 5 minutes. This step was performed in dark. After protein staining, Actin filaments were stained by Phalloidin iFlour 488 reagents (Thermo Fisher, catalog number: 12379). The nucleus was stained by DAPI from Electron Microscopy Sciences (PA, USA). The signals

were detected by using Carl Zeiss LSM900 confocal microscopy with Airyscan 2. Image analysis was done by using ImageJ[57,72].

2.13. Apoptosis analysis after Z-VAD-FMK treatment

To confirm the caspase-dependent apoptosis pathway involvement in the apoptosis process, the cells were provided pretreatment with 30μM Z-VAD-FMK (Santacruz biotechnology, Catalog number: SC3067) for 2 hours. After that, both 4T1 and MDA-MB-231 cells were treated with a combination of 10μM Iminodibenzyl and 100μM DGLA for 48 hours. After 48 hours of treatment, the cells were collected by trypsinization, and apoptosis analysis was performed as mentioned in 2.6.[52,54,55].

Additionally, approximately 0.1 x 10^6 cells were seeded and incubated overnight. The next day, an experiment was divided into three groups, and cells were treated accordingly. Cells in group "A" were provided Vehicle, group "B" was treated with a combination of Iminodibenzyl and DGLA, and group "C" was pretreated with 30μM Z-VAD-FMK (for 2 hours) and then provided combination treatment. During 48 hours of treatment, cells were incubated with culture medium (37°C, 5% CO_2) mixed with Polarity Sensitive Indicator of Viability & Apoptosis (pSIVA) and propidium iodide (ab129817) for imaging under time-lapse through Lionheart FX Automated Microscope microscopy over time. Green fluorescence indicated pSIVA positive cells. The percentage of pSIVA positive cells was quantified at different time points in the same field.

2.14. Zymography

To perform the gelatin gel zymography, 4T1 cells were seeded and treatments were provided for 48 hours as mentioned in 2.4. After treatment, the conditioned media from different treatment groups was collected and concentrated using Vivaspin 6 MWCO 3000 concentrator spin columns. The protein content in each group was analyzed using a BCA protein assay kit as

mentioned in 2.10.2. The concentrated media (~20µg protein) was then diluted with Bio-Rad Zymogram sample buffer and loaded on Novex 10% Zymogram Plus (Gelatin) Protein Gels. After electrophoresis, the zymography gel was incubated on a shaker in zymogram renaturation buffer for one hour. Then, the gel was washed with deionized water and incubated for 36 hours in a zymogram develop buffer at 37℃. The gelatin gel was then stained with Coomassie Blue R-250 staining solution for 2 hours at room temperature and then destained using a destaining solution (10% glacial acetic acid, 40% methanol, and 50% deionized water). The gels were then imaged by the Li-Cor Odyssey XL System and MMP activity was analyzed.

2.15. Orthotopic breast cancer model

The orthotopic breast cancer model was performed to analyze *in vivo* therapeutic potency of Iminodibenzyl to exert a paradigm shift of COX-2 to produce an anti-cancer effect. The protocol to conduct the animal study was approved by Institutional Animal Care and Use Committee (IACUC) at North Dakota State University. A total of 24 female Nu/J mice were purchased from Jackson Laboratory (ME, USA). The mice were housed four per cage in the pathogen-free innovive IVC system with water and food ad libitum. After two weeks of acclimatization, an orthotopic tumor was induced by implanting 0.25 x 10^6 cells in the fourth mammary fat pad[73-76]. The animals were housed for seven days for the tumor to grow. Once the tumor reached the desired size, the animals were randomly divided into four groups having six animals in each group based on their treatment regimen. During the study, animals were dosed daily with Vehicle, DGLA (5mg/mouse, oral gavage (p.o.)) (Cayman chemicals, MI, USA), Iminodibenzyl (20mg/kg, intraperitoneal (i.p.)), and a combination of Iminodibenzyl ((20 mg/kg, i.p.) + DGLA (5 mg/mouse, p.o.)). During the treatment period, the change in animal weight and the tumor volume (($V=L \times W^2$) / 2 (L: longest axis; W: shortest axis)) were noted every three days. At the endpoint, the animals were

euthanized with pentobarbital overdose (200 mg/kg, *i.p.*), and blood, tumors, and vital organs (liver, spleen, heart, and kidneys) were collected for analysis.

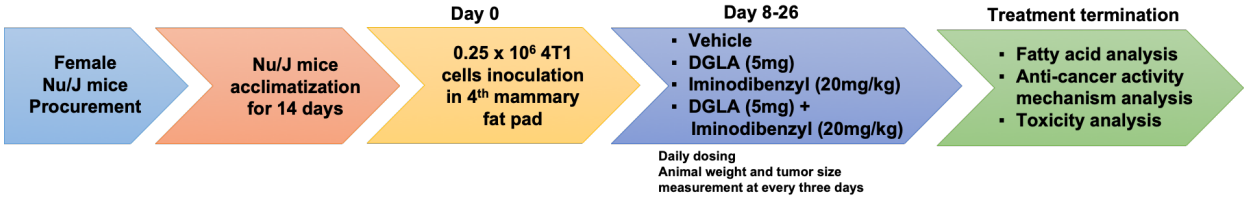

Scheme 4. Animal study plan. A total of 24 mice were used for the *in vivo* experiment as described above (6 mice/group × 4 groups). 0.25 million 4T1 cells were implanted in the 4th mammary fat pad of the mouse to develop an orthotopic breast cancer model. After one week of growth, the mice were randomized into four treatment groups, including 1) Vehicle, 2) DGLA (5mg/mouse), 3) Iminodibenzyl (20mg/kg), and 4) Combination of Iminodibenzyl (20mg/kg) and DGLA (5mg/mouse). During the study, the tumor size was measured every three weeks by using a digital Vernier caliper to measure tumor growth. At the end of the study, animals were euthanized by pentobarbital overdose, and blood, organs, and tumors were collected for post-analysis.

2.16. Fatty acid and prostaglandin analysis

2.16.1. Fatty acid and prostaglandin extraction from tumor

The ω-6s (DGLA and AA) and PGs (PGE_2 and PGE_1) present in the tumor were quantified *via* LC/MS approach. Briefly, approximately 0.1g tumor tissues from three mice from each treatment group were weighed and immersed in liquid nitrogen to freeze. After freezing, the tumor was crushed in a mortar and pastel to a fine powder. The tumor powder was then transferred to a glass test tube, and mixed with 2.55ml of water and 0.45ml of methanol. After adding 5µl internal standards (AA-d8, DGLA-d6, PGE1-d4, and PGE2-d9), the mixture was vortexed for 1-2 minutes and set on ice for 30-45 minutes. Then, the mixture was centrifuged for 15 minutes at 3,000 rpm and the supernatant was collected. The pH of the supernatant was adjusted to 3.0 using 6 N HCl followed by solid phase extraction was done using a SampliQ Silica C18 ODS cartridge. The free fatty acids and PGs were eluted out with 2ml ethyl acetate from a cartridge, which was previously activated by methanol and HPLC grade water. The eluted solution was vacuumed to dryness by vacufuge and reconstituted with 100µl ethanol for HPLC/MS analysis.

2.16.2. HPLC/MS analysis of fatty acid and prostaglandin from tumor

The HPLC/MS system (Agilent 1200 series HPLC system and Agilent 6300 LC/MSD SL ion trap mass spectrometer) was used to quantify the DGLA, AA, and PGs from the tumor. The C18 Zorbax Eclipse-XDB column (3.5µm), 5.0µl sample injection, and a flow rate of 0.8 ml/minute was used to separate different fatty acids and prostaglandins. The used mobile phases were H_2O with 0.01% Acetic acid (mobile phase A) and Acetonitrile with 0.01% Acetic acid (mobile phase B) with gradient of 0-12 minutes (isocratic), 68% A and 32% B; 12-14 minutes, 68 to 44% A and 32 to 56% B; 14-28 minutes (isocratic), 44% A and 56% B; 28-30 minutes, 44 to 14% A and 56 to 86% B; 30-38 minutes, 14 to 4% A and 86 to 95% B; and 38-44 minutes (isocratic), 5% A and 95% B.

In MS settings electrospray ionization was kept in negative mode with total ion current chromatograms in full mass scan mode from m/z 50 to m/z 600. The nebulizer pressure was kept at 15 psi, dry gas flow rate at 5 L/minute, dry temperature at 325°C; compound stability at 20%, and a number of scans were set to 50.

For quantification for fatty acids and PGs, an internal standard curve of solutions having gradient concentrations of DGLA, AA, PGE_1, PGE_2, and a constant concentration of internal standards DGLA-d6, AA-d8, PGE1-d4, PGE2-d9 was prepared. Extracted ion current were used to quantify the peak area of PGE_1 (m/z 353), PGE1-d4 (m/z 357), PGE_2 (m/z 351), PGE2-d9 (m/z 360), DGLA (m/z 305), AA (m/z 303), AA-d8 (m/z 311) and DGLA-d6 (m/z 311), respectively. The concentrations of fatty acids and PGs in the samples were calculated by extrapolating the values of the ratios, obtained from the peak areas of the analytes to their corresponding internal standards, to the standard curve[57,72].

2.17. 8-HOA quantification from tumor

2.17.1. 8-HOA extraction from tumor

Approximately, 0.1g tumor tissues from three mice from each treatment group were weighed, immersed in liquid nitrogen, and smashed into powder, which was then transferred to a glass test tube. It was then mixed with 1ml of water, 500µl of methanol containing hexanoic acid as an internal standard, 50µl of 1.0 N HCl, and 3ml of Dichloromethane. The mixture was then vortexed and centrifuged to collect the organic layer. The extraction procedure was repeated twice, and the combined dichloromethane layers were evaporated to dryness using a vacufuge evaporator. The sample was reconstituted with 50µl of 1.0% diisopropylethylamine in acetonitrile (v/v) and derivatized with 50µl of 1% PFB-bromide in acetonitrile (v/v). The reaction mixture was then heated at 37°C for 30 minutes and then the acetonitrile layer was removed using a vacuum evaporator. The residue was reconstituted in 100µl of dichloromethane and subjected to GC/MS analysis[57,72] as described in 2.9.

2.18. Iminodibenzyl quantification

2.18.1. Extraction

To extract the Iminodibenzyl, 0.1g tumor and organs from animals from each treatment group were crushed into a fine powder (after immersing them in liquid nitrogen) and then transfer to the glass test tube. The powder was then mixed with 3ml of ethanol and vortexed for 30 seconds and then the tumor/organ suspension was kept on ice for one hour. Followed by incubation, the solution was centrifuged, and the supernatant was collected. The extraction procedure was repeated twice, and the combined supernatants were dried under a vacuum. The extracted Iminodibenzyl was resuspended in 100µl ethanol and subjected to HPLC analysis.

2.18.2. HPLC analysis of Iminodibenzyl

The Agilent 1200 series HPLC system was used to quantify Iminodibenzyl in the organs and tumor tissue. The analysis was performed by using an established method using 10 mM ammonium acetate buffer (pH adjusted to 2.21 with glacial acetic acid) – methanol (50 + 50, v/v) as a mobile phase, 37°C column temperature, and C18 Zorbax column (3.5µm). Iminodibenzyl from the samples was quantified from developed Iminodibenzyl dose vs. area under the curve[77].

2.19. Western analysis using tumor tissue

2.19.1. Protein extraction

Approximately, 0.05g of tumor tissues from three mice from each treatment group were weighed, immersed into liquid nitrogen, and smashed into powder using a mortar and pestle. The powder was then mixed with modified RIPA lysis buffer premixed with protease and phosphatase cocktail inhibitor and sonicated at 5 second cycle for 25 seconds and kept on ice for 30-45 minutes. After incubation, the suspension was centrifuged at 13000rpm for 10 minutes and clear protein supernatant was collected. Then the Western blot analysis for different proteins was performed according to the procedure mentioned in 2.10.

2.20. HDAC activity analysis from tumor samples

The protein from the tumors harvested from animals was extracted in a similar manner mentioned in 2.18.1. Protein was quantified by the BCA protein assay kit as mentioned in 2.10.2. Approximately 50µg protein from each sample was loaded in a plate and HDAC activity analysis was done as mentioned in 2.11.

2.21. Immunohistochemistry analysis

Immunofluorescence analysis was done to analyze the D5D, E-Cadherin, MMP-2, Vimentin, and Ki-67 protein level in tumor tissue at Advanced Imaging & Microscopy Laboratory,

NDSU. Briefly, freshly collected tumor tissues were fixed with 10% v/v formaldehyde and embedded in paraffin blocks. Tissues sections of 5μm thickness were cut and placed on a glass slide followed by heated at 70°C for 1 hour. The slides were then deparaffinized by immersing in xylene for three minutes (x3). The xylene solution was removed by dipping the slides 15-20 times in 100% methanol (x3). The tumor section was then rehydrated by immersing in 95% and 70% alcohol solution. Epitope retrieval was done by heating the slide (having sections) in a pressure cooker for 30 minutes with sodium citrate buffer. The slides were then washed with TBST to removed excess buffer. The tumor section was then blocked with 5% goat serum and then incubated with primary antibodies for 1 hour at room temperature followed by washing with TBST was performed to remove unbound antibodies. The sections were then incubated with corresponding secondary antibodies for 1 hour at room temperature in dark and then washed with TBST. The tumor sections were then incubated with DAPI solution to stain the nuclei. In the end, the tumor section was covered with the glass coverslip, and images were taken by using LSM 900 with Airyscan 2.0.

2.22. Hematoxylin and Eosin (H&E) staining

H&E staining was performed to analyze any pathological abnormality and presence of metastatic nodules in the vital organs. Briefly, freshly collected vital organs were fixed with 10% v/v formaldehyde and embedded in paraffin blocks. Tissues sections of 5μm thickness were cut and placed on a glass slide and then the H&E staining procedure was performed at Advanced Imaging & Microscopy Laboratory, NDSU. The pathological abnormality was determined by observing the images of tissues under an inverted microscope (Leica Microsystems Model DMi8) in the bright field mode.

2.23. Statistical analysis

GraphPad Prism 9 software was used to perform statistical analyses. The complete randomized design was applied for grouping *in vivo* mouse study. The data was presented as Means ± Standard Error of the Mean (SEM). Data were analyzed by multiple comparisons test using one-way or two-way ANOVA followed by Bonferroni analysis. Statistical significance was shown by differences with a minimum of $P<0.05$.

3. THE ANTI-CANCER EFFECT OF IMINODIBENZYL ALONG WITH DGLA ADMINISTRATION IN TRIPLE-NEGATIVE BREAST CANCER CELLS

It is well established that ω-6-PUFAs such as DGLA upon metabolism by D5D forms AA, which is further peroxidized by COX-2 in cancer microenvironment to precancerous PGE_2[78]. The generated PGE_2 acts through various cellular pathways resulting in uncontrolled cancer cell proliferation, inhibition of cancer cell apoptosis, increased migration, and metastasis (Scheme 1 in Introduction)[79]. On the contrary, D5D inhibition by siRNA/shRNA/3WJ-NP has been found to redirect DGLA metabolism to 8-HOA, resulting in anti-cancer effect[51-53,55,57,72]. Notably, all the above-mentioned approaches to deliver RNAi modality to the cancer cell are limited by major limitations such as physiological degradation by endonucleases, off-target side effects, and inability to cross the cellular membrane due to the presence of negative charge on the phosphate backbone[61,80]. Hence, to execute the paradigm shift of the COX-2 approach and to translate our approach in the clinics to suppress cancer growth, we identified different reported D5D inhibitors, such as Sesame, Iminodibenzyl, CP-24879, and Curcumin. Then, based on the IC_{50} value, determined by analyzing the amount of DGLA left after 2 hours of incubation in rat liver microsomes, we found Iminodibenzyl as a potent D5D inhibitor as it has the lowest IC_{50} (104nM) compared to CP-24879 (144nM), Curcumin (148nM), and Sesame (346nM) (Table 1). By D5D activity inhibition, the DGLA metabolism was diverted to an alternative pathway to produce 8-HOA. On analyzing 8-HOA, after 48 hours of incubation with a combination of DGLA and different D5D inhibitors in colon cancer cell line, only Iminodibenzyl was able to produce 8-HOA above the threshold value (>0.5μM) (Table 1 in Introduction). Additionally, to determine therapeutic output, the percentage reduction in survival fraction, by D5D inhibitors and/or DGLA treatment, a proliferation assay was performed. The analysis showed a significant reduction in

survival fraction by Iminodibenzyl and DGLA treatment compared to Sesame or CP-24879 with DGLA treatment in colon cancer cells (Table 1 in Introduction). From the preliminary experiments, we found Iminodibenzyl as the potent D5D inhibitor among four identified ones as it produced the high 8-HOA, resulting in a significant reduction in survival fraction in colon cancer cells[81]. Based on the above findings, we postulated that administration of Iminodibenzyl will stimulate the COX-2 paradigm shift in COX-2 overexpressed breast cancer cell lines causing DGLA peroxidation to produce 8-HOA, which will produce anti-cancer activity.

3.1. Iminodibenzyl and DGLA treatment reduced cancer cell viability

In the initial analysis, the cell viability assay was performed to determine the suitable *in vitro* dose of DGLA and Iminodibenzyl for 4T1 and MDA-MB-231 breast cancer cells. When cells were treated with gradient doses of DGLA (1 to 500μM) or Iminodibenzyl (0.1 to 50μM) for 48 hours, no significant cytotoxic effect was observed on cancer cell lines except the highest employed dose of DGLA (500μM) and Iminodibenzyl (50μM) (Figure 1 and Figure 2). Surprisingly, when cells were provided combination treatment with Iminodibenzyl and DGLA, a significant reduction in cell viability was observed from Iminodibenzyl (10μM) and DGLA (100μM) in 4T1 and MDA-MB-231 cells (Figure 3, $P<0.001$), implicating the beneficial synergistic effect (δ score: 38.68 by ZIP model) of the drug combination at a lower dose. Hence, to achieve the ideal outcome and to avoid unexpected toxicity, we used 10μM Iminodibenzyl + 100μM DGLA in subsequent *in vitro* studies.

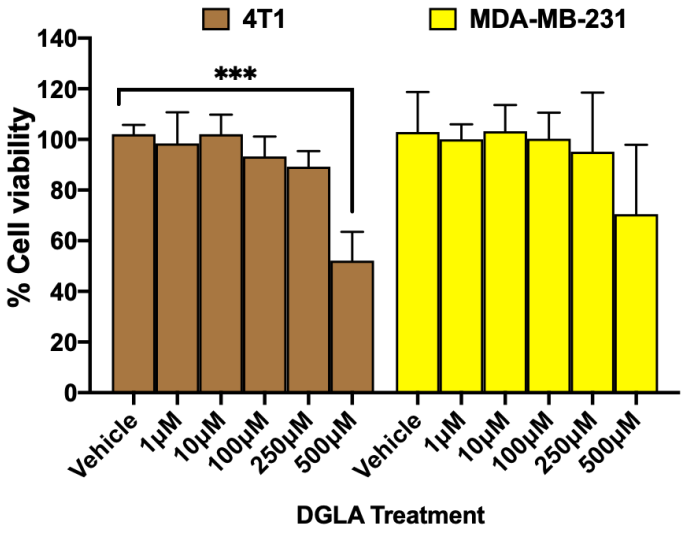

Figure 1. Effect of DGLA on breast cancer cells viability after 48 hours of treatment. 4T1 and MDA-MB-231 cells were treated with different concentrations of DGLA for 48 hours, followed by an MTT assay was performed. Data represented as mean ± SEM with at least three separate experiments. The cell viabilities for different treatment groups were calculated by considering the Vehicle group's cell viability as 100%. ****P<0.001 vs.* Vehicle.

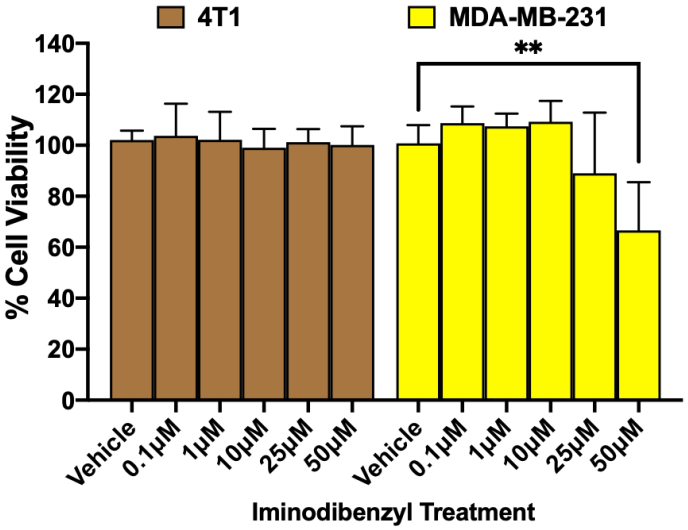

Figure 2. Effect of Iminodibenzyl on breast cancer cells viability after 48 hours of treatment. 4T1 and MDA-MB-231 cells were treated with different concentrations of Iminodibenzyl for 48 hours, followed by an MTT assay was performed. Data represented as mean ± SEM with at least three separate experiments. The cell viabilities for different treatment groups were calculated by considering the Vehicle group's cell viability as 100%. ***P<0.01 vs.* Vehicle.

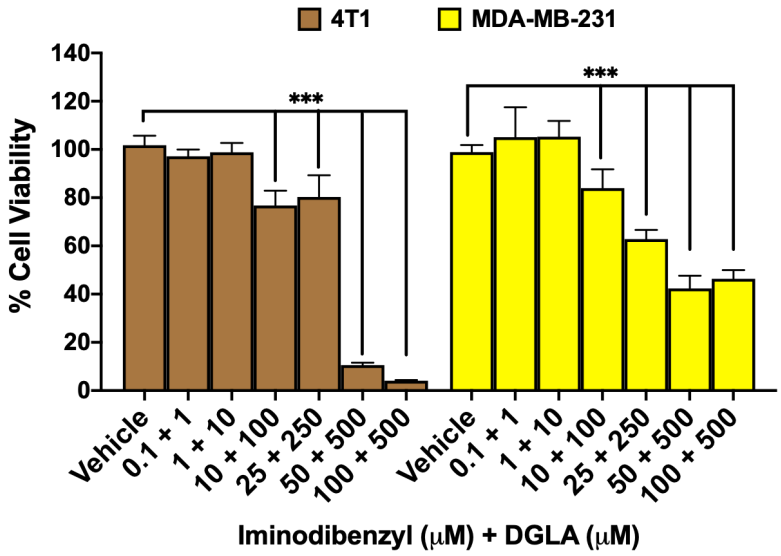

Figure 3. Effect of Iminodibenzyl and DGLA combination on breast cancer cells viability after 48 hours of treatment. 4T1 and MDA-MB-231 cells were treated with different concentrations of Iminodibenzyl and DGLA for 48 hours, followed by an MTT assay was performed. Data represented as mean ± SEM with at least three separate experiments. The cell viabilities for the different treatment groups were calculated by considering the Vehicle group's cell viability as 100%. ****P<0.001 vs.* Vehicle.

3.2. Iminodibenzyl and DGLA combination treatment caused 8-HOA production

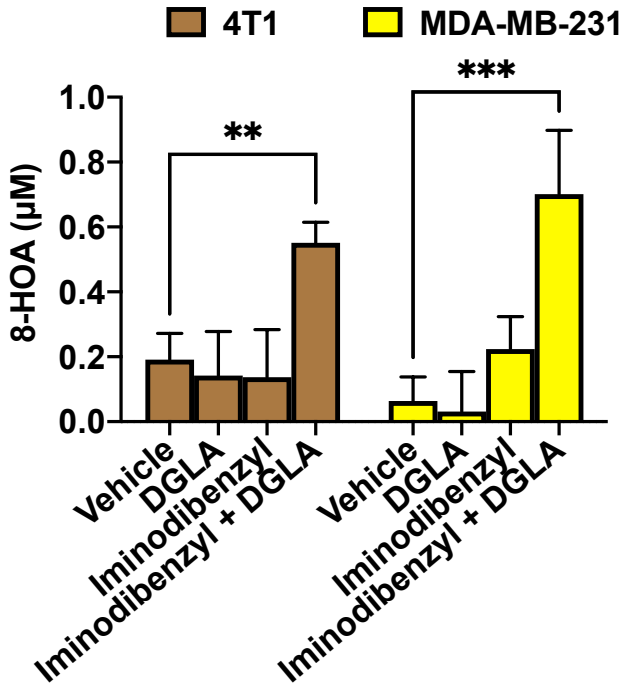

Figure 4. Iminodibenzyl and DGLA combination treatment caused 8-HOA production in breast cancer cells. 4T1 and MDA-MB-231 cells were treated with Vehicle, DGLA, Iminodibenzyl, and combination of DGLA and Iminodibenzyl for 48 hours followed by which GC/MS analysis was done to quantify derivatized 8-HOA. N=3; Data represented as mean ± SEM. ****P<0.001,* ***P<0.01 vs.* Vehicle.

To investigate the mechanism of the drug combination and feasibility of Iminodibenzyl as a D5D activity inhibitor in breast cancer cells, we quantified the 8-HOA level in breast cancer cells treated with 10µM Iminodibenzyl and 100µM DGLA. 8-HOA is an exclusive distinctive C-8 oxygenation product from DGLA, which abstract •H from the atmosphere and form free radical adduct, making quantification difficult. To avoid the limitation, we have derivatized 8-HOA by widely used Pentafluorobenzyl-bromide (PFB-Br)[82]. On analysis, a significant increase in the 8-HOA level in COX-2 overexpressing 4T1 and MDA-MB-231 cancer cells was observed (Figure 4, *P<0.01* and *P<0.001*, respectively). Notably, we did not find any significant change in 8-HOA

level, when cells were provided treatment with Vehicle, DGLA, or Iminodibenzyl alone (Figure 4).

3.3. Iminodibenzyl and DGLA treatment reduced survival fraction in breast cancer cells

In our previous studies, we have observed a significant reduction in cancer cell proliferation after DGLA treatment in D5D knockdown cells[52,55,56]. Based on the Iminodibenzyl property to divert DGLA metabolism by D5D activity inhibition, we performed a colony formation assay to assess the outcome of different treatments on cancer cell proliferation. We found no prominent effect on cancer cell proliferation when 4T1 cancer cells were treated with Vehicle and 10μM Iminodibenzyl. However, a significant decrease in the number of colonies was observed on providing concomitant treatment of Iminodibenzyl and DGLA (Figure 5 $P<0.001$), which implicated a reduction in cancer cell proliferation. Interestingly, when cells were provided with 100μM DGLA treatment, a significant increase in 4T1 cell proliferation was observed (Figure 5, $P<0.01$). This effect could be due to DGLA's metabolism to cancer cell proliferation stimulating PGE_2 by overexpressed COX-2 in cancer cells.

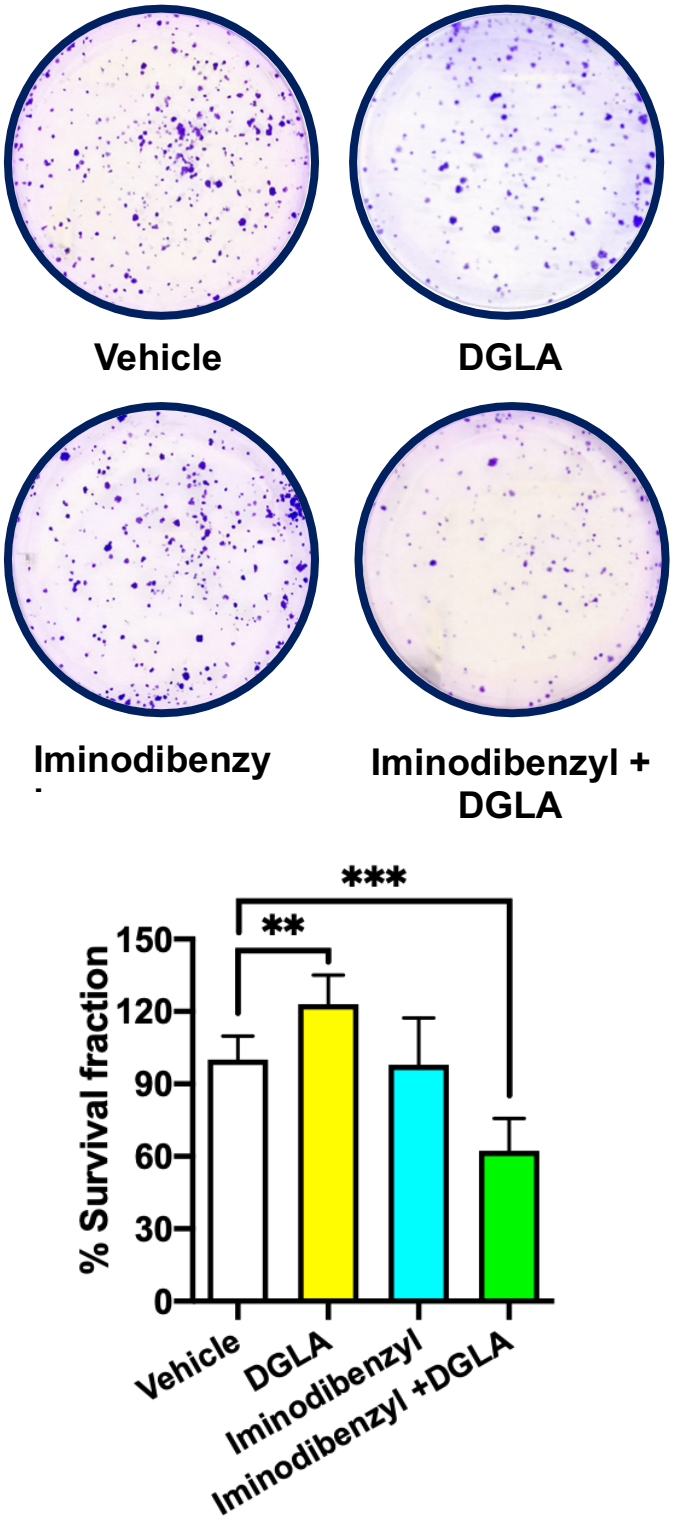

Figure 5. Colony formation assay to analyze breast cancer cell survival. Representative images of colonies from different treatment groups and calculated percentage survival fraction. N=3; Data represented as mean ± SEM. ****P<0.001, **P<0.01 vs.* Vehicle.

3.4. Breast cancer cells undergo apoptosis after Iminodibenzyl and DGLA treatment

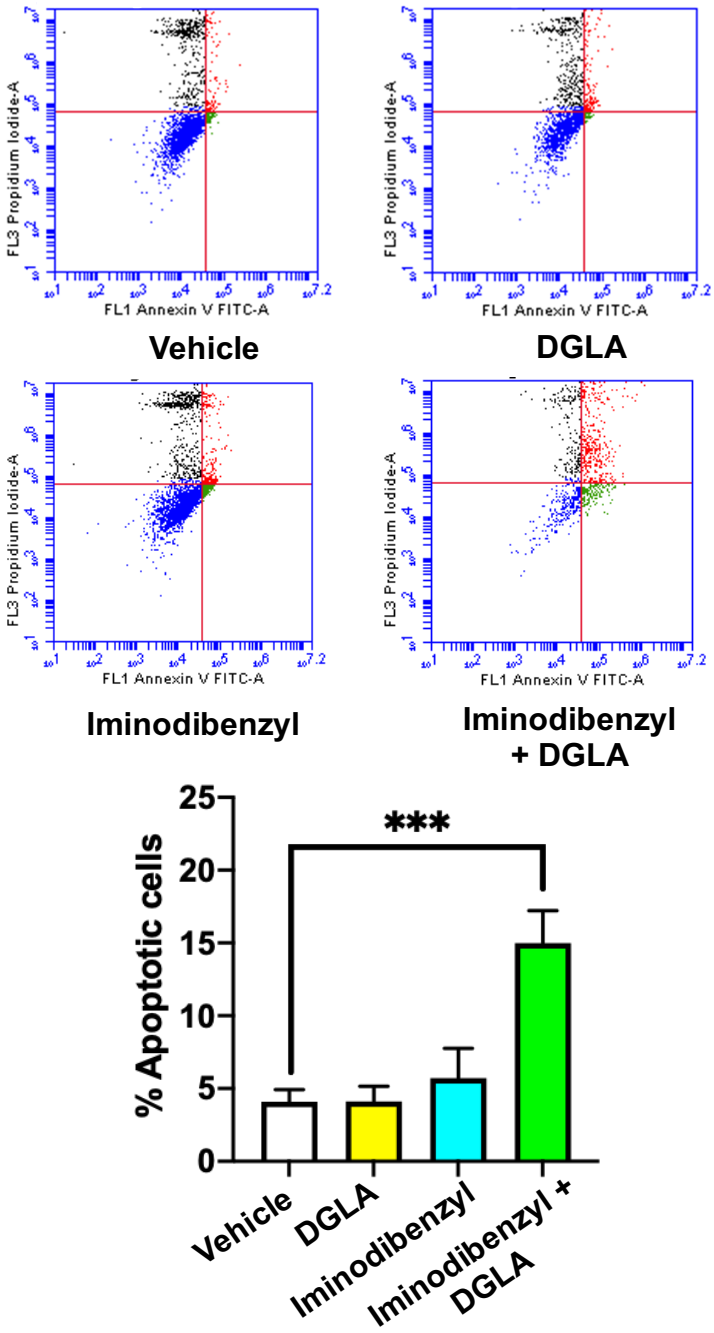

Figure 6. Apoptosis analysis after 48 hours of treatment with Iminodibenzyl and/or DGLA in 4T1 cancer cells. Apoptosis analysis was performed by PI-Annexin V FITC double staining method by using a flow cytometer. Representative images of single run from different treatment groups are shown. The bar graph is the percentage of apoptotic cells from the Q3 quadrant. N=3; Data represented as mean ± SEM. ****P<0.001 vs.* Vehicle.

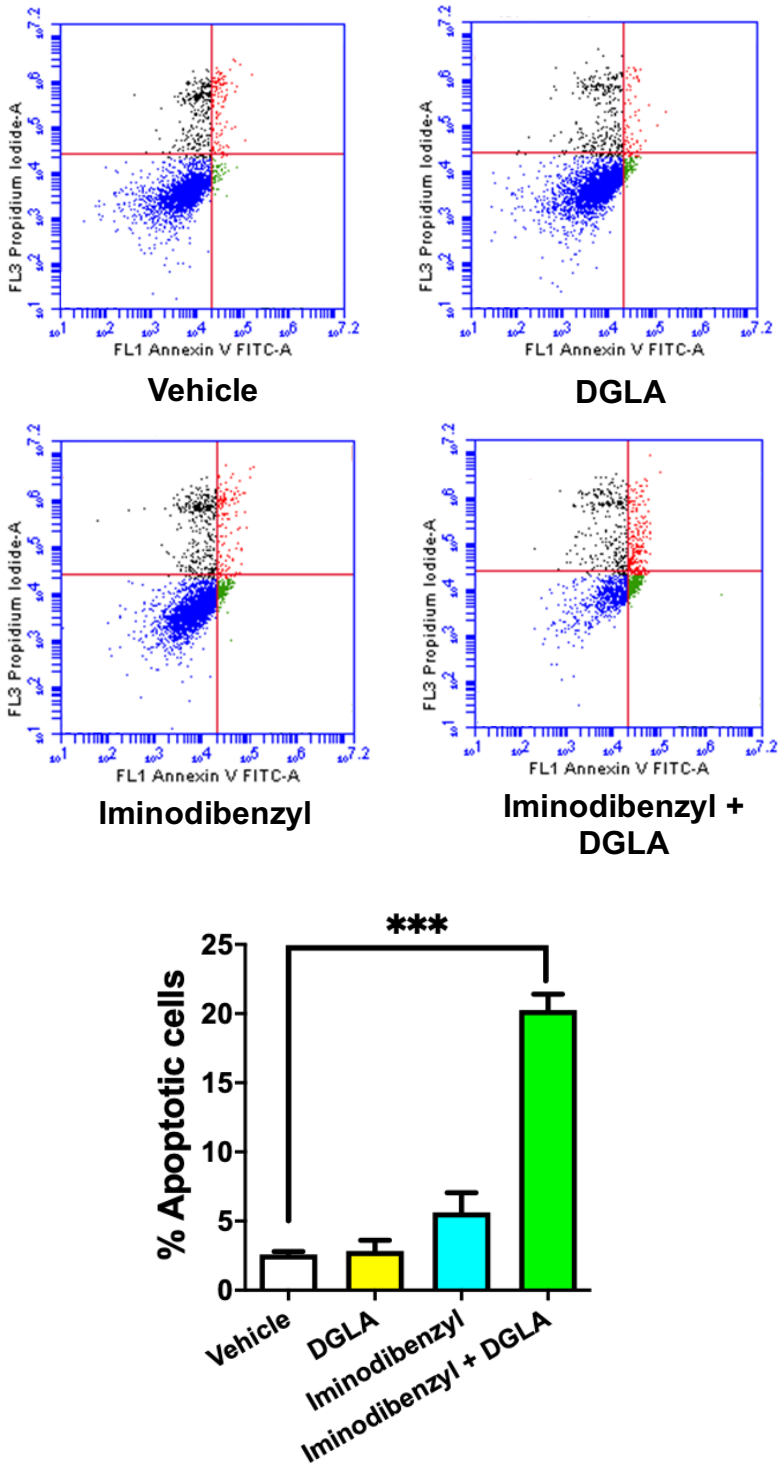

Figure 7. Apoptosis analysis after 48 hours of treatment with Iminodibenzyl and/or DGLA in MDA-MB-231. Apoptosis analysis was performed by PI-Annexin V FITC double staining method by using a flow cytometer in 4T1 cells. Representative images of single run from different treatment groups are shown. The bar graph is the percentage of apoptotic cells from the Q3 quadrant. N=3; Data represented as mean ± SEM. ****P<0.001 vs.* Vehicle.

As per Yu et al., and Yang et al., treatment with exogenous 8-HOA or 8-HOA produced after treatment with DGLA in D5D-KD cells showed a significant increase in early apoptotic cells[52,55,56]. Here, we attempted to analyze the percentage of apoptotic cells after 48 hours of treatment with Iminodibenzyl and DGLA by PI-Annexin V FITC staining using a flow cytometer. On analysis, we found that treatment with Vehicle, DGLA, or Iminodibenzyl did not have any effect on breast cancer cell apoptosis. However, when cells were provided concomitant treatment with Iminodibenzyl and DGLA, a significant increase in the percentage of apoptotic cells were observed in 4T1 and MDA-MB-231 breast cancer cells (Figure 6 and Figure 7, $P<0.001$).

3.5. Iminodibenzyl fueled COX-2 catalyzed DGLA peroxidation caused a reduction in breast cancer cell migration

To further evaluate the effect of different treatments; Vehicle, DGLA, Iminodibenzyl, and Iminodibenzyl and DGLA on cancer cell migration, we performed the wound healing assay on 4T1 and MDA-MB-231 cells. In this assay, the cellular wound was created by using the sterile pipette tip after the formation of a cell monolayer, and growth media was changed from media containing 10% FBS to serum-free media mixed with various treatments. Following treatment, the reduction in wound size was measured at 24 and 48 hours of the treatment by using bright-field microscopy. On analysis, we found a significant decline of cancer cell migration rate resulting in larger wound size in 4T1, and MDA-MB-231 cancer cells at 24 hours and 48 hours of treatment with DGLA and Iminodibenzyl (Figure 8, $P<0.001$ and Figure 10, $P<0.05$). The transwell migration assay was also performed to confirm the findings obtained from the wound healing assay. Transwell migration assay also showed similar findings of reduced 4T1 cancer cell migration (larger bright spots) in the group of cells provided simultaneous treatment with

Iminodibenzyl and DGLA (Figure 9, *P<0.01*). Notably, we did not observe any inhibitory effect on cancer cell migration when cells were treated with DGLA (Figure 8, 9, and 10).

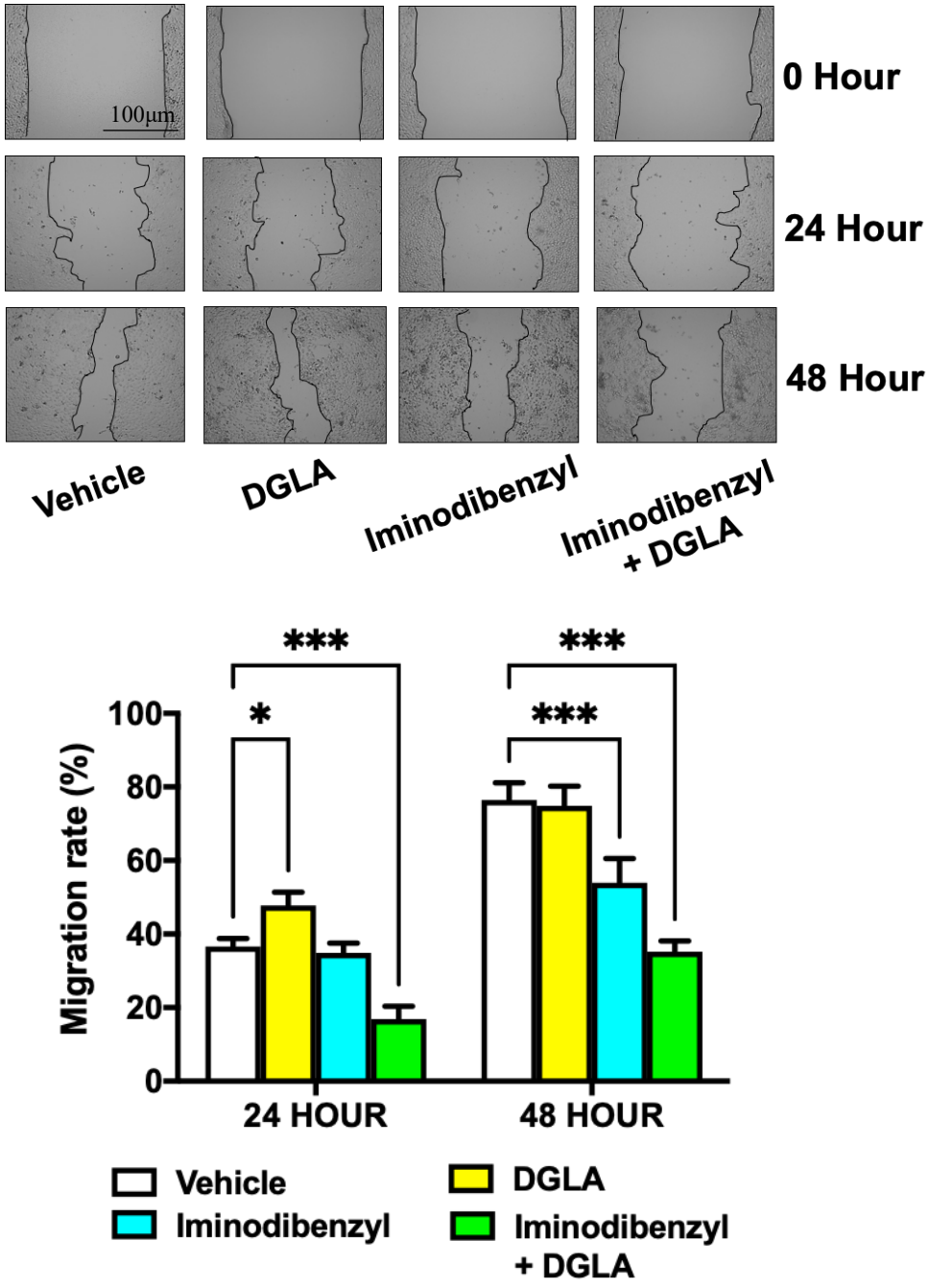

Figure 8. Percentage migration rate at 24 and 48 hours in 4T1 cells. The wound area was measured at 0, 24, and 48 hours to determine the effect of different treatments on migration rate. The upper panel in the figure show the wound size at different time points. Percentage migration rate was analyzed by comparing the wound area at 24- and 48-hours with 0-hour time point. N=3; Data represented as mean ± SEM. ****P<0.001, *P<0.05 vs.* Vehicle.

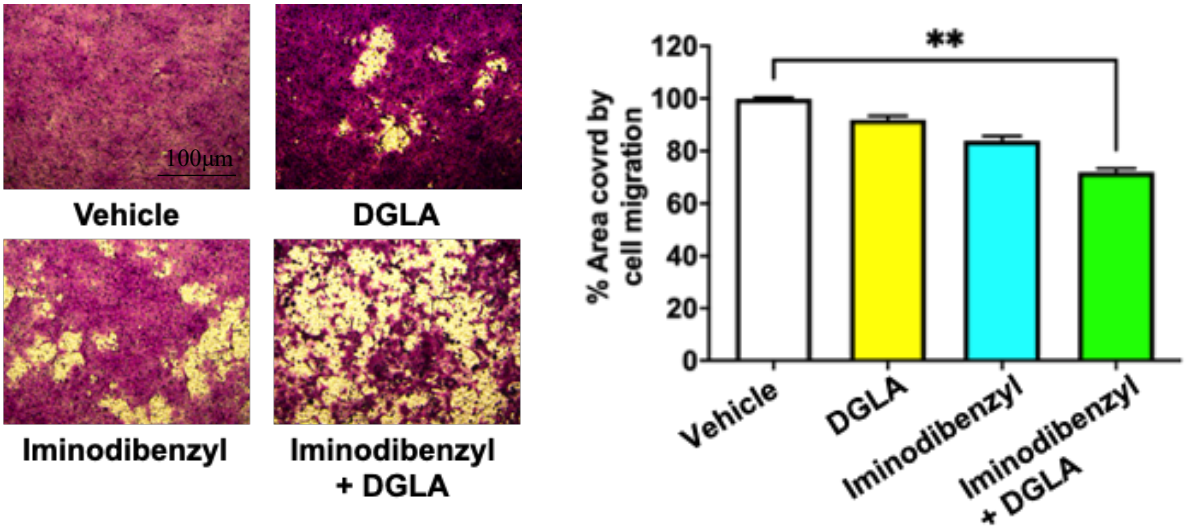

Figure 9. Transwell migration assay after 48 hours of treatment with DGLA and/or Iminodibenzyl in 4T1 cells. Representative images of the area covered after cell migration after 48 hours of treatment. The bar graph shows the percentage area covered by the 4T1 breast cancer cells after 48 hours of treatment. Data analysis was done by comparing the area with Vehicle treated group. N=3; Data represented as mean ± SEM. ***P<0.01 vs.* Vehicle.

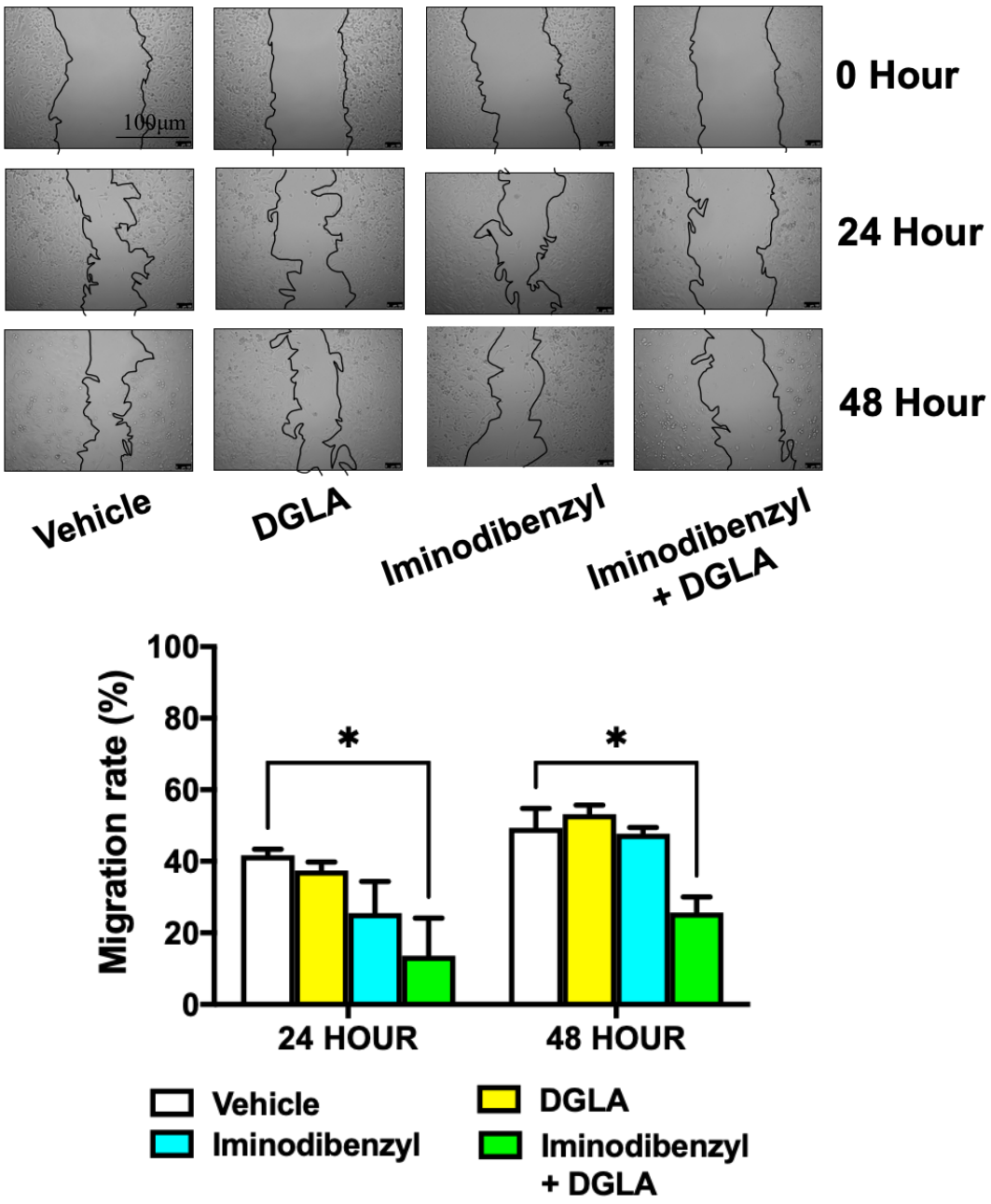

Figure 10. Percentage migration rate at 24 and 48 hours in MDA-MB-231 cells. The wound area was measured at 0, 24, and 48 hours to analyze the effect of DGLA and/or Iminodibenzyl on migration rate. The upper panel in the figure show the wound size at different time points. Percentage migration rate was quantified by comparing the wound area at 24 and 48 hours with 0-hour time point. N=3; Data represented as mean ± SEM. *$P<0.05$ *vs.* Vehicle.

3.6. COX-2 dependence to exhibit derogatory effect on cancer cell growth

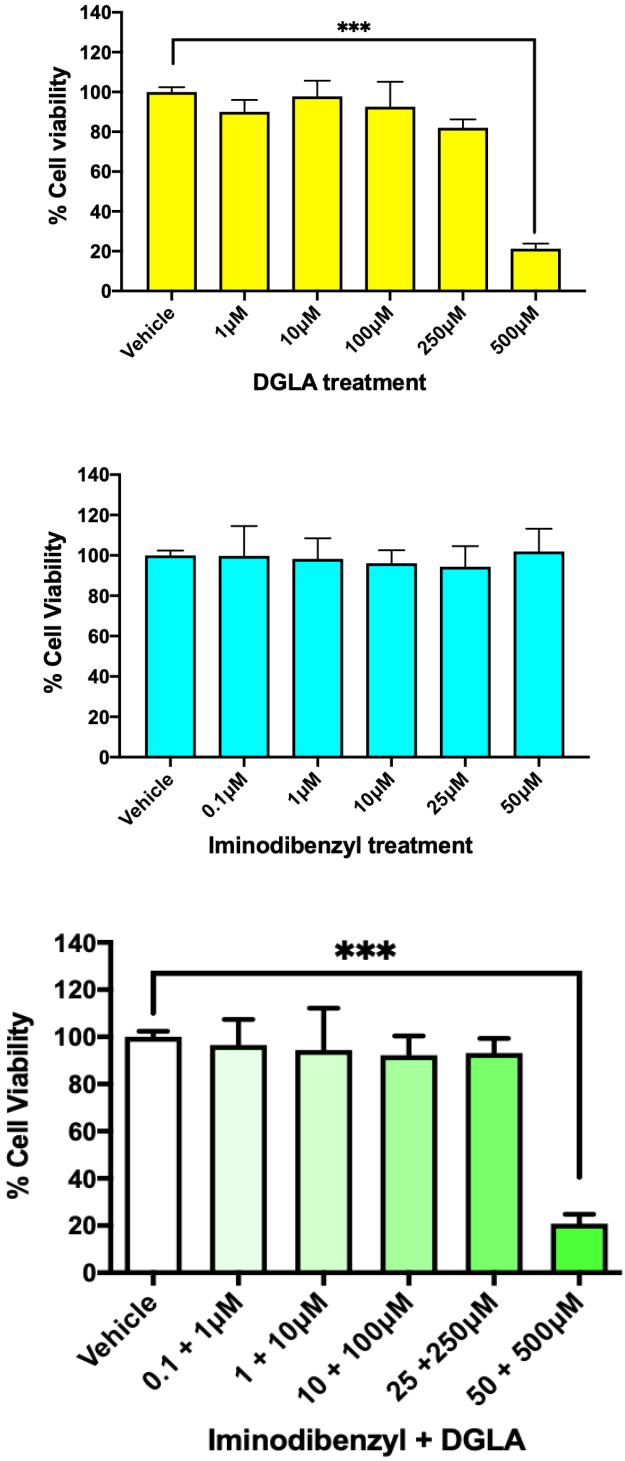

Figure 11. Cell viability assay in MCF-12a cells. Cell viability assay after 48 hours of treatment with gradient doses of DGLA, Iminodibenzyl, and combination of Iminodibenzyl and DGLA. Data analysis was done by comparing cell viability to Vehicle treated group of cells. N=3; Data is represented as mean ± SEM. ****P<0.001 vs.* Vehicle.

As per the paradigm shift of COX-2 approach, COX-2 is hypothesized to be a prime requirement for DGLA peroxidation to occur. To analyze the COX-2 role, we utilized a COX-2 negative non-cancerous mammary epithelial MCF-12a cell line and provided 48 hours of treatment with similar doses of DGLA, Iminodibenzyl, and a combination of Iminodibenzyl and DGLA as provided for 4T1 and MDA-MB-231. On analysis, unlike cancer cells, no effect on cell viability was noted on either Iminodibenzyl or DGLA alone or in combination with Iminodibenzyl, except highest employed dose of 500µM (Figure 11).

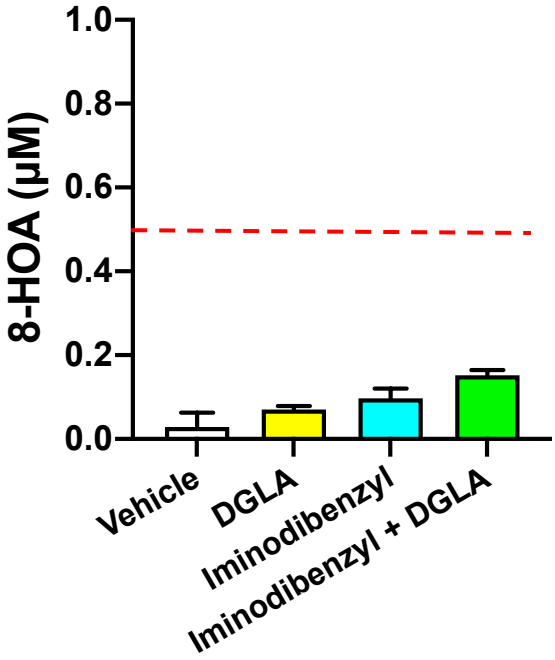

Figure 12. 8-HOA analysis in MCF-12a cells. GC/MS analysis to quantify 8-HOA after 48 hours of treatment with Vehicle, DGLA, Iminodibenzyl, and combination of Iminodibenzyl and DGLA. The red dotted line indicates the minimum threshold (0.5µM) of 8-HOA required to produce a therapeutic effect. N=3; Data is represented as mean ± SEM.

Additionally, to determine whether single-agent treatment or combination treatment could produce any 8-HOA, MCF-12a cells were treated with Vehicle, DGLA, Iminodibenzyl, and combination of Iminodibenzyl and DGLA for 48 hours and followed by that GC/MS analysis was

done. On analysis, we found neither of the treatment was able to produce 8-HOA above the threshold level (0.5μM) needed to produce any therapeutic effect (Figure 12).

3.7. Limitations

To validate and compare the therapeutic effectiveness of a new therapeutic strategy, a positive control is required. However, in our approach, we have identified four different D5D inhibitors and have chosen the most potent one (Iminodibenzyl) for the research work. Hence, we lack a chemically synthesized or naturally occurring standard compound, which will produce 8-HOA in cancerous environment. Hence, lack of the positive control is considered as the limitation of the approach of D5D activity inhibition.

In transwell migration assay, a serum containing media was used as a chemoattractant to lure the cancer cells across the membrane and inhibitory effect of the treatment on cell migration was analyzed for 48 hours. Since, 4T1 has a doubling time of ~14-15 hours, the cells might have undergone proliferation and have produced false positive outcome. However, more evidence that is concrete is required to distinguish anti-proliferative vs. anti-migrative effect exerted during the analysis.

3.8. Conclusion and discussion

COX-2 is one of the most well-known identified markers in breast cancer specimens. As per the various reports, COX-2 is overexpressed in 58-93% of the tumor samples[14,16,18]. The inducible COX-2 is an upstream enzyme responsible for the metabolism of downstream n-6 AA to cancer growth-promoting PGE_2[17,79,83,84]. Therefore, the COX-2 inhibition strategy was considered an effective strategy to manage breast cancer. However, the result obtained from clinical studies employed selective and non-selective COX-2 inhibitors with/without other

chemotherapeutic agents were inconclusive[33,34,85]. On the contrary, COX-2 inhibitors produced life-threatening cardiovascular adverse events that resulted in the death of clinical patients[31,35,85].

However, earlier findings from our group highlighted an additional unique C-8 oxygenation pathway of DGLA (precursor of AA) metabolism by COX-2 induced peroxidation to produce exclusive anti-cancer free radical metabolite, 8-HOA[49]. To divert the DGLA metabolism from cancer inducing pathway to cancer inhibiting pathway, our group has tried D5D siRNA/shRNA/3WJ D5D siRNA NP and achieved the cancer growth inhibition in the colon, pancreatic, and lung cancer animal studies[51,55,72,86]. However, all the above-mentioned approaches are difficult to execute clinically as it requires in-patient treatment and most importantly, it is limited by shortcomings of RNAi therapy[61,80]. To overcome the limitations, we have identified chemically synthesized or naturally present D5D inhibitors and characterized the most potent D5D activity inhibitor Iminodibenzyl by various preliminary screening assays[81]. Since Iminodibenzyl role in a COX-2 paradigm shift in breast cancer to achieve cancer growth inhibition was unexplored, here we have hypothesized that Iminodibenzyl treatment would divert the DGLA metabolism to 8-HOA that would help in achieving breast cancer growth inhibition.

In this chapter, we have performed preliminary functional endpoint experiments to validate the cancer growth inhibitory effect produced by Iminodibenzyl and/or DGLA. Iminodibenzyl administration halted the D5D activity resulting in a shift of DGLA peroxidation to 8-HOA in the COX-2 overexpressed tumor microenvironment. As a result of which, when 4T1 and MDA-MB-231 breast cancer cells were treated with Iminodibenzyl and DGLA, a significant surge in 8-HOA was observed. The produced 8-HOA in breast cancer cells might lead to cell viability reduction in 4T1 and MDA-MB-231 cells. On the contrary, COX-2 null mammary epithelial MCF-12a cells did not show how sufficient level of 8-HOA and did not affect the cell viability of epithelial cells,

which was possibly due to negative COX-2 expression. This phenomenon emphasizes the importance and role of COX-2 to produce 8-HOA after DGLA and Iminodibenzyl combination treatment in cancer cells. Notably, higher concentrations (500μM DGLA alone or with Iminodibenzyl) showed a toxic effect on cells, which is possibly due to other off-target effects. For example, ω-6-PUFAs like linoleic acid (LA) and gamma-linolenic acid (GLA) at high concentrations have been found to cause significant reduction in cell viability by inducing reactive oxygen or carbonyl species formation and/or activating apoptosis by various mechanisms such as caspase-dependent mechanism[87,88]. In cancer, cell apoptosis, proliferation, and migration are the most important characteristics to be considered for therapeutic analysis. Iminodibenzyl administration diverted the DGLA metabolism to cancer inhibiting compound 8-HOA, which led to a reduction in cancer cell survival (Survival analysis by MTT assay) and cell migration (Wound healing assay and transwell migration assay). Additionally, cancer cells underwent apoptosis when Iminodibenzyl and DGLA were provided as a treatment. Notably, when DGLA was provided as a treatment in cancer cells, increased cancer cell survival or proliferation was seen (a greater number of colonies). The observed effect could be due to the direct conversion of DGLA to AA and then to PGE_2 promoting cancer cell growth.

In summary, results from this chapter provided evidence about Iminodibenzyl role in DGLA metabolism to 8-HOA, resulting in reduced cancer cell survival, reduced migration, and increased apoptosis with DGLA administration in COX-2 expressing breast cancer cells.

4. ELUCIDATION OF THE *IN VITRO* GROWTH INHIBITORY MECHANISMS AFTER IMINODIBENZYL AND DGLA TREATMENT IN BREAST CANCER CELLS

COX enzymes are the inductive enzymes catalyzing the first step in the prostanoids synthesis. Among COXs, COX-2 is majorly involved in catalyzing AA conversion to PGE_2, which activates various molecular pathways leading to cancer cell development, resistance to apoptosis, progression, and metastasis (Scheme 1 in Introduction). COX-2 was the target of research in a multitude of extensive pathological conditions, including inflammation, and different cancers like colon, gastric, lung cancer, and breast cancer[24,89,90]. Clinical studies evaluating COX-2 expression quantification from breast cancer specimens concluded overexpression in 42% of the analyzed samples[91]. The exploration of COX-2 as a target for cancer therapeutics has been in a limelight for decades. However, the first clinical study analyzing the role of COX-2 selective inhibitor celecoxib for familial adenomatous polyposis (FAPs) occurred in the 1990s, where celecoxib exerted reduction in adenomatous polyps in patient[92]. After this initial application, the use of COX-2 inhibitors was raised in cancer management. However, during this period the serious cardiovascular effects were also observed[15] with OX-2 inhibitors . Hence, the use of COX-2 inhibitors was halted in 2005 for the use in clinical studies for cancer management.

Recently, our research group came up with the approach where instead of inhibiting COX-2 by inhibitors, we are exploiting overexpressed COX-2 in cancer cells to metabolize the upstream n-6 fatty acid. As per this approach, upstream D5D enzyme inhibition halts the DGLA metabolism to AA resulting in DGLA accumulation in cancer cells. This results in DGLA metabolism redirection to unique short-lived metabolite 8-HOA and other therapeutically non-significant metabolites by overexpressed COX-2, which have cancer growth inhibitory activity[49]. Until now, we have validated this approach by D5D siRNA/shRNA/ 3-WJ D5D siRNA NP in colon,

pancreatic, lung, and breast cancer[50,55,57,72]. However, these approaches are limited by endonuclease mediated physiological degradation, possible off-targeted side effects, low availability at the site of action, and in patient treatment[80]. However, to bridle the limitations and to master the COX-2 paradigm shift approach, as mentioned in chapter-3, based on literature and preliminary analysis, we screened out a potent D5D activity inhibitor Iminodibenzyl[81,93]. Iminodibenzyl is a lead moiety for widely used antipsychotics, Imipramine and Desipramine, acting as dopaminergic antagonists blocking alpha and beta adrenoreceptors in the brain[94]. As per the preliminary screening, Iminodibenzyl has a strong D5D activity inhibition property with IC50 of 104nM[81]. Recently, Iminodibenzyl is also reported to exert cancer growth inhibitory effect in xenograft and syngeneic lung cancer models produced by A549 and Lewis lung carcinoma cell line[93]. Additionally, when Iminodibenzyl was provided in combination with DGLA in 4T1 and MDA-MB-231 cell lines, diverted metabolism of DGLA to 8-HOA was observed with a simultaneous reduction in breast cancer cell proliferation, reduction in cancer cell migration, and upregulated cancer cell apoptosis (Chapter 3). However, the molecular mechanism of action behind the exerted therapeutic effect is still unexplored. In the future, after understanding the molecular mechanism, a combination therapy working through different therapeutic pathways can be designed to provide additive or synergistic effect with the Iminodibenzyl based therapeutic approach.

4.1. Activation of the caspases dependent mechanism after Iminodibenzyl and DGLA treatment

Our earlier reports also suggested that on providing DGLA as a treatment to D5D knockdown cells, a significant increase in apoptosis occurred by activation of caspase-dependent death mechanism[51]. Additionally, in chapter 3, we have seen that when Iminodibenzyl and DGLA

combination was provided as a treatment, a significant increase in apoptotic cells was observed, however, the mechanism responsible for the witnessed effect is unexplored. In this aim, we have used Western and immunofluorescent approaches to elucidate possible molecular mechanisms behind apoptosis and reduced cancer cell migratory effect. Here, we have provided 48 hours of Vehicle, DGLA, and/or Iminodibenzyl treatment to 4T1 and MDA-MB-231 cancer cells, and the protein was extracted using lysis buffer. After lysis, the protein was collected and measured using the BCA protein estimation method, and 50µg of protein was loaded to a Western blot gel and electrophoresis was performed. After running the samples on the gel, the proteins were transferred to a PVDF membrane and incubated with primary and corresponding secondary antibodies. First, we analyzed the protein expression of procaspase-3, procaspase-9, and cleaved caspase-3 in 4T1 cancer cells. The analysis showed a significant decrease in procaspase-9 level with 10µM Iminodibenzyl, and the combination of 10µM Iminodibenzyl and 100µM DGLA treatment (Figure 13, $P<0.05$). Consequently, cleaved caspase-3 (C. Caspase-3) analysis showed a significant increase in its levels on providing simultaneous treatment with 10µM Iminodibenzyl and 100µM DGLA (Figure 13, $P<0.001$). However, we did not observe any modulatory effect on apoptosis markers by DGLA treatment (Figure 13).

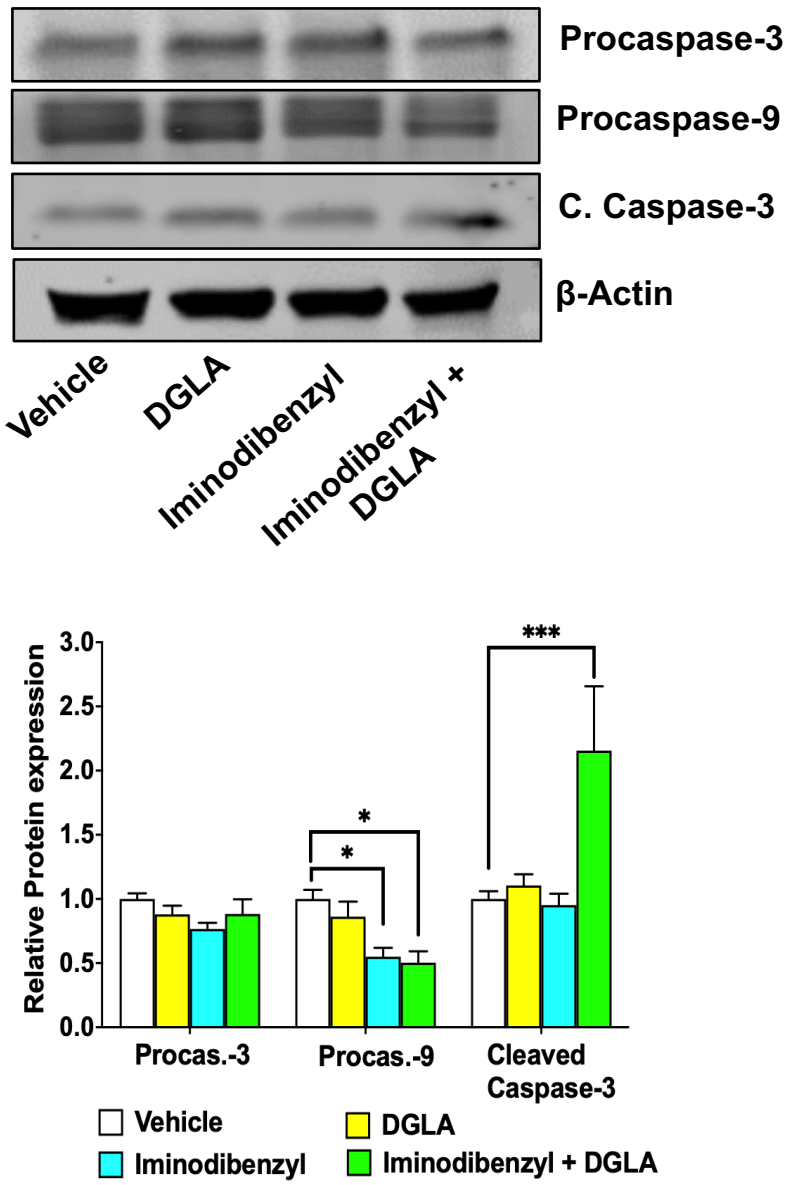

Figure 13. Iminodibenzyl and DGLA treatment activated the caspases in 4T1 cancer cells. Western blot and densitometry analysis of Procaspase-3, Procaspase-9, and Cleaved Caspase-3 in 4T1 breast cancer cells treated with Iminodibenzyl and/or DGLA for 48 hours. The protein expression level in the vehicle was normalized to 1, β-Actin serves as a loading control. Data is represented as mean ± SEM with at least three separate experiments. *P***<0.001, *P<0.05 vs.* Vehicle.

Additionally, we also analyzed the anti-apoptotic protein BCl_2. BCl_2 is a member of the pro-survival family of proteins, which determined whether a cell undergoes apoptosis or not[95]. When cells were provided Iminodibenzyl alone and/or in combination with DGLA, it caused a significant reduction in anti-apoptotic protein BCl_2 expression (Figure 14, *P<0.001*).

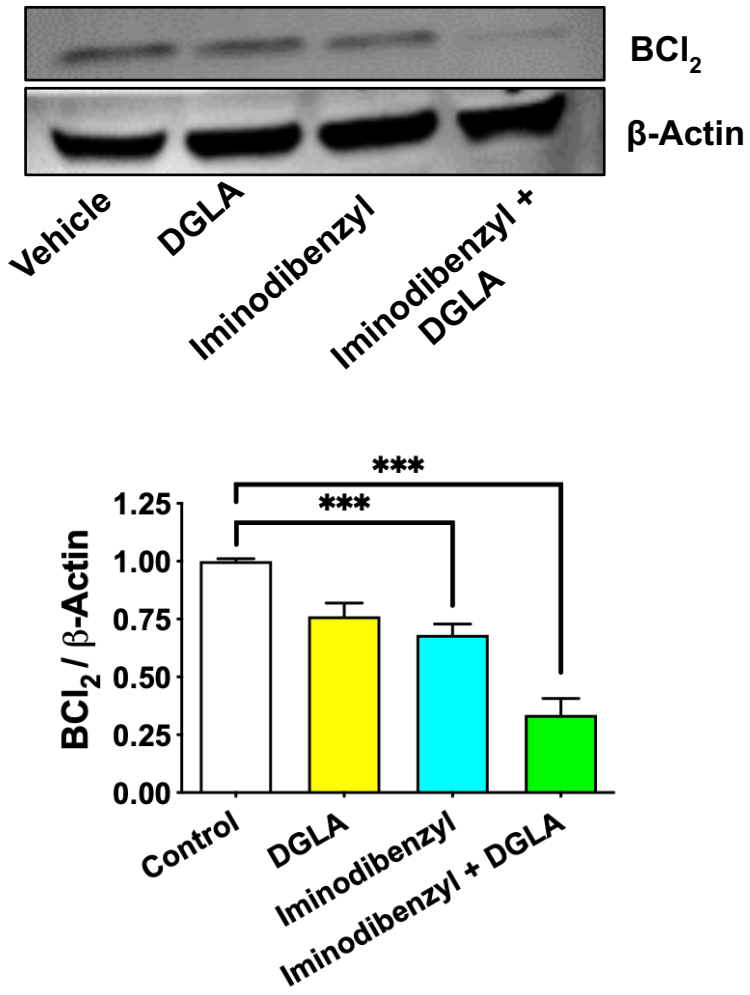

Figure 14. Iminodibenzyl and DGLA treatment downregulated anti-apoptotic protein in 4T1 cells. Western blot analysis and densitometry analysis of BCl_2 in 4T1 breast cancer cells treated with Iminodibenzyl, DGLA, and a combination of Iminodibenzyl and DGLA for 48 hours. The protein expression level in the vehicle was normalized to 1, β-Actin serves as a loading control. Data is represented as mean ± SEM with at least three separate experiments. ****P<0.001 vs.* Vehicle.

Additionally, treatment with DGLA and Iminodibenzyl have caused a significant cleavage of PARP as observed from a reduction of PARP and a significant increase in C. PARP protein (Figure 15, *P<0.001*).

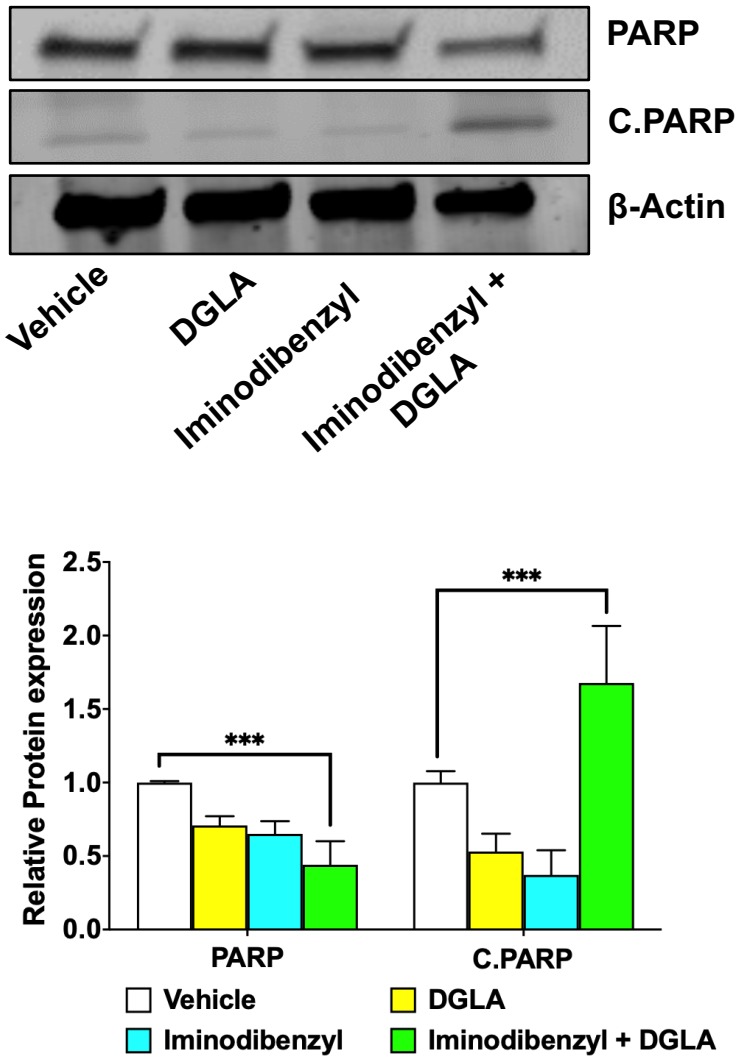

Figure 15. Combination treatment modulated PARP level. Western blot analysis and densitometry analysis of PARP and C. PARP from protein samples extracted after treating 4T1 cells with Iminodibenzyl, DGLA, and a combination of Iminodibenzyl and DGLA for 48 hours. The protein expression level in the vehicle was normalized to 1, β-Actin serves as a loading control. Data is represented as mean ± SEM with at least three separate experiments. ****P<0.001 vs.* Vehicle.

Similar to 4T1 cells, on treating MDA-MB-231 cells with Iminodibenzyl and DGLA, a significant reduction in procaspase-3 (Figure 16, *P<0.05*) and significant upregulation of C. PARP (Figure 17, *P<0.001*) was observed. Notably, a moderate change but not significant was exerted by Iminodibenzyl and DGLA treatment on BCl_2 and total PARP levels (Figure 16 and 17).

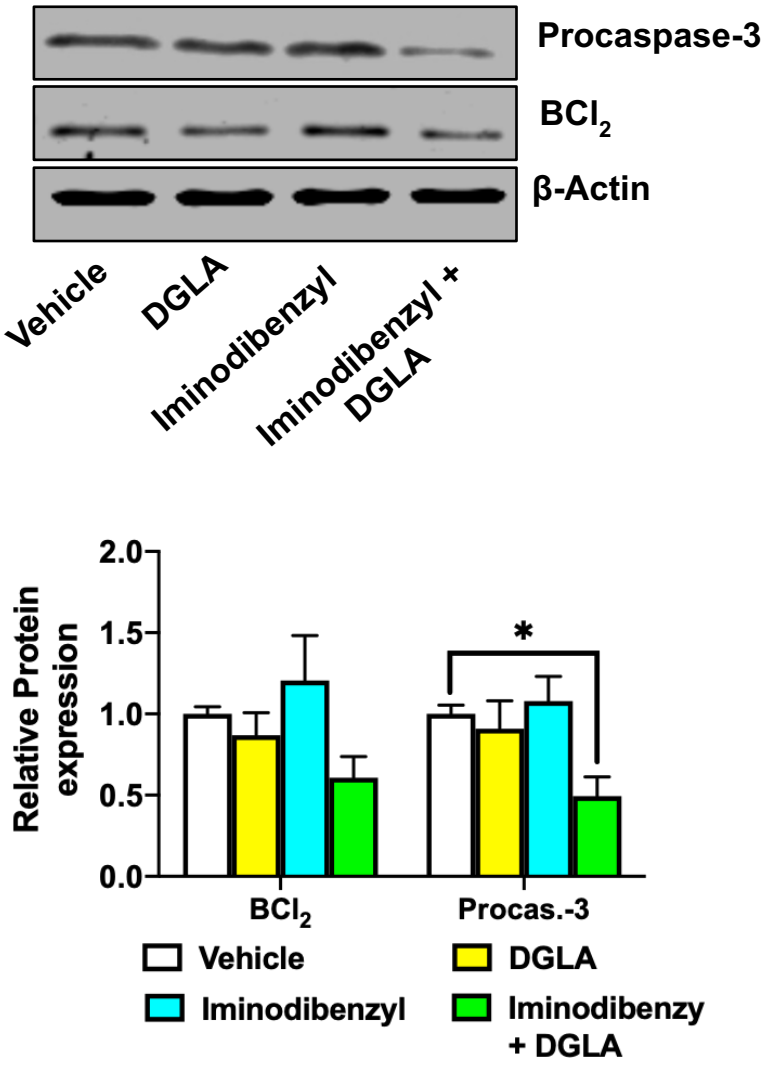

Figure 16. Iminodibenzyl and DGLA treatment downregulated Procaspase-3 and BCl_2. Western blot analysis and densitometry analysis of Procaspase-3 and BCl_2 from protein samples extracted after treating MDA-MB-231 cells with Iminodibenzyl, DGLA, and a combination of Iminodibenzyl and DGLA for 48 hours. The protein expression level in the vehicle was normalized to 1, β-Actin serves as a loading control. Data is represented as mean ± SEM with at least three separate experiments. *$P<0.05$ *vs.* Vehicle.

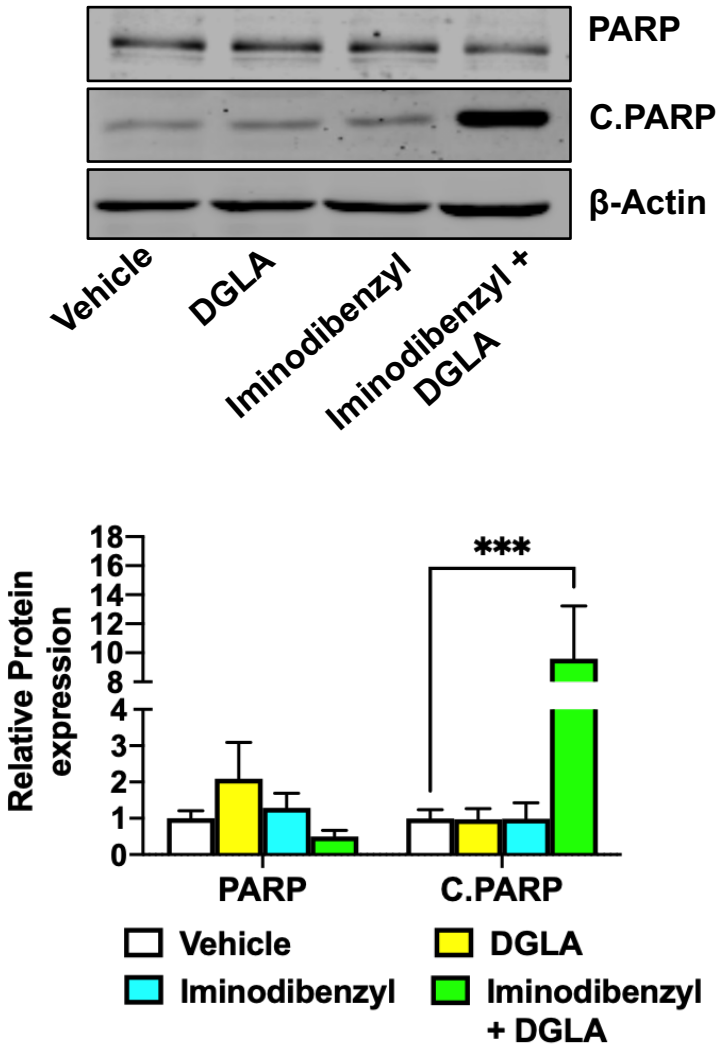

Figure 17. Iminodibenzyl and DGLA treatment promoted PARP breakdown to C. PARP. Western blot analysis and densitometry analysis of PARP and C. PARP in MDA-MB-231 breast cancer cells treated with Iminodibenzyl, DGLA, and a combination of Iminodibenzyl and DGLA for 48 hours. The protein expression level in the vehicle was normalized to 1, β-Actin serves as a loading control. Data is represented as mean ± SEM with at least three separate experiments. ****P<0.001* *vs.* Vehicle.

4.2. Validation of involvement of caspase dependent death mechanism

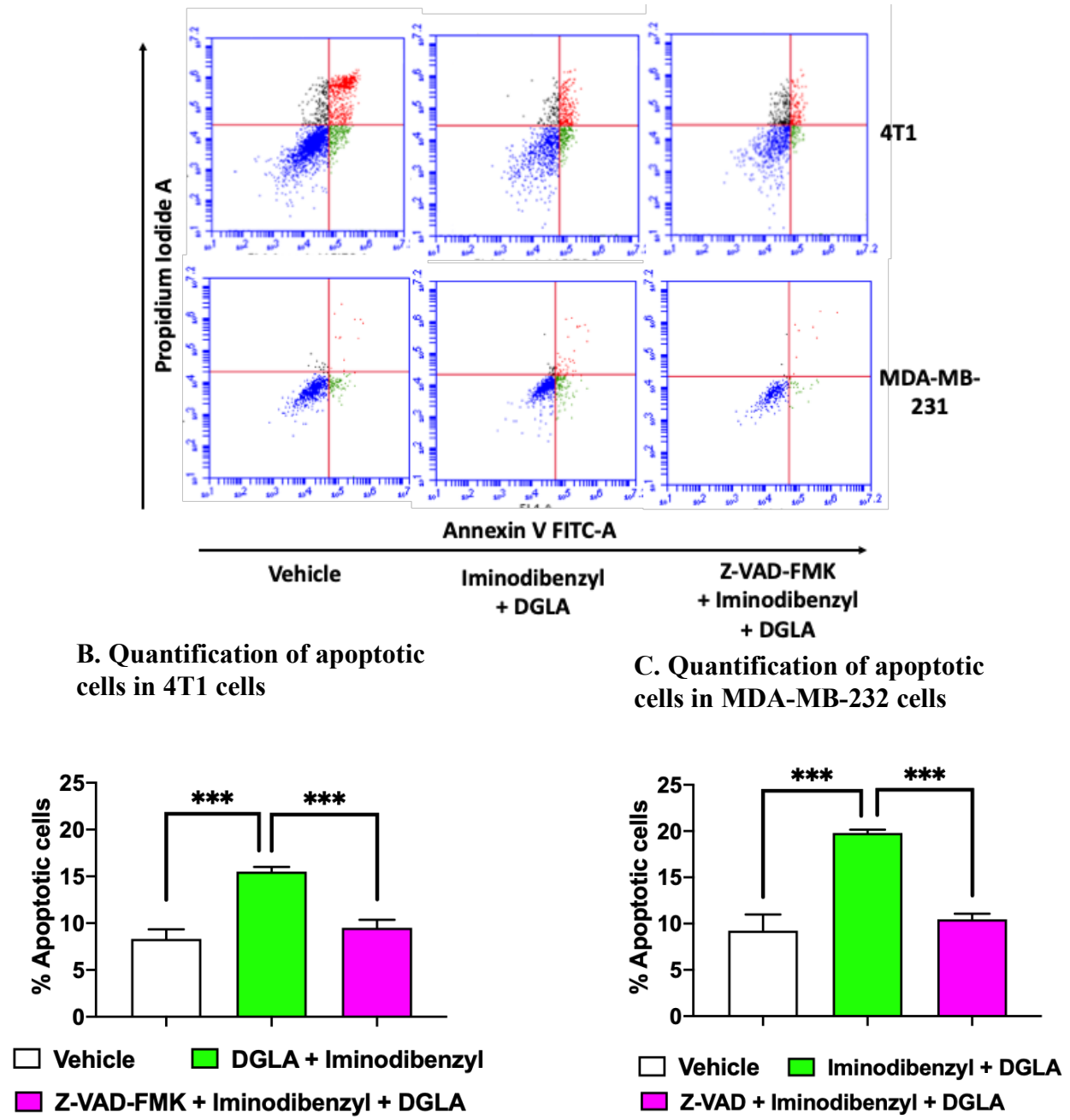

Figure 18. Z-VAD-FMK pretreatment decreased the apoptotic effect exerted by Iminodibenzyl and DGLA combination. A. Flow cytometry analysis of breast cancer cells pretreated with 30µM Z-VAD-FMK, followed by combination of Iminodibenzyl and DGLA for 48 hours. B. Percentage apoptotic cells quantification in 4T1 cells. C. Percentage apoptotic cells quantification in MDA-MB-231 cells. Data represent mean ± SEM with at least three separate experiments. ****P<0.001* *vs.* Vehicle or Iminodibenzyl + DGLA.

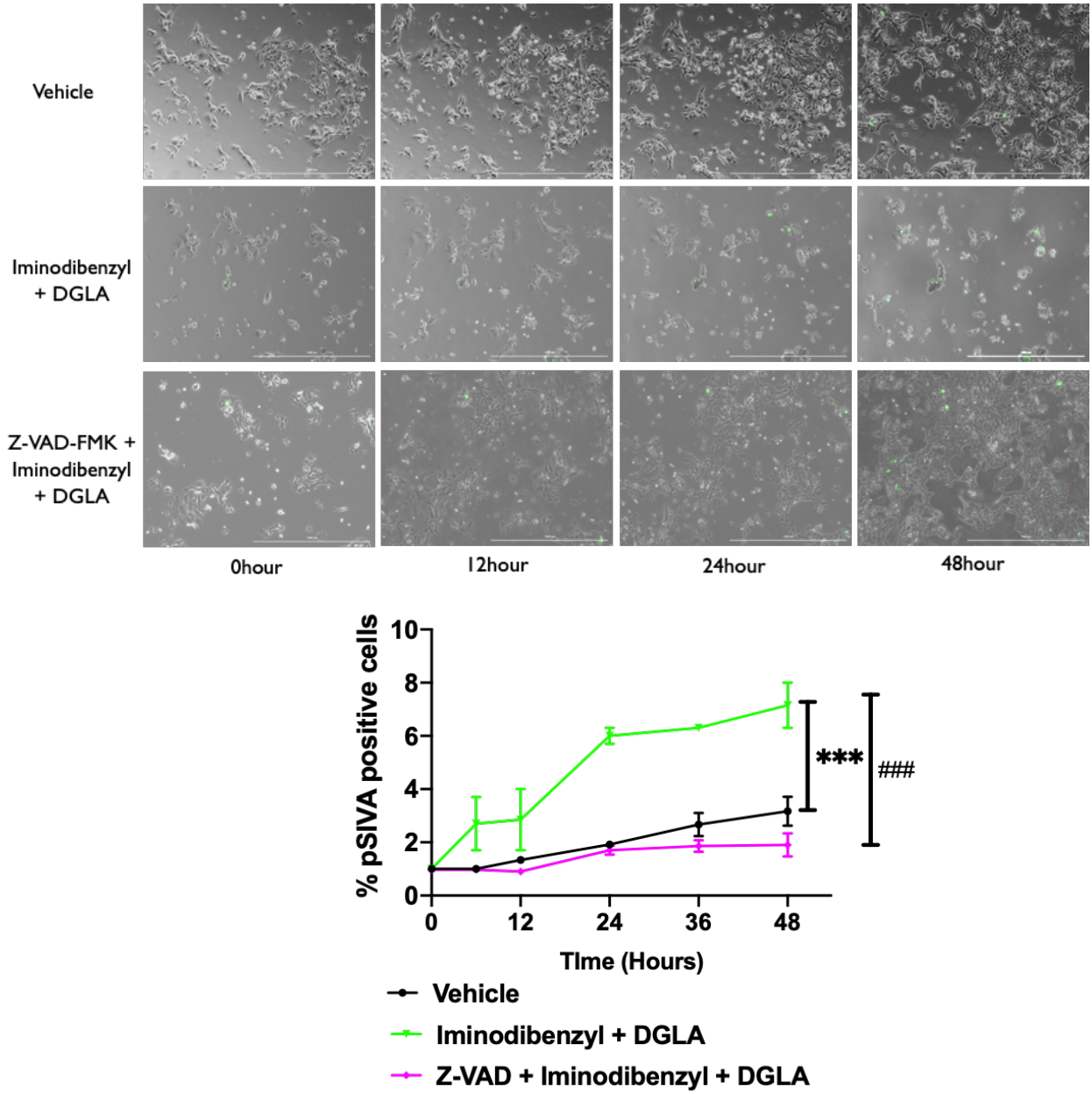

Figure 19. Z-VAD-FMK pretreatment overcame the apoptotic effect of combination treatment. 4T1 breast cancer cells were pretreated with nonspecific irreversible caspase inhibitor Z-VAD-FMK for 2 hours and then the medium was replaced with fresh growth media having various treatments and pSIVA dye. The plate was then subjected to a kinetic apoptosis analysis by using Lionheart FX at various time points and apoptosis rate was measured. Data is represented as mean ± SEM with at least three independent fields. ***$P<0.001$ *vs.* Vehicle and $^{###}P<0.001$ *vs.* Iminodibenzyl + DGLA at 48 hours.

Caspases are key mediators involved in the apoptosis pathway. Modulation of their level is involved in various pathological conditions such as cancer. To confirm the caspase-dependent

death mechanism, we have used Z-VAD-FMK. It is a cell-permeable, irreversible caspase inhibitor. To confirm the caspase-dependent apoptotic mechanisms, we treated cells with 30μM Z-VAD-FMK for 2 hours before providing cells the combination treatment and performed apoptosis analysis. We observed a significant increase in the percentage of apoptotic 4T1 and MDA-MB-231 cells (PI-Annexin V analysis) after Iminodibenzyl and DGLA combination treatment (Figure 18, $P<0.001$). Whereas pretreatment with Z-VAD-FMK recuperated the percentage of apoptotic cells to the vehicle-treated cells (Figure 18, $P<0.001$). Additionally, we also performed polarity-sensitive indicators of viability and apoptosis (pSIVA) imaging analysis. In line with the PI-Annexin analysis, we found that DGLA and Iminodibenzyl could result in a significant increase in the percentage of apoptotic breast cancer cells (Figure 19, $P<0.001$). Notably, the pretreatment of Z-VAD-FMK diminished the DGLA and Iminodibenzyl induced apoptosis in pSIVA imaging (Figure 19, $P<0.001$).

4.3. Combination treatment causes HDAC activity reduction

In our earlier studies, we have demonstrated that exogenous 8-HOA or DGLA derived 8-HOA could inhibit HDAC activity in cancer cells[54,55,57,86]. Hence, here we hypothesized that the combination of Iminodibenzyl and DGLA would have a dampening effect on HDAC activity via endogenous 8-HOA production in breast cancer cells. To perform the HDAC activity, we use the protein extracted from the cells after providing different treatments. On examination, we observed a significant reduction of HDAC activity in 4T1 and MDA-MB-231 cells treated with Iminodibenzyl and DGLA combination (Figure 20, $P<0.001$). Notably, we also noted a significant reduction in HDAC activity in 4T1 cells treated with Iminodibenzyl alone (Figure 20, $P<0.05$).

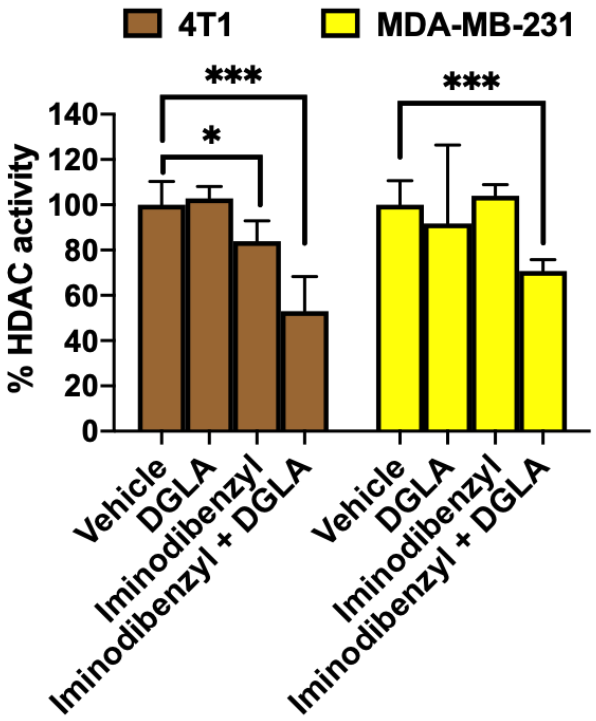

Figure 20. Combination treatment of Iminodibenzyl and DGLA caused a reduction in HDAC activity. HDAC activity was performed from protein samples extracted from breast cancer cells after various treatments for 48 hours. The activity was performed by using a standard HDAC colorimetry activity kit. Data represent mean ± SEM with at least three separate experiments. ****P<0.001, *P<0.05 vs.* Vehicle.

Abnormal histone acetylation has an essential role in tumor development by epigenetically inhibiting the tumor suppressor genes, and hence histone deacetylase inhibition has become the ideal target for cancer therapeutics. HDAC inhibitors exhibit their anti-cancer activity by stimulating acetylation of core histone protein, which impacts gene transcription resulting in apoptosis and degradation of misfolded proteins[96]. As noted above, Iminodibenzyl administration redirected the DGLA metabolism to 8-HOA, which also exerted a significant reduction in HDAC activity. The reduced HDAC activity linked with upregulation of AcH_3 in 4T1 and MDA-MB-231 cancer cells (Figure 21 and 22, *P<0.001* and *P<0.05*).

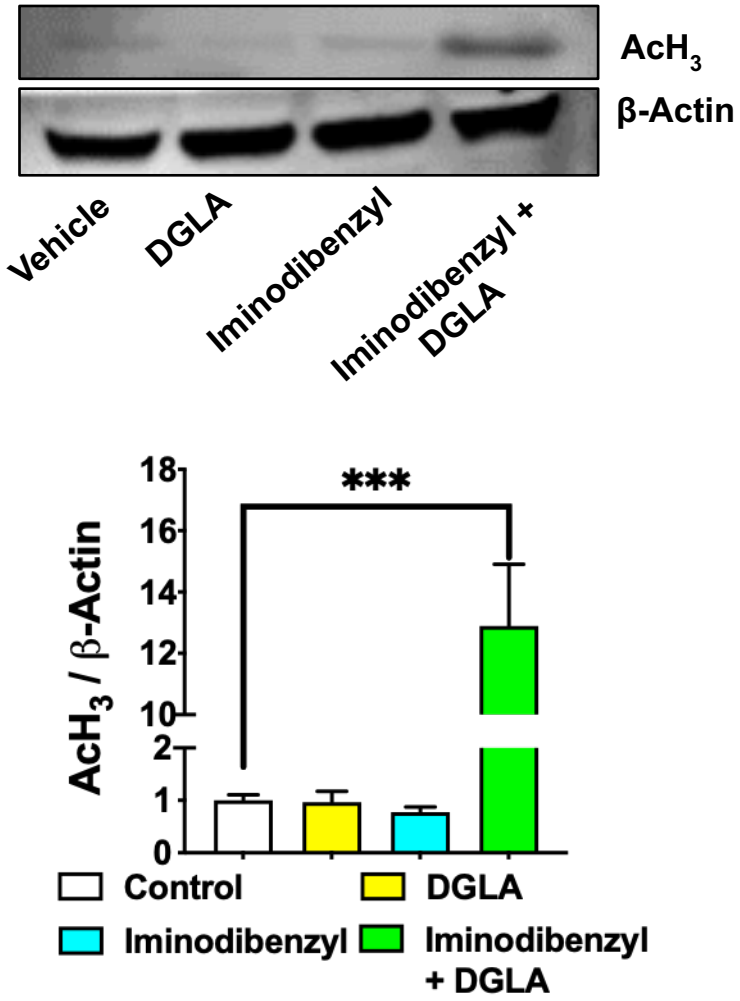

Figure 21. Iminodibenzyl and DGLA treatment stimulated histone acetylation. Western blot analysis and densitometry analysis of AcH_3 in 4T1 breast cancer cells treated with Iminodibenzyl, DGLA, and a combination of Iminodibenzyl and DGLA for 48 hours. The protein expression level in the vehicle was normalized to 1, β-Actin serves as a loading control. Data is represented as mean ± SEM with at least three separate experiments. ****P<0.001 vs.* Vehicle.

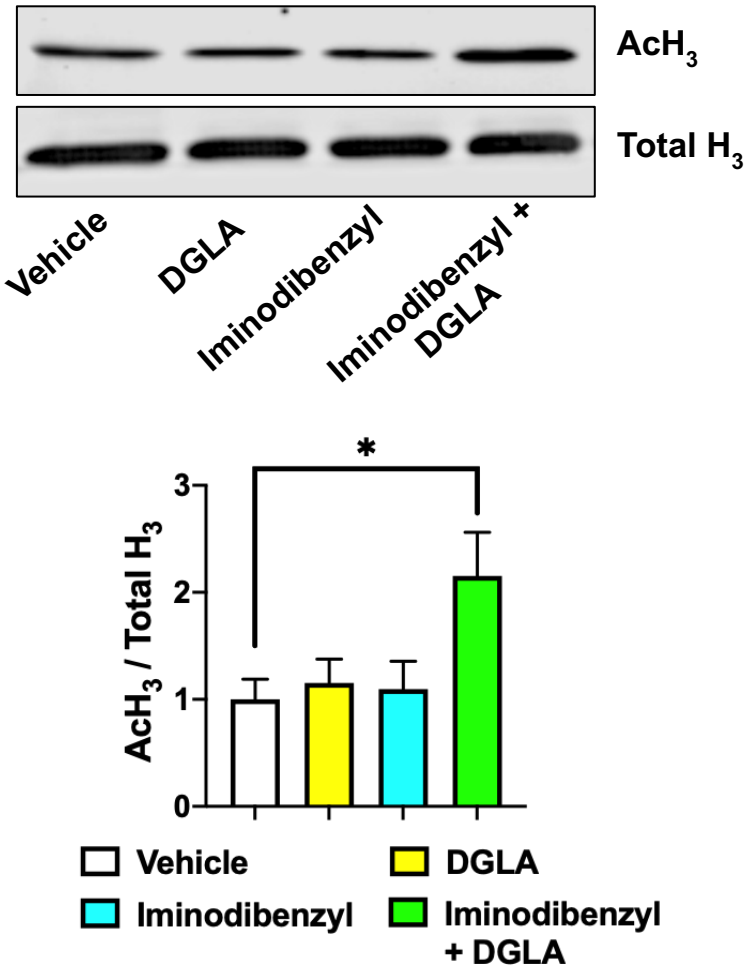

Figure 22. Combination treatment upregulated histone acetylation in MDA-MB-231 cells. Western blot analysis and densitometry analysis of AcH_3 and Total H_3 in MDA-MB-231 breast cancer cells treated with Iminodibenzyl, DGLA, and a combination of Iminodibenzyl and DGLA for 48 hours. The protein expression level in the vehicle was normalized to 1, β-Actin serves as a loading control. Data is represented as mean ± SEM with at least three separate experiments. *$P<0.05$ *vs.* Vehicle.

4.4. Iminodibenzyl diverted DGLA metabolism resulted in reduction in lamellipodia and filopodia

Cell migration is a highly controlled process involving many proteins, which regulate fundamental process of cell movement[97]. It is a dynamic and multistep process of protrusion of the cell membrane, formation of new focal adhesions, tractional forces to move, and retraction and detachment[98]. Focal adhesion (FA) dynamics (assembly and disassembly of FA) is an incessant

process encompassing synchronization between FA and actin cytoskeleton (F-Actin) leading to cell migration[99]. The regulation of attachment between F-actin and integrins via other proteins within FAs is essential for regulating cell protrusion and retraction. Additionally, multiple findings available depicting the role of FA kinase (FAK) as a prime regulator of signaling pathways causing cancer pathogenesis[100]. FAK is a unique controller of FAs association and dissociation, which is a fundamental process for efficient uni/multidirectional cell movement[100,101] . Paxillin is another crucial cytoskeletal and scaffolding protein hired initially to budding FAs at cell front and is obligatory for FA at cell front during cell migration[102]. Additionally, paxillin networks with vinculin at FAs permitting recruitment of F-actin, and other cytoskeletal-related proteins[103]. A recent report by Carisey et al., also provide concluding evidence that vinculin is also one of the important proteins controlling intra- and extracellular processes mandatory for reorganization of FAs to coordinate cell migration[104].

In chapter 3, it was observed that treatment with Iminodibenzyl and DGLA caused significant reduction in cancer cell migration. To explore the possible mechanism behind the observed therapeutic effect, F-Actin, Paxillin, Vinculin, and FAK analysis was done by immunofluorescent staining and Western blot.

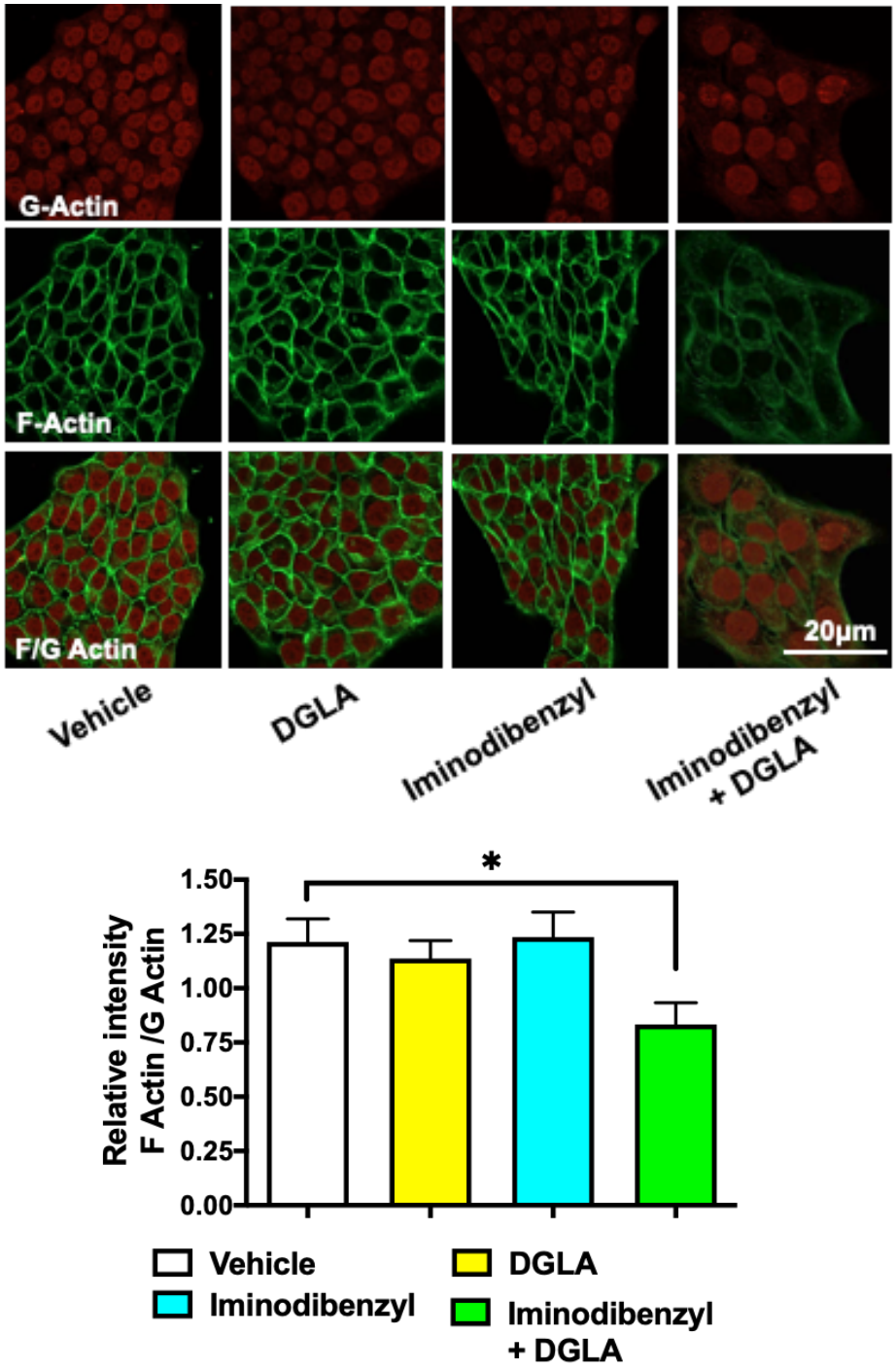

Figure 23. Concomitant treatment with Iminodibenzyl and DGLA reduced the F-Actin level in 4T1. Immunofluorescent and quantitative analysis of F-Actin and G-Actin after 48 hours of treatment with Iminodibenzyl and/or DGLA. Images were acquired from three separate experiments and data analysis was done by ImageJ software. *$P<0.05$ *vs.* Vehicle.

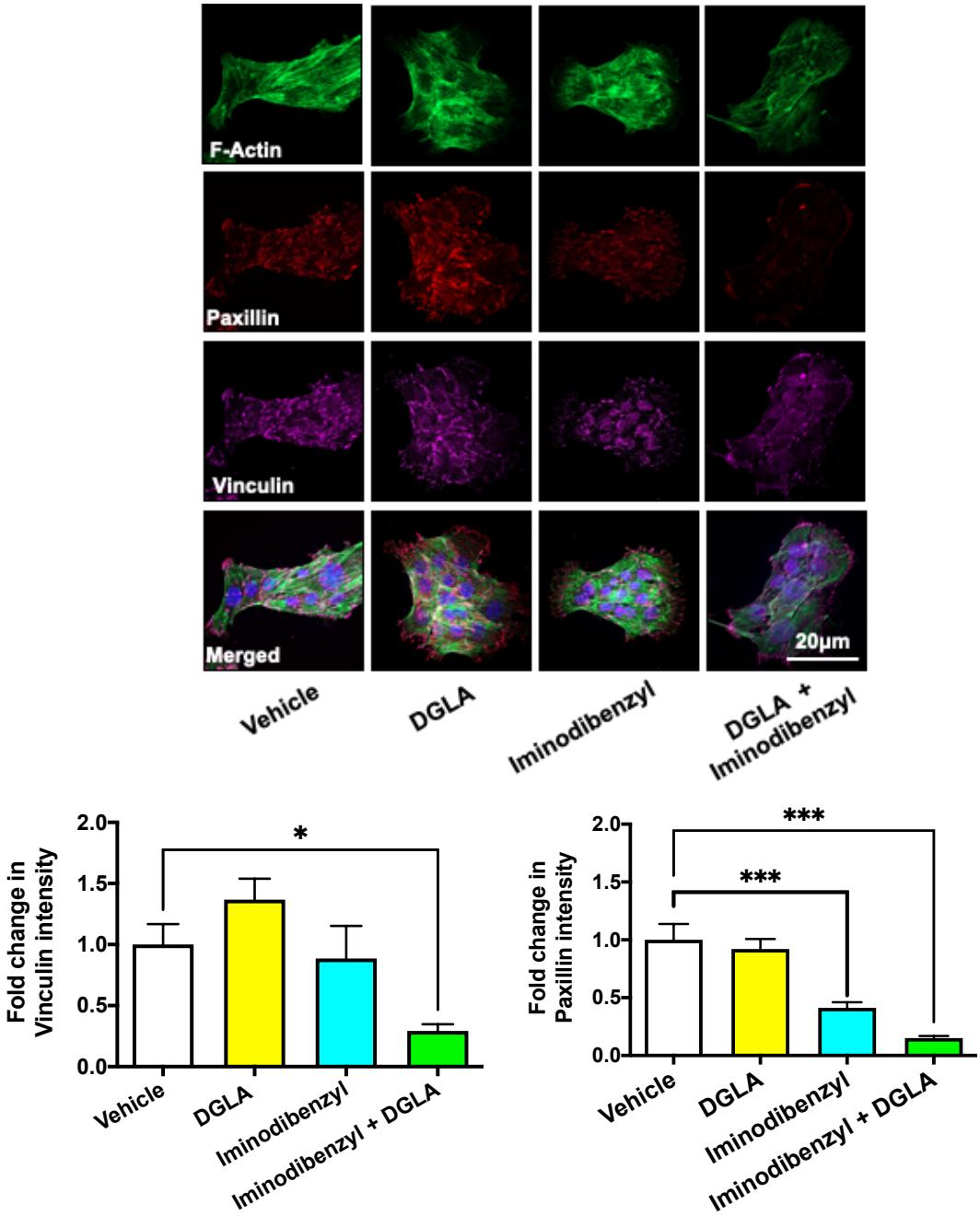

Figure 24. Combination treatment with Iminodibenzyl and DGLA reduced the paxillin and Vinculin in 4T1. Immunofluorescent and quantitative analysis of Paxillin and Vinculin after 48 hours of treatment with Iminodibenzyl and/or DGLA. After treatment, the cells were blocked, permeabilized, and stained with primary antibodies of Paxillin and Vinculin followed by corresponding secondary antibodies. The F-Actin was stained by Phalloidin Alexa 488, and nuclei were stained by using DAPI. Images were acquired from three separate experiments and data analysis was done by ImageJ software. ****P<0.001, *P<0.05 vs.* Vehicle.

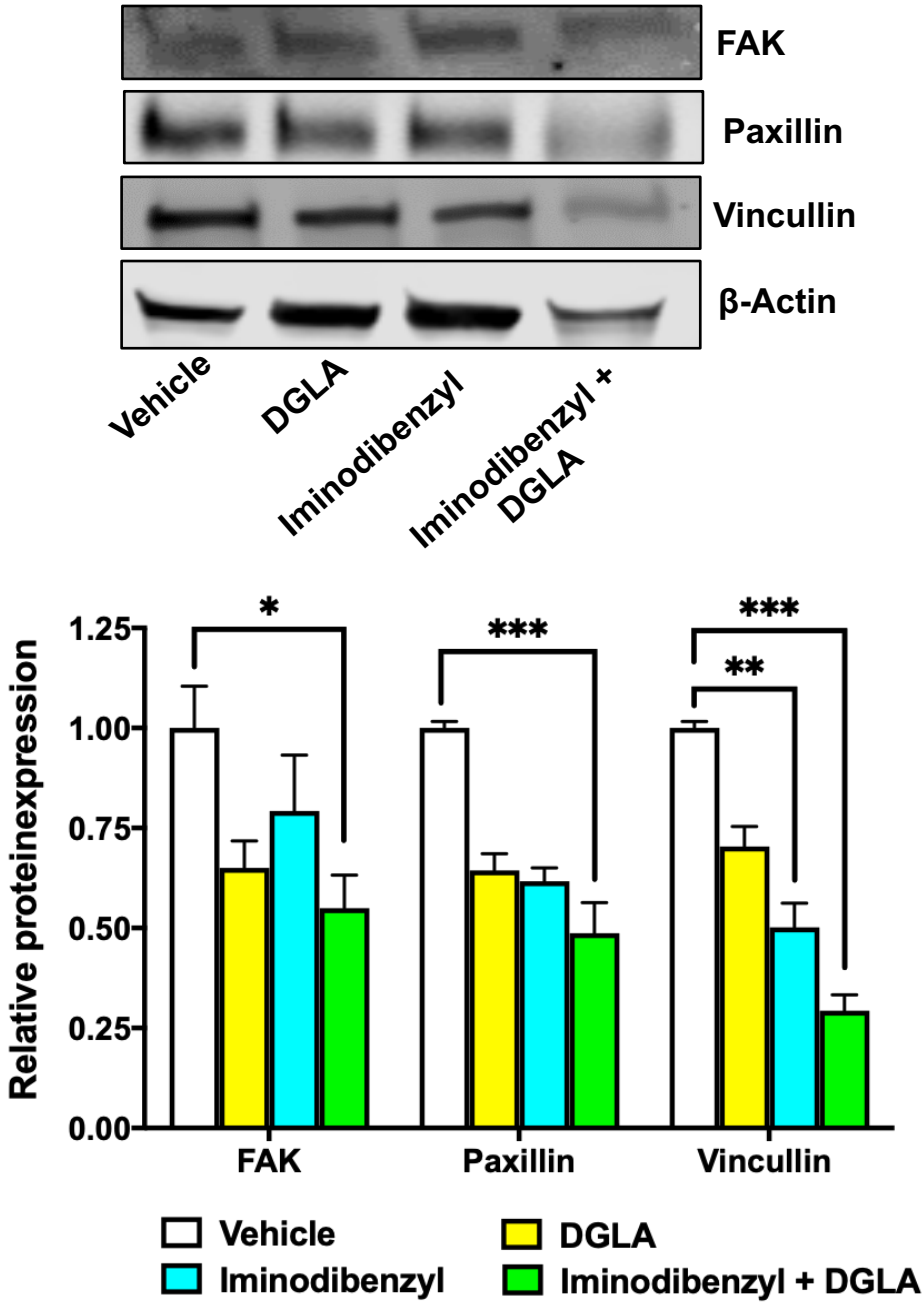

Figure 25. Combination treatment reduced the Lamellipodia and Filopodia in 4T1 cancer cells. Western blot analysis and densitometry analysis of FAK, Paxillin, and Vinculin in 4T1 breast cancer cells treated with Iminodibenzyl and/or DGLA for 48 hours. The protein expression level in the vehicle was normalized to 1, β-Actin serves as a loading control. Data represent mean ± SEM with at least three separate experiments. ****P<0.001, **P<0.01, and *P<0.05 vs.* Vehicle.

On performing immunofluorescent staining to analyze F-Actin, we observed significant reduction in F-Actin level on treatment with Iminodibenzyl and DGLA in 4T1 cancer cells (Figure

23, *P<0.05*). Additionally, when Paxillin and Vinculin levels were analyzed by immunocytochemistry study, a significantly reduced Paxillin and Vinculin level were found (Figure 24, For vinculin *P<0.05* and for paxillin *P<0.001*). The immunofluorescent findings of Paxillin and Vinculin were further confirmed by Western blot analysis, which also showed significantly reduced Paxillin and Vinculin level in 4T1 breast cancer cells on providing Iminodibenzyl and DGLA as a treatment (Figure 25, *P<0.001*). Additionally, concomitant treatment with Iminodibenzyl and DGLA also produced significant reductions in FAK (Figure 25, *P<0.05*). Notably, both Immunofluorescent and Western blot analysis showed reduced Paxillin (Figure 24, *P<0.001*) and Vinculin (Figure 25, *P<0.01*) with Iminodibenzyl treatment. The observed reduced cell migration maker after Iminodibenzyl treatment have been observed before by other research groups after using Imipramine (Structurally similar analog), which is due to the inherent nature of the compound to affect FAK phosphorylation[105].

4.5. Concomitant treatment with Iminodibenzyl and DGLA reduced MMP activity

During breast cancer progression EMT is another important phenomenon occurring, causing cancer cells to migrate to distant lymph nodes to form metastatic nodules. During EMT many molecular changes occur, out of which release of MMPs in the extracellular environment and adaptation of the mesenchymal phenotype are few of them. MMPs are a group differentially expressed zinc dependent endopeptidases that can destroy the basement membrane and promote cell invasion to systemic circulation and metastasis[106]. For a metastatic growth, cancer cells must cross the basement membranes and transverse to the distant lymph nodes after entry into and exit from the blood stream. The collagen IV, primary component of basement membrane, is degraded mostly by collagenase MMPs such as MMP-2 and MMP-9. These MMPs may therefore play a critical role in the conversion of in situ breast cancers to invasive lesions[107]. To analyze the effect

of treatments, gelatin gel zymography was performed. Here, the cells were treated with Vehicle, DGLA, Iminodibenzyl, and Iminodibenzyl and DGLA for 48 hours. After 48 hours of treatment, the growth media were collected and concentrated followed by protein concentration was measured, gelatin gel zymography was performed. After performing the zymography MMP-2 and MMP-9 activity was analyzed. On analyzing the gelatinase activity, it was found that simultaneous treatment with Iminodibenzyl and DGLA caused significant reduction in the MMP-2 (Figure 26, $P<0.05$) and MMP-9 (Figure 26, $P<0.01$) activity, while DGLA or Iminodibenzyl did not exert any effect on MMPs activity.

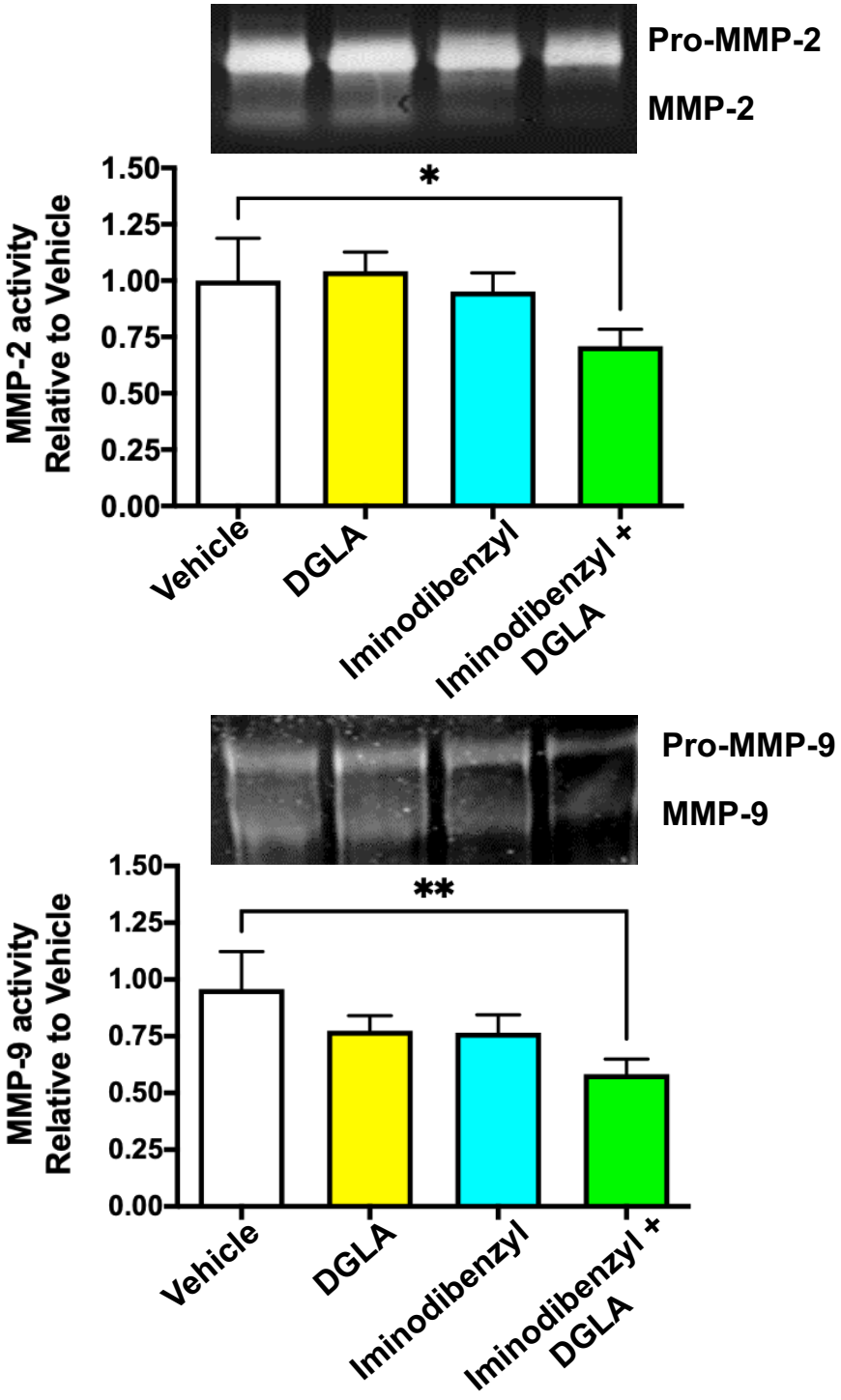

Figure 26. Gelatin zymography to detect the effect of combination treatment on MMP activity. Gelatin gel zymography was performed after concentrating the conditioned growth media of the treated cells. The samples were loaded and the modulatory effect of various treatments on MMP-2 and MMP-9 activity was determined. Images were acquired by using Licor Odyssey. The activity level in the Vehicle treated group was normalized to 1. Data represent mean ± SEM with at least three separate experiments. ***P<0.01, *P<0.05 vs.* Vehicle.

4.6. Concurrent treatment with Iminodibenzyl and DGLA modulated EMT protein markers

EMT is a very complex process by which epithelial cells lose the adherent and tight intercellular junctions keeping them in a cluster and adapt mesenchymal properties responsible for increased motility, crossing the basal membrane enabling them to enter systemic circulation to migrate to distance causing breast tumor progression and metastasis[108]. However, when 4T1 breast cancer cells were provided treatment with Iminodibenzyl and DGLA, significant reduction in mesenchymal markers Snail and MMP-2 was observed (Figure 27, $P<0.001$ (for snail) and $P<0.01$ (for MMP-2)). Additionally, combination treatment also caused significant upregulation of E-Cadherin level (Figure 27, $P<0.001$), which allow the cells to remain in cluster. Interestingly, we did not observe any effect on vimentin level (Figure 27).

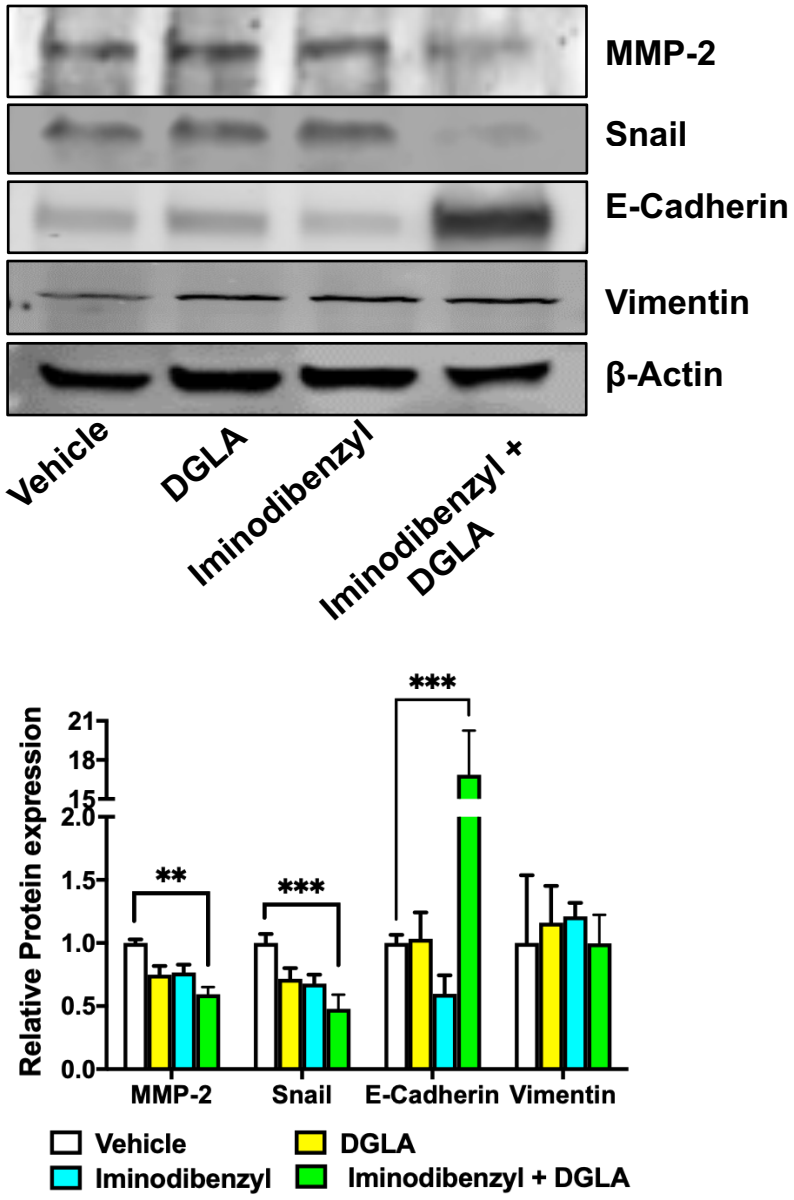

Figure 27. EMT marker level analysis from 4T1 cells provided simultaneous treatment with Iminodibenzyl and DGLA. Western blot analysis and densitometry analysis of MMP-2, Snail, E-Cadherin, and Vimentin in 4T1 breast cancer cells treated with Iminodibenzyl and/or DGLA for 48 hours. The protein expression level in the Vehicle was normalized to 1, β-Actin serves as a loading control. Data represent as a mean ± SEM with at least three separate experiments. ****P<0.001, **P<0.01 vs.* Vehicle.

4.7. Treatment with Iminodibenzyl and DGLA reduced the β-Catenin level in breast cancer cells

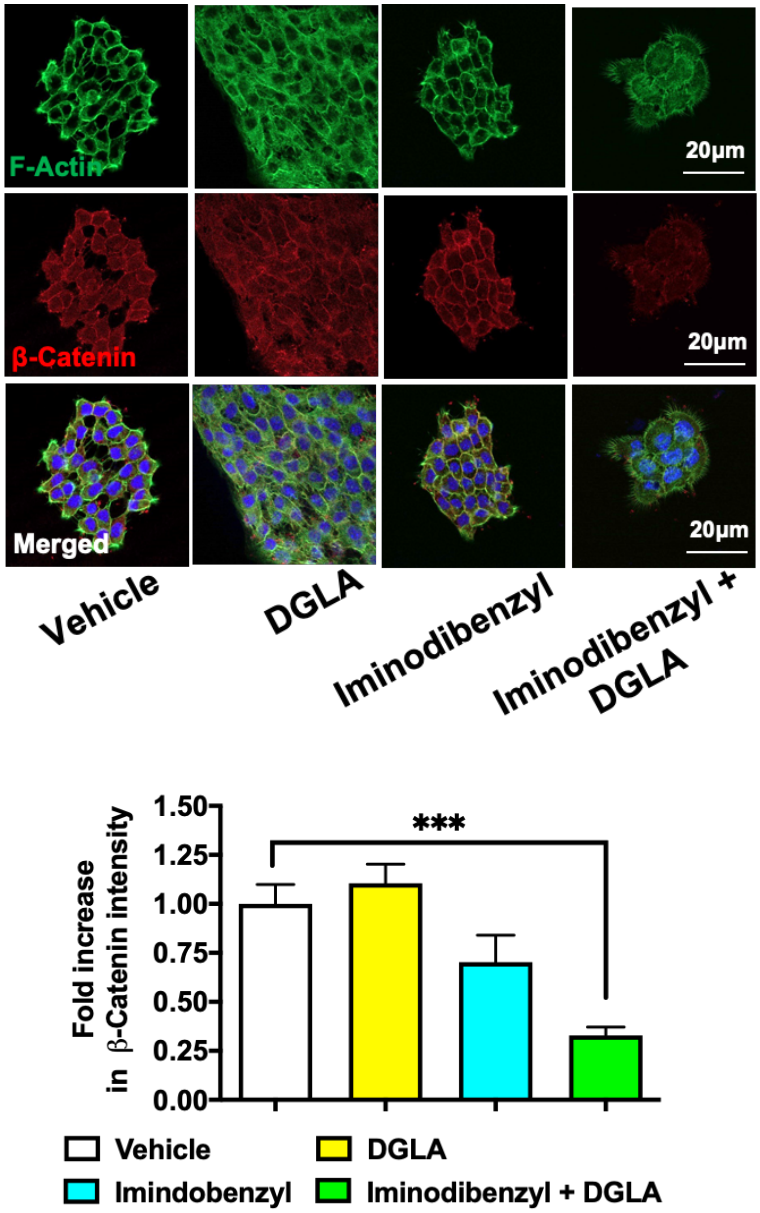

Figure 28. Treatment with Iminodibenzyl and DGLA reduced the β-Catenin in breast cancer cells. Immunofluorescent and quantitative analysis of β-Catenin after 48 hours of treatment with Iminodibenzyl and/or DGLA. The cells were stained with primary β-Catenin and corresponding secondary antibody. The F-Actin was stained by Phalloidin Alexa 488, and nuclei were stained by using DAPI. Images were acquired from three separate experiments and data analysis was done by ImageJ software. ****P<0.001, vs.* Vehicle.

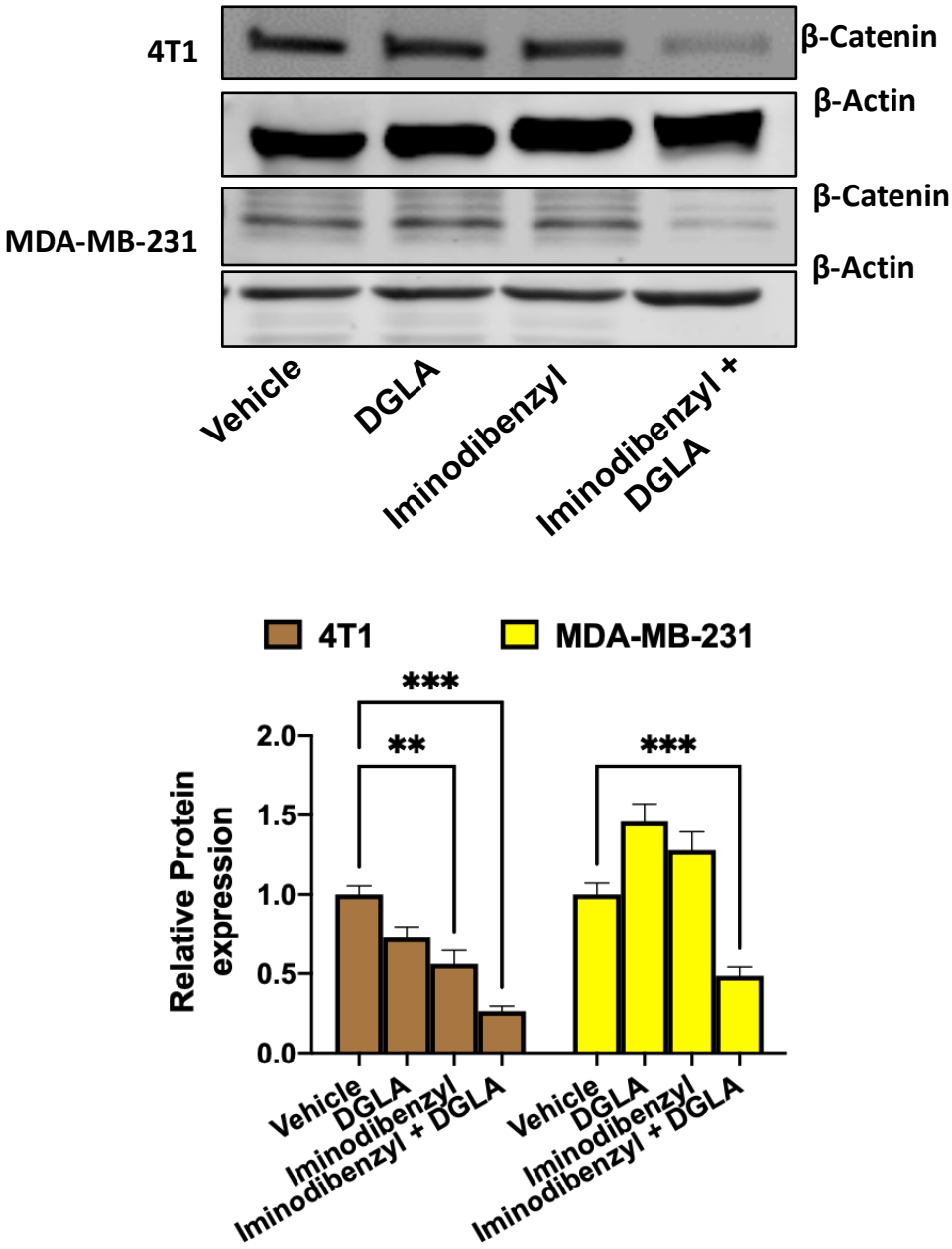

Figure 29. Concurrent treatment with Iminodibenzyl and DGLA reduced the β-Catenin level in 4T1 and MDA-MB-231cancer cells. Western blot analysis and densitometry analysis of β-Catenin in breast cancer cells treated with Iminodibenzyl and/or DGLA for 48 hours. The protein expression level in the vehicle was normalized to 1, β-Actin serves as a loading control. Data represent mean ± SEM with at least three separate experiments. ****P<0.001, **P<0.01 vs.* Vehicle.

β-catenin is a vital protein in several signaling pathways. It interacts with E-cadherin (critical regulator of intercellular adhesion) in plasma membrane[109]. The subcellular distribution

of β-catenin greatly affects the phenotype and behavior of the breast cancer cells[109]. In one of the study, aberrant expression of β-catenin 64.5% of the clinical breast cancer samples[110]. Accumulation of cytoplasmic β-catenin is a malignant marker for breast cancer. In malignant condition, it is translocated to the nucleus where it modulates various transcriptional factors to activate downstream target genes associated with increased growth and invasion[110]. By considering the importance of β-catenin, we performed fluorescent and relative protein expression analysis to detect the β-catenin level after treatment with Iminodibenzyl and / or DGLA. On analysis we found that, when 4T1 and MDA-MB-231 cells were treated with concurrent Iminodibenzyl and DGLA, significant reduction in β-catenin protein fluorescence intensity (Figure 28, $P<0.001$) and protein expression via Western was observed (Figure 29, $P<0.001$). Interestingly, we also observed notable reduction in protein expression when Iminodibenzyl was provided as a treatment in 4T1 cells (Figure 29, $P<0.01$).

4.8. Limitations

D5D enzyme is located on endoplasmic reticulum[111] of the cell and we think that majority of the therapeutic mechanisms of actions responsible for anti-cancer effect are occurring in the cytoplasmic area of the cell. However, we have not validated the exact location of therapeutic action, which we will explore in our future studies. There are multiple mechanisms responsible for induction of EMT in breast cancer cells including treatment with tissue growth factor- β (TGF-β). From our attempt, we successfully noted conversion of MCF-7 epithelial phenotype to mesenchymal phenotype accompanied by reduction in E-cadherin level. However, TGF-β treatment was not able to stimulate COX-2 level, a mandatory factor required to produce anti-cancer effect, in the less invasive MCF-7 breast cancer cells. Hence, we concluded that TGF-β induced model is not suitable to study EMT in our strategy.

Wnt controlled β-catenin undergo degradation after amino terminal serine/threonine phosphorylation by glycogen synthase kinase-3 (GSK-3) in conjunction with tumor dampening protein Axin and adenomatous polyposis coli (APC)[112]. Here, we have determined modulation in β-catenin level after various treatment through immunofluorescent and Western analysis, however the possible role of GSK-3, Axin, and APC is still unexplored.

4.9. Conclusion and discussion

As per the finding from Yu et al., administration of DGLA in D5D-KD breast cancer cells (4T1 and MDA-MB-231), cause generation of 8-HOA. The produced 8-HOA caused increase in apoptotic cells by activating caspase dependent pathway. Additionally, the unique metabolite product 8-HOA also reduced the cancer cell migration and invasion by reducing EMT markers[56]. In Chapter 3, we have found that administration of Iminodibenzyl diverted the DGLA metabolism from pro-tumorigenic pathway to anti-cancer pathway by producing significantly high level of 8-HOA in cancer cells. The produced 8-HOA from Iminodibenzyl and DGLA led to increased percentage apoptosis, and reduced breast cancer cell survival. However, the molecular mechanism behind the observed therapeutic end effect was still unexplored. Elucidation of the molecular mechanism assists in designing a new combination therapeutic strategy targeting different therapeutic pathways for better therapeutic outcome. In this chapter, we have used immunofluorescent and Western approach, and biochemical assays to explore the caspase dependent death mechanism and EMT markers.

During apoptosis, the intrinsic death pathway regulated by BCl_2 is evoked, which activates the caspase cascade initiator procaspase-9 followed by procaspase-3. The activated procaspase-3 then fragmented to cleaved caspase-3 to induce apoptosis[113-115]. The combination treatment of Iminodibenzyl and DGLA activated the intrinsic apoptosis death mechanism in *in vitro*, which is

also confirmed using pan-caspase inhibitor Z-VAD-FMK. Abnormal histone acetylation has an essential role in tumor development by epigenetically inhibiting the tumor suppressor genes, and hence histone deacetylase inhibition has become the ideal target for cancer therapeutics[116]. HDAC inhibitors exhibit their anti-cancer activity by stimulating acetylation of core histone protein, which impacts gene transcription resulting in apoptosis and degradation of misfolded proteins[116]. Iminodibenzyl administration redirected the DGLA metabolism to 8-HOA, which also exerted a significant reduction in HDAC activity[93]. The reduced HDAC activity linked with upregulation of AcH_3, which could activate the intrinsic apoptosis pathway to achieve tumor cell apoptosis and reduced cell proliferation.

During metastasis, the tumor cell migrates through the extracellular matrix (ECM) for intravasation into lymphatic and blood vessels. This is achieved by various types of movement like chemoattractant mediated chemotaxis and environmental gradient mediated haptotaxis[117]. Chemotaxis is one of the mechanisms through which cancer cells migrate. Cancer cell migration is a complex mechanism that necessitates coordination between specific cellular processes such as aggregation and dispersal of focal adhesions (FAs), polymerization of the actin filament, etc.[118]. The FA formation is commenced by the interaction of integrins with corresponding ligands followed by recruitment of various proteins such as focal adhesion kinase (FAK), vinculin, and paxillin[119]. Additionally, actin filament, specifically F-actin is also involved in processes like filopodia, lamellipodia, and invadopodia, which help cancer cells to move and invade distant sites to colonize[119]. Reduced FAK, paxillin, and vinculin levels supported the findings of reduced filopodia and lamellipodia in 4T1 breast cancer cells, which might have resulted in reduced cancer cell migration as visible from large wound size in wound healing assay. During cancer metastasis, EMT is an important complex phenomenon leading to metastatic nodule formation at the distant

site. It is mediated by intricate crosstalk between tumor cells and adjacent stroma and cannot be fully simulated *in vitro*[120]. Breast tumor cells excrete zinc-dependent proteases such as MMP-2 and MMP-9, which damage an integral part of the basal membrane, type IV collagen, resulting in cancer cells' entry into the systemic circulation. Iminodibenzyl along with DGLA administration caused a differential reduction in MMP-9 and MMP-2 activity and expression inferring reduced ability to invade, indicating a possible independent effect on MMPs expression and activity. Furthermore, increased E-Cadherin, a single-span transmembrane protein essential for tight inter-epithelial cell connections, was showing improved protection against metastasis ability of the 4T1 and MDA-MB-231 cancer cells. Snail and Vimentin are other markers responsible for tumor recurrence and tumor cell metastasis[121], which was found to be significantly reduced with the Iminodibenzyl and DGLA combination treatment.

Several studies have demonstrated the relation between the canonical Wnt/β-catenin pathway and upregulated proliferation, survival, and metastasis by modulating the intrinsic apoptosis pathway and EMT in breast cancer[122-126]. β-catenin is an appealing target due to its ability to abolish cancer relapse[127]. From *in vitro* analysis, we have perceived that Iminodibenzyl and DGLA combination caused downregulation of β-catenin, which could be another possible mechanism leading to breast cancer cell apoptosis and reduced cell proliferation. The downregulated β-catenin also has an inhibitory role in EMT markers.

In summary, when combination of Iminodibenzyl and DGLA was provided as a treatment to 4T1 and MDA-MB-231 cancer cells, activation of caspase dependent death pathway was activated, evident from cleaved caspase-3, which was validated by recuperated apoptosis after Z-VAD-FMK pretreatment. Additionally, combination treatment also reduced the HDAC activity, which might be one of the mechanism responsible for anti-cancer effect. After acute administration

of Iminodibenzyl and DGLA, reduction in FA protein markers and EMT markers were observed, which might have caused a reduction in cancer cell migration.

5. DETERMINATION OF *IN VIVO* EFFECT OF IMINODIBENZYL AND DGLA SUPPLEMENTATION ON BREAST CANCER GROWTH IN FEMALE NU/J MICE

In chapter 3 and 4, it was observed that Iminodibenzyl diverted the DGLA metabolism from cancer promoting pathway (DGLA/AA/PGE_2) to cancer inhibiting (DGLA/8-HOA) pathway resulting in increased apoptosis, and reduced breast cancer cell proliferation and migration by modulation of various molecular pathways. However, the *in vitro* system cannot completely mimic the complex in clinic physiological environment and hence validation is required in *in vivo* system. To determine *in vivo* cancer growth inhibitory effect, an orthotopic tumor model using immune-deficient female nude mice, commonly used model for breast cancer research, was used.

In this model, 4T1 TNBC cell line was used to develop the breast cancer model. 4T1 cell line induced orthotopic breast cancer model is widely used model offering multiple advantages over other breast cancer cell lines; significant molecular similarities with human TNBC[128], cancer cells upon implanting likely to form metastatic nodules in 7-10 days from the day of implantation etc[57,73-76,129]. The protocol to conduct in vivo study was prior approved by IACUC (Protocol number A17065). The orthotopic model was developed by using immune deficient nude mouse. The immune-deficient mice (J:Nu, 002019, The Jackson Lab) are homozygous for the *Foxn1^{nu}* mutation, which makes the mice nude (hairless) and athymic. The lack of thymus in these mice blocks the differentiation and maturation of T cells, resulting in an immunodeficiency which allowed implantation of tumor cell xenografts. After receiving the animals from the Jackson lab, they were acclimatized for two weeks with unlimited food and water ad libitum. After two weeks of acclimatization, 0.25 x 10^6 mycoplasma free 4T1 cells were inoculated in 4th mammary fat pad of the mouse by 20-gauge syringe and housed for another week for tumor to grow[57]. After one week, the animals were randomized in four treatment groups; Vehicle, DGLA (5mg/mouse, p.o.),

Iminodibenzyl (20mg/kg, i.p.), and combination of Iminodibenzyl (20mg/kg, i.p.) and DGLA (5mg/mouse, p.o.). During the study period, animals were treated daily, and the tumor volume (by using a digital vernier caliper) and body weight (using a weighing balance) was measured every three days. At the end of the study period, animals were euthanized, and blood, organs, and tumors were collected for post analysis (Scheme 4 in 2.15.). The samples were used for fatty acid, free radical metabolite, pharmacokinetics, immunohistochemistry, and relative protein expression analysis.

5.1. Anti-cancer effect exerted by combination of Iminodibenzyl and DGLA

After one week of tumor cell implantation, the animals were randomized in four different groups and provided different treatment. In group A, animals were provided Vehicle as a treatment. In group B, DGLA (5mg) was provided as a treatment through oral gavage. In group C, Iminodibenzyl (20mg/kg) was provided as a treatment through i.p. route and in group D, combination of Iminodibenzyl (20mg/kg) through i.p. route and DGLA through oral gavage provided as a daily treatment. During the study period, animal weight and tumor volume was measured periodically to analyze fold change in tumor size with different treatment. From the tumor volume measurement and visual inspection of the tumors at the end of the study, we noticed a significant decline in tumor volume in the group of animals receiving a combination of Iminodibenzyl (20mg/kg) and DGLA (5mg) as a treatment (Figure 30, $P<0.01$ and Figure 31), while animals in Vehicle and DGLA treatment groups did not exert any significant effect on the tumor growth. It is important to note that animals in the Iminodibenzyl treatment group exhibited a moderate reduction in tumor volume (Figure 30). During the treatment period, we did not observe any significant change in animal weight (Figure 32). On providing Vehicle, DGLA, and Iminodibenzyl single agent treatment, the measured average fold change in tumor volume was

35.49 ± 7.34, 39.36 ± 6.37, and 18.82 ± 2.94, while the tumor volume in combination treatment provided group of animals was 9.55 ± 4.57 from the start of the treatment.

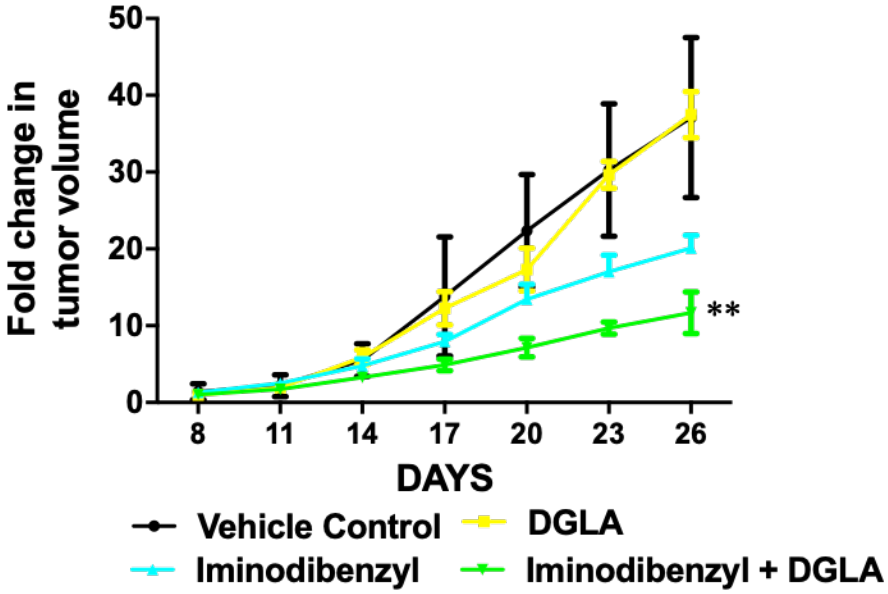

Figure 30. Fold change in tumor volume vs. days after different treatments. Tumor volume measured by using digital Vernier caliper. Tumor volume at day 8 is considered as one-fold and change in tumor volume was quantified based on that. Data is represented as a mean ± SEM from six animals (in each group). ***P<0.01 vs.* Vehicle at 26 days.

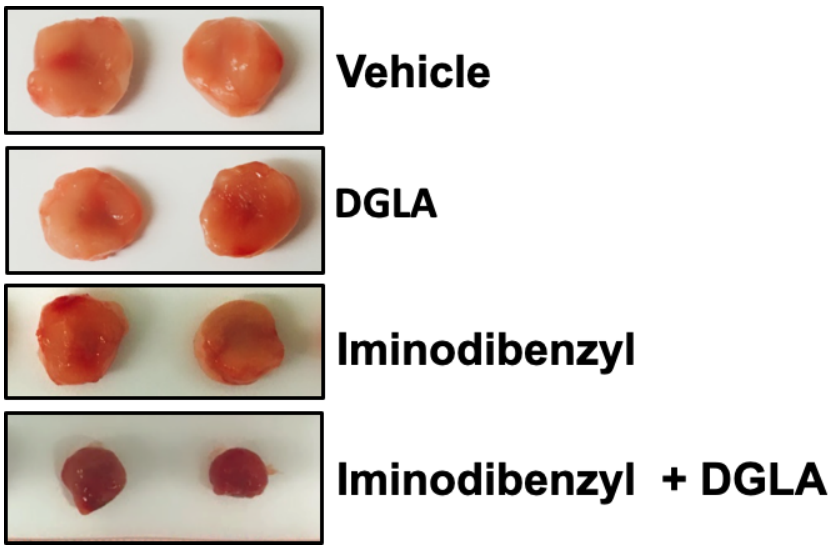

Figure 31. Representative images of the tumor from different treatment groups.

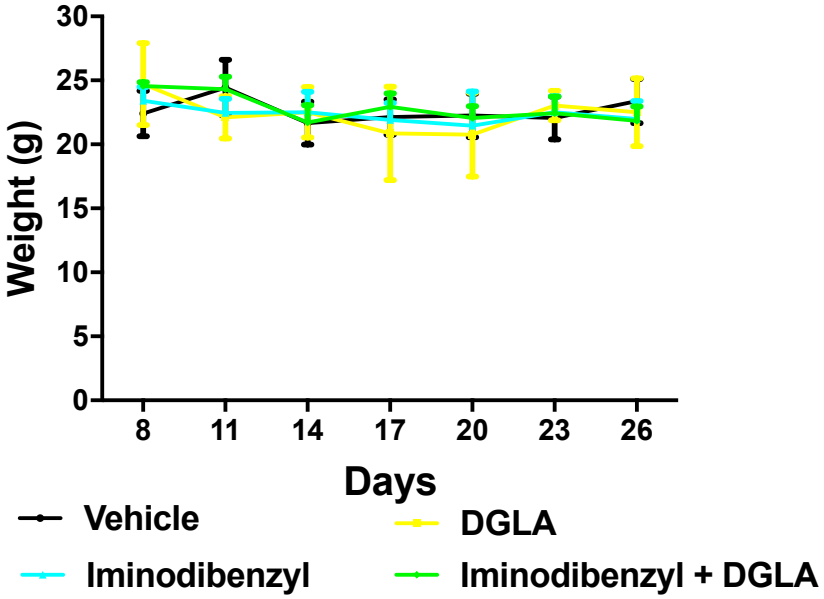

Figure 32. Change in animal weight (g) during the treatment period. During the animal dosing period the weight of the animals were captured periodically every three days by digital weighing balance. Data is represented as a mean ± SEM from six animals (in each group).

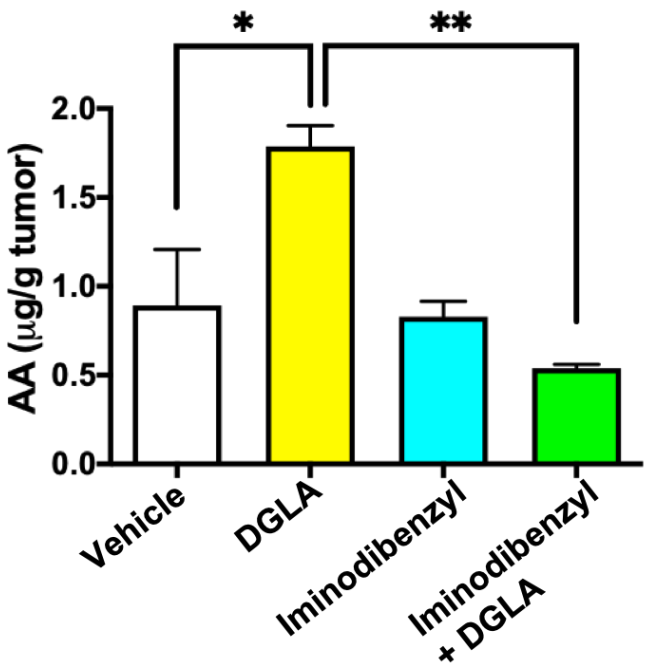

Figure 33. Fold change in AA from tumor samples by LC/MS. AA quantification from tumor samples harvested from animals provided different treatments. Data is represented as a mean ± SEM from three animals. *$P<0.05$ *vs.* Vehicle and **$P<0.01$ *vs.* DGLA.

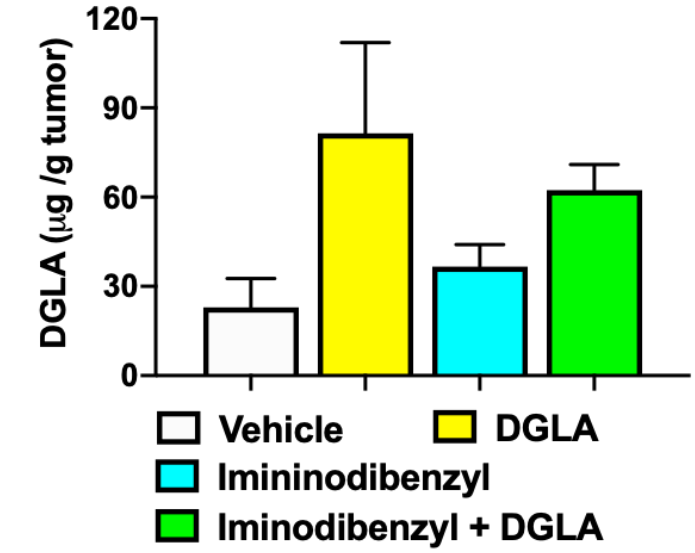

Figure 34. Quantification of DGLA (µg) from tumor samples (g) by LC/MS. DGLA were quantified from tumor samples by solid phase extraction followed by LC/MS approach. Data is represented as a mean ± SEM from three animals.

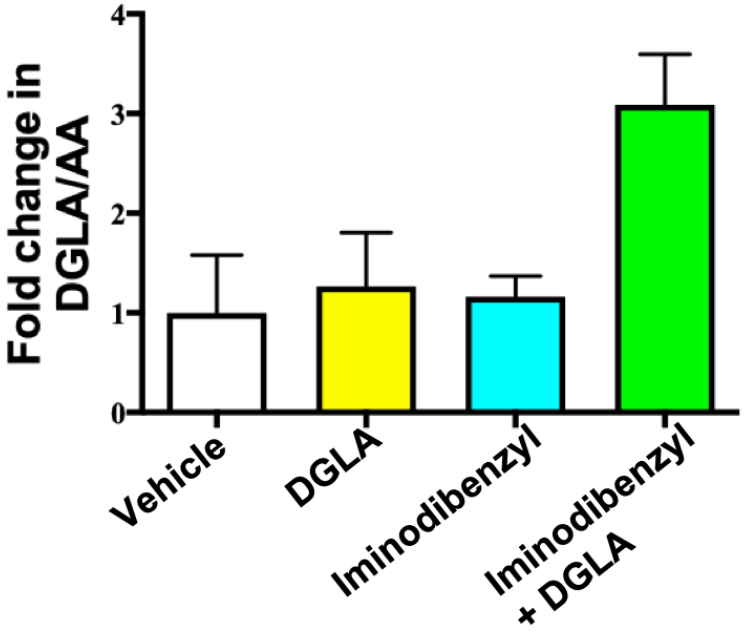

Figure 35. Fold change in DGLA/AA from tumor samples by LC/MS. DGLA and AA were quantified from tumor samples by LC/MS approach and then fold change in DGLA/AA was determined. Data is represented as a mean ± SEM from three animals.

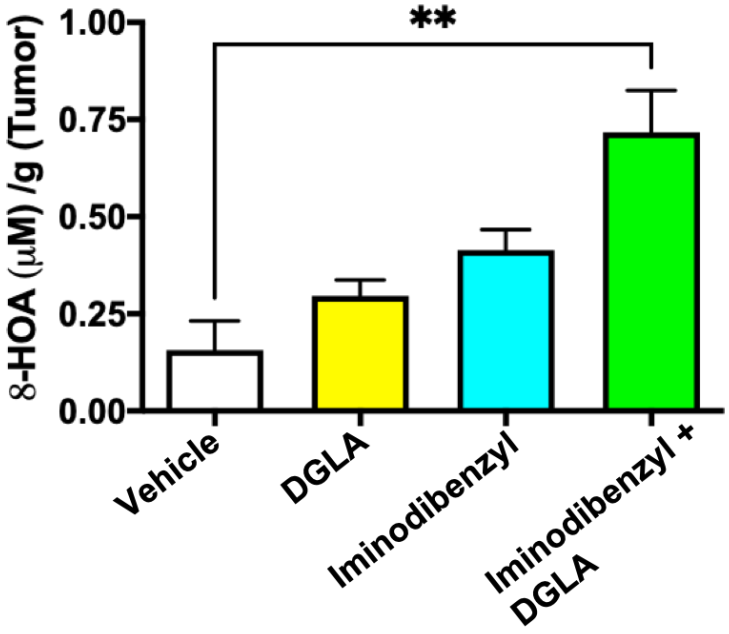

Figure 36. 8-HOA analysis from tumor samples. GC/MS analysis to quantify 8-HOA from tumor samples extracted from animals provided different treatments. Data is represented as mean ± SEM from three individual animals from each group. ***P<0.01 vs.* Vehicle.

Previously, we and others have observed that administration of DGLA in D5D KD cancer cells (by D5D shRNA or 3WJ-D5D siRNA nanoparticles) exhibit diversion of DGLA metabolism from DGLA/AA/PGE_2 to DGLA/8-HOA[51,57]. This was also evident by reduced AA and increased DGLA/AA level in tumors[56,57]. Additionally, in chapter 3 (Figure 4) and previously published findings also suggested that Iminodibenzyl also divert DGLA metabolism to 8-HOA. To analyze Iminodibenzyl stimulated COX-2 fueled DGLA metabolism *in vivo*, we performed liquid-liquid extraction of different tumor samples and did the derivatization reaction with PFB to form 8-HOA-PFB to quantify 8-HOA by GC/MS. On extrapolating the area into the standard curve, we found significantly high level of 8-HOA in animals provided combination of Iminodibenzyl and DGLA, whereas no significant change was observed in 8-HOA level in tumor samples harvested from animals provided DGLA or Iminodibenzyl (Figure 36, *P<0.01*). Additional, solid phase extraction of tumor samples followed by LC/MS analysis led us to know that animals from combination

treatment groups have significantly increased AA level (vs. vehicle). Contrary, animals administered Iminodibenzyl along with DGLA showed significantly reduced AA content (vs. DGLA treatment group), which could be due to the inhibited D5D activity by Iminodibenzyl causing diversion of DGLA metabolism (Figure 33, $P<0.01$). This finding was further supported by increased DGLA and DGLA/AA levels in animals provided DGLA alone or in combination (Figure 34 and 35).

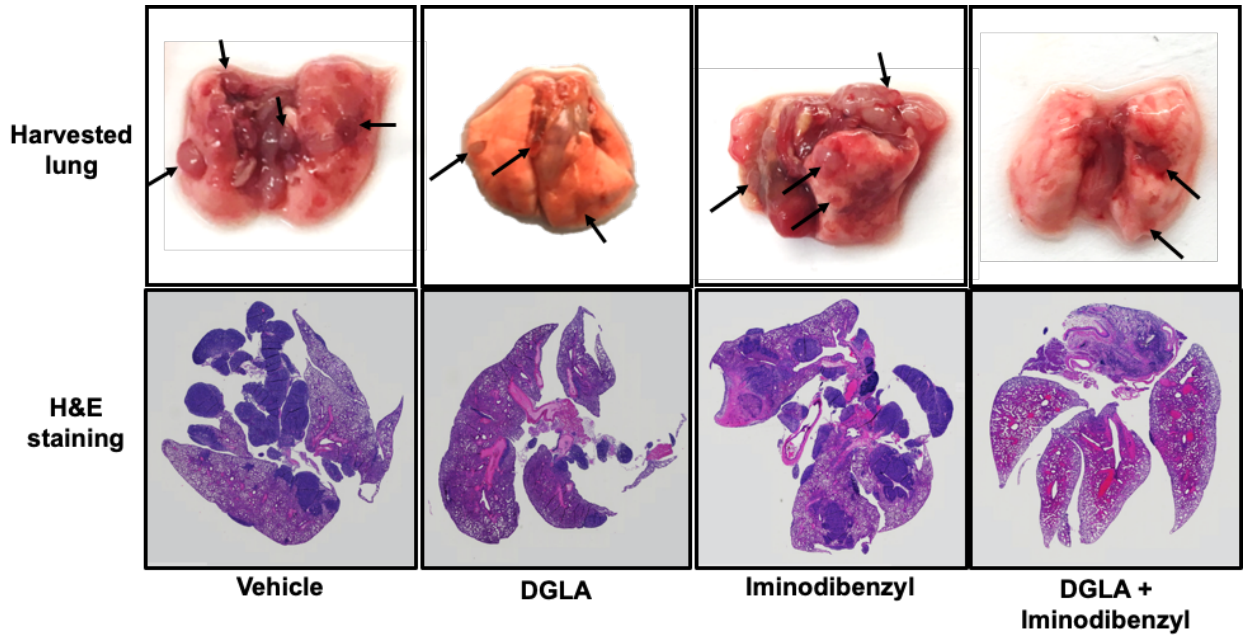

Figure 37. Qualitative and quantitative analysis of lung metastatic nodule from animals provided different treatments. The top panel show the 2D image of the lung with maximum nodules from respective treatment groups and the arrows show lung metastatic nodules. The bottom panel show the H&E staining image of the lung section from animals.

In our previous experiments, we have seen that 4T1 cells in orthotopic breast cancer model migrate to distant site and form metastatic nodules[57]. To analyze the effect of Iminodibenzyl mediated altered DGLA metabolism on metastatic nodules, we quantified the lung metastatic nodules by visually as well as through H&E staining. From visual inspection we detected significantly less number (n=6) of metastatic lung nodules in the group of animals that received

simultaneous treatment of Iminodibenzyl and DGLA compared to animals administered Vehicle (n=17), DGLA (n=9), or Iminodibenzyl (n=8) (Figure 37).

To elucidate the probable *in vivo* mechanism of action behind reduced tumor size and metastatic lung nodule, we analyzed the relative expression of different markers involved in apoptosis and EMT. Immunohistochemistry analysis showed a significant reduction in proliferative marker Ki-67 was found in tumor samples from animals provided combination treatment (Figure 38, $P<0.01$). C.PARP expression further showed a significant increase in fluorescent signal with concurrent treatment with Iminodibenzyl and DGLA (Figure 39, $P<0.01$). This finding was further supported by increased relative C. PARP expression (Fig. 40, $P<0.05$). Procaspase-3 and an anti-apoptotic protein BCl_2 analysis in tumors showed similar findings as that of *in vitro* analysis, which was a significant reduction in the procaspase-3 and BCl_2 protein levels in tumors harvested from the combination treatment of Iminodibenzyl and DGLA (Figure 40, $P<0.05$ and Figure 46, $P<0.01$). However, we did not see any significant changes in all these proteins in animals treated with Iminodibenzyl or DGLA. HDAC activity analysis of protein samples extracted from Iminodibenzyl and DGLA treated animals showed a significant reduction in HDAC activity (Figure 41, $P<0.01$). We also detected a notable reduction in HDAC activity in tumor samples obtained from animals treated with Iminodibenzyl alone with no significant changes in other treatment groups (Figure 41). D5D protein level analysis by Immunohistochemistry (Figure 42) showed no significant change in D5D protein levels with any of the provided treatments, which suggested no significant effect of any treatment on D5D level.

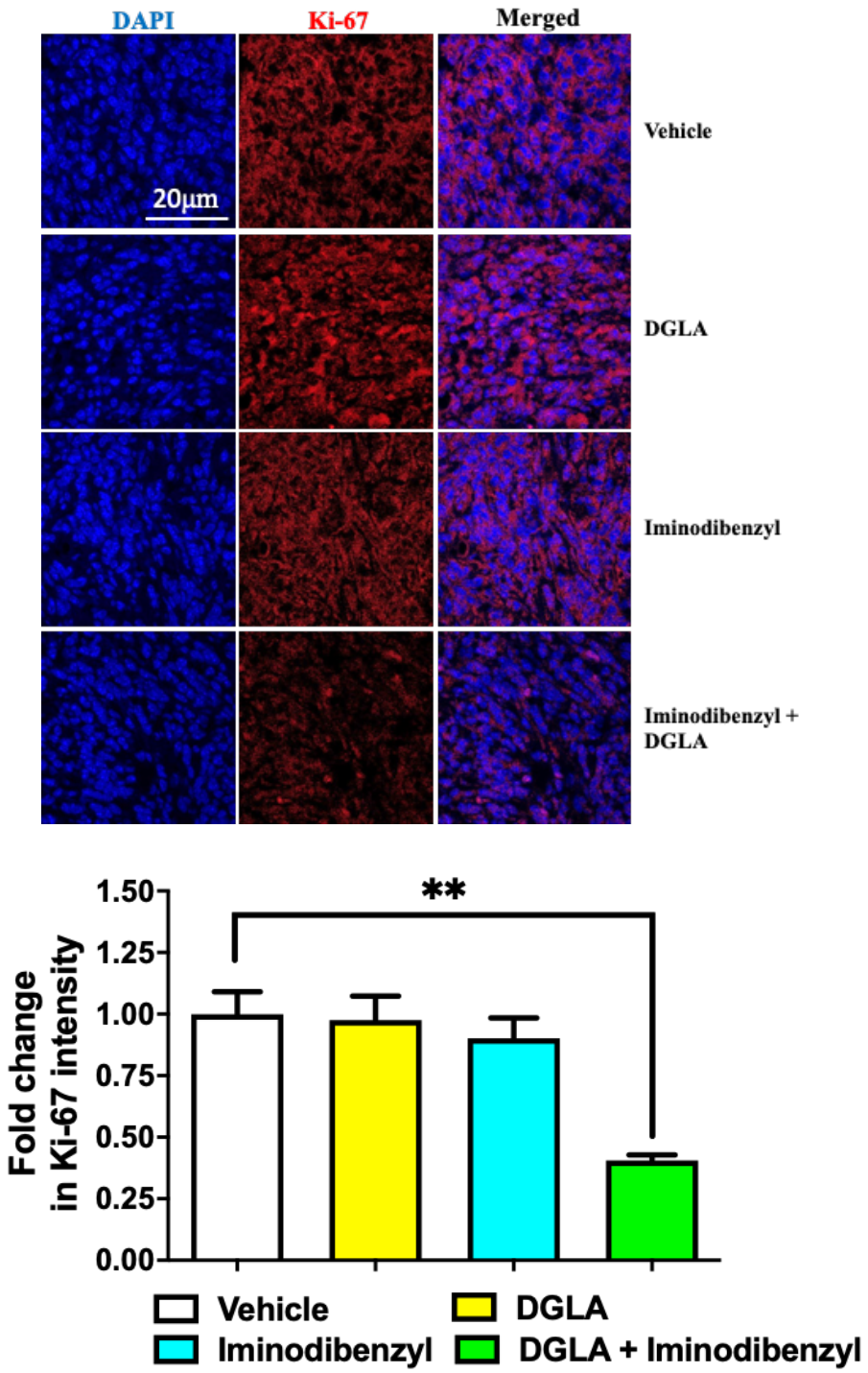

Figure 38. Qualitative and quantitative immunofluorescence analysis of proliferation marker Ki-67 protein expression in tumors. Representative images for Ki-67 expression in tumor tissues. Ki-67 was stained in red; cell nuclei were counter stained with DAPI in blue. Mean intensity of Ki-67 in each sample was quantified as an index of its expression level in tumor tissue. Data is represented as Mean ± SEM from three tumors. ***P<0.01 vs.* Vehicle.

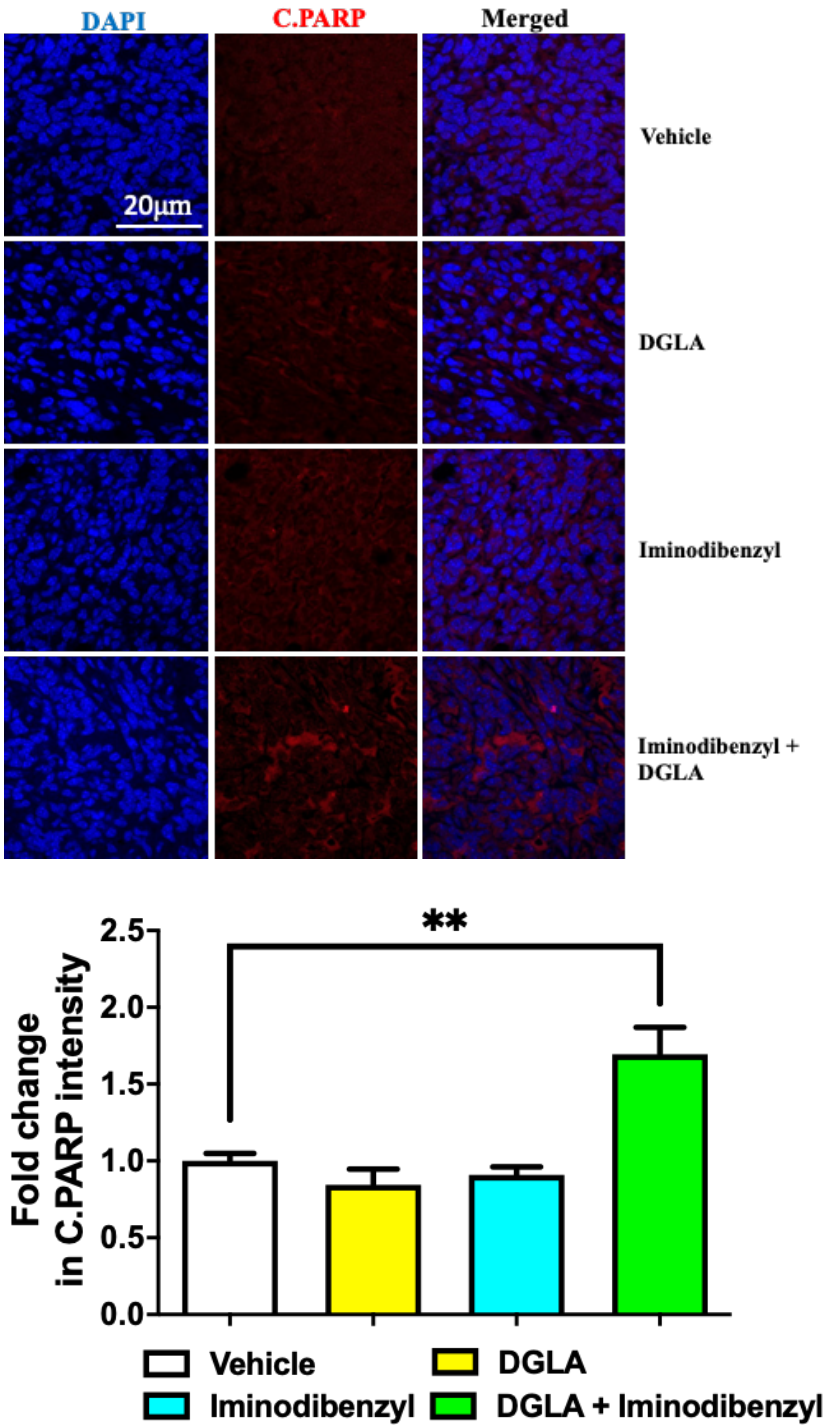

Figure 39. Qualitative and quantitative immunofluorescence analysis of apoptosis marker C. PARP protein expression in tumors. Representative images for C. PARP expression in tumor tissues. C. PARP was stained in red; cell nuclei were counter stained with DAPI in blue. Mean intensity of C. PARP in each sample was quantified as an index of its expression level in tumor tissue. Data is represented as Mean ± SEM from three tumors. ***P<0.01 vs.* Vehicle.

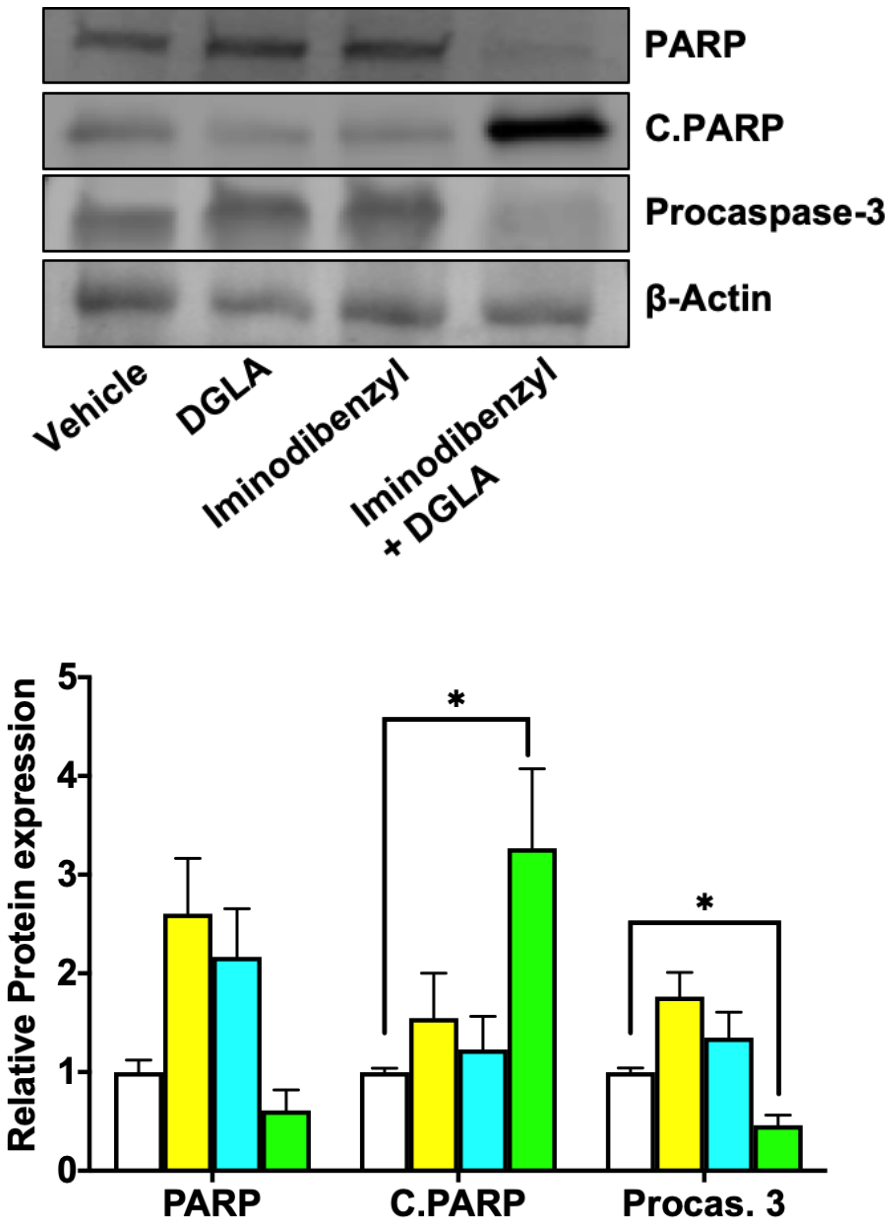

Figure 40. Apoptosis marker level analysis from tumor samples. Western blot analysis and densitometry analysis of PARP, C. PARP, and Procaspase-3 in breast tumor tissue harvested from nude mice provided different treatments. The protein expression level in the Vehicle was normalized to 1, β-Actin serves as a loading control. Data represent as a mean ± SEM with at least three separate experiments. *$P<0.05$ *vs.* Vehicle.

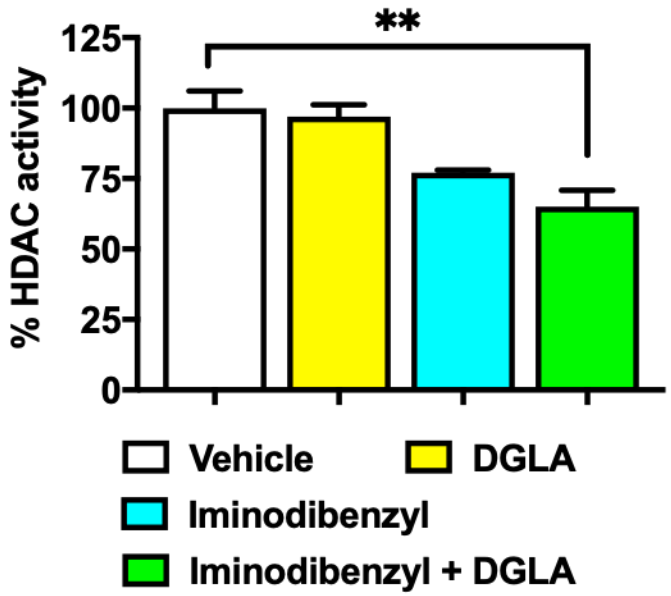

Figure 41. Percentage HDAC activity analysis in tumor samples. HDAC activity was performed from protein samples extracted from breast tumors harvested from different groups of animals. The activity was performed by using a standard HDAC colorimetry activity kit and HDAC activity in Vehicle group was considered as 100%. Data is represented as mean ± SEM. N=3, and ***P<0.01 vs.* Vehicle.

To elucidate the probable in *vivo* mechanism of action behind observed lung metastatic nodule, we analyzed the protein expression of various EMT markers. Immunohistochemistry analysis showed a significant increase in E-Cadherin (Figure 43, *P<0.001*), and reduction in MMP-2 (Figure 44, *P<0.01*) and Vimentin level (Figure 45, *P<0.01*) in tumor samples obtained from animals simultaneously administered Iminodibenzyl (20mg/kg) and DGLA (5mg). We did not find any significant change in any analyzed EMT markers (MMP-2, Vimentin, and E-Cadherin) in tumors extracted from animals treated with Vehicle, DGLA, or Iminodibenzyl alone (Figure 43, 44, and 45).

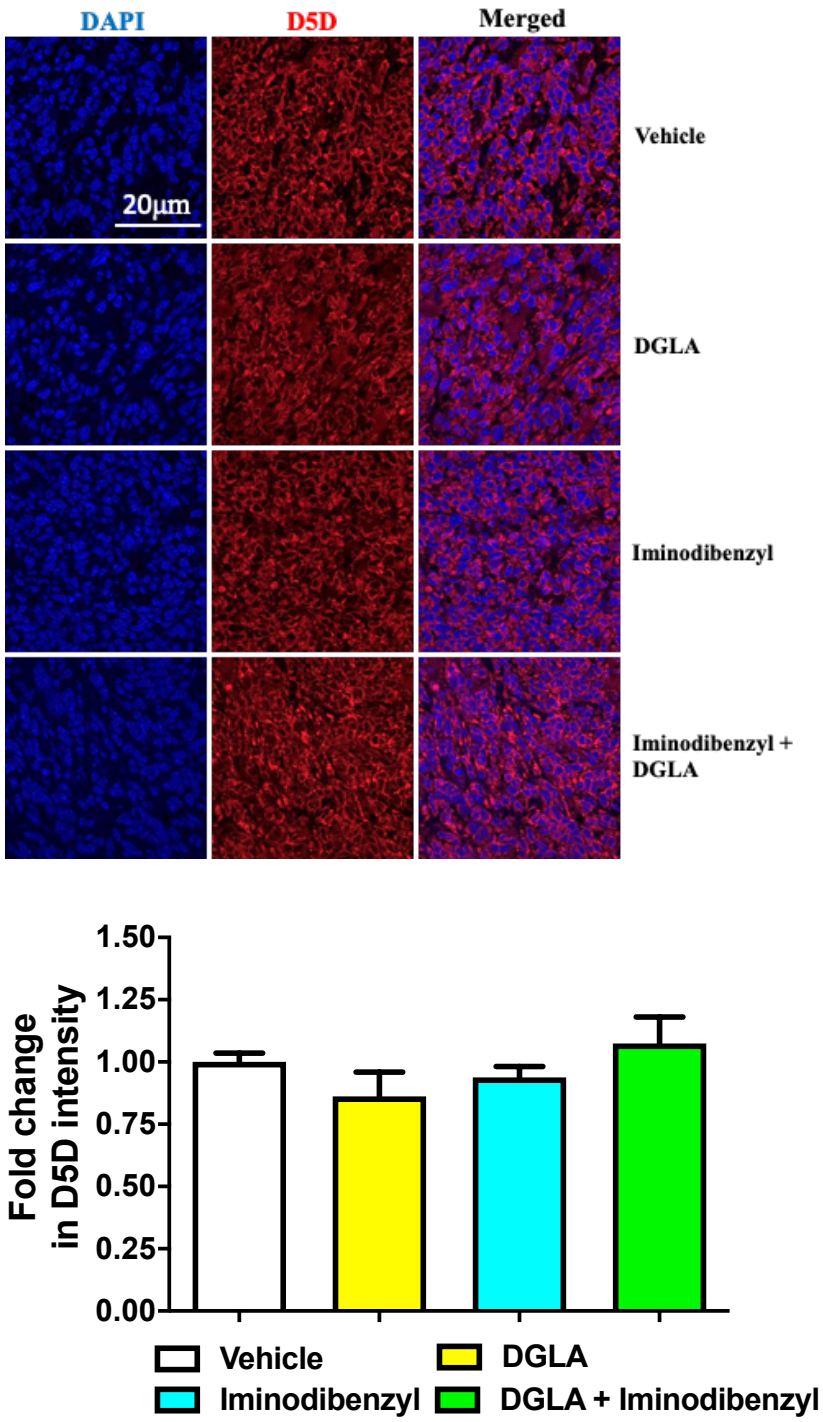

Figure 42. Qualitative and quantitative immunofluorescence analysis of D5D protein expression in tumors. Representative images for D5D expression in tumor tissues. D5D was stained in red; cell nuclei were counter stained with DAPI in blue. Mean intensity of D5D in each sample was quantified as an index of its expression level in tumor tissue. Data is represented as Mean ± SEM from three tumors.

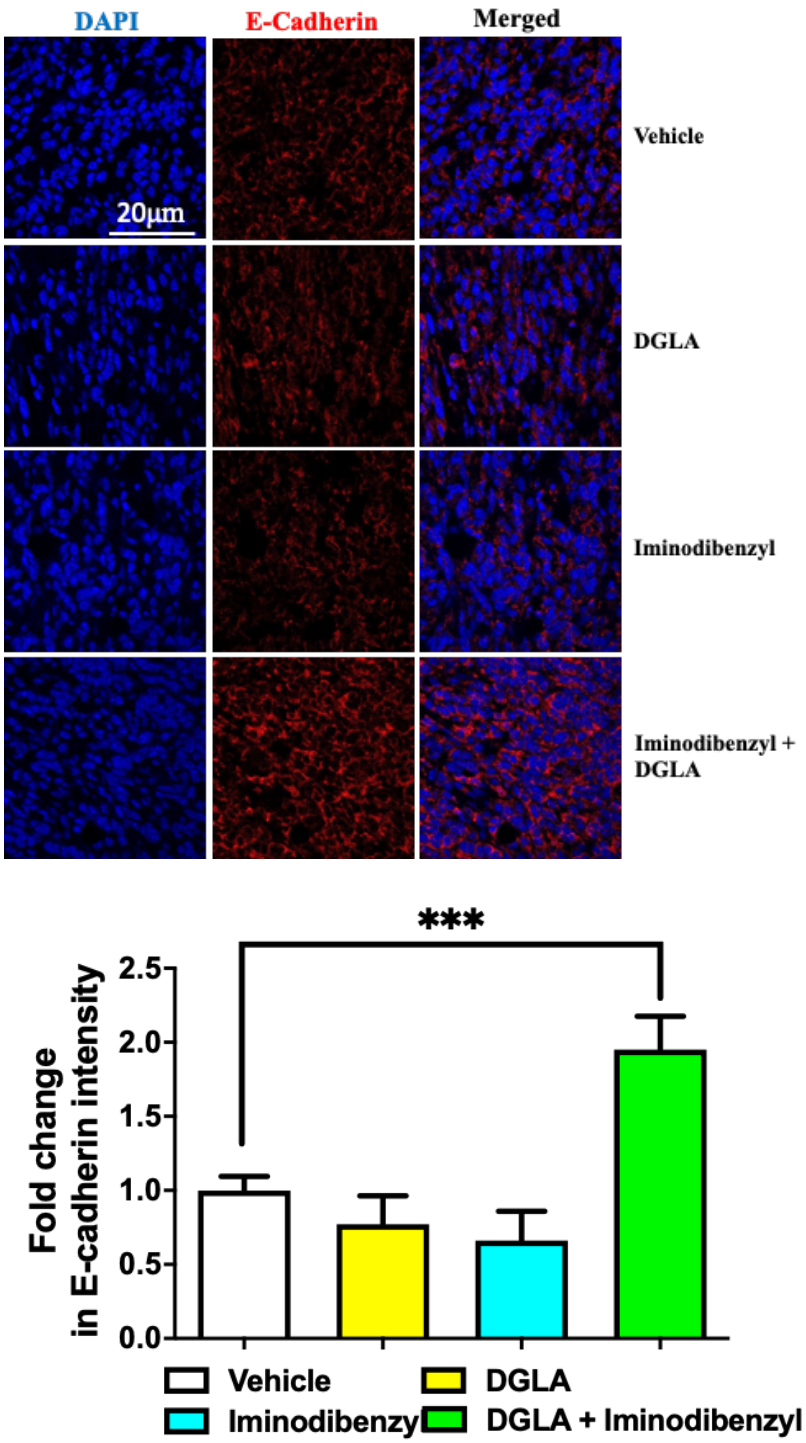

Figure 43. Qualitative and quantitative immunofluorescence analysis of EMT marker E. Cadherin protein expression in tumors. Representative images for E-Cadherin expression in tumor tissues. E. Cadherin was stained in red; cell nuclei were counter stained with DAPI in blue. Mean intensity of E. Cadherin in each sample was quantified as an index of its expression level in tumor tissue. Data is represented as Mean ± SEM from three tumors. ****P<0.001 vs.* Vehicle.

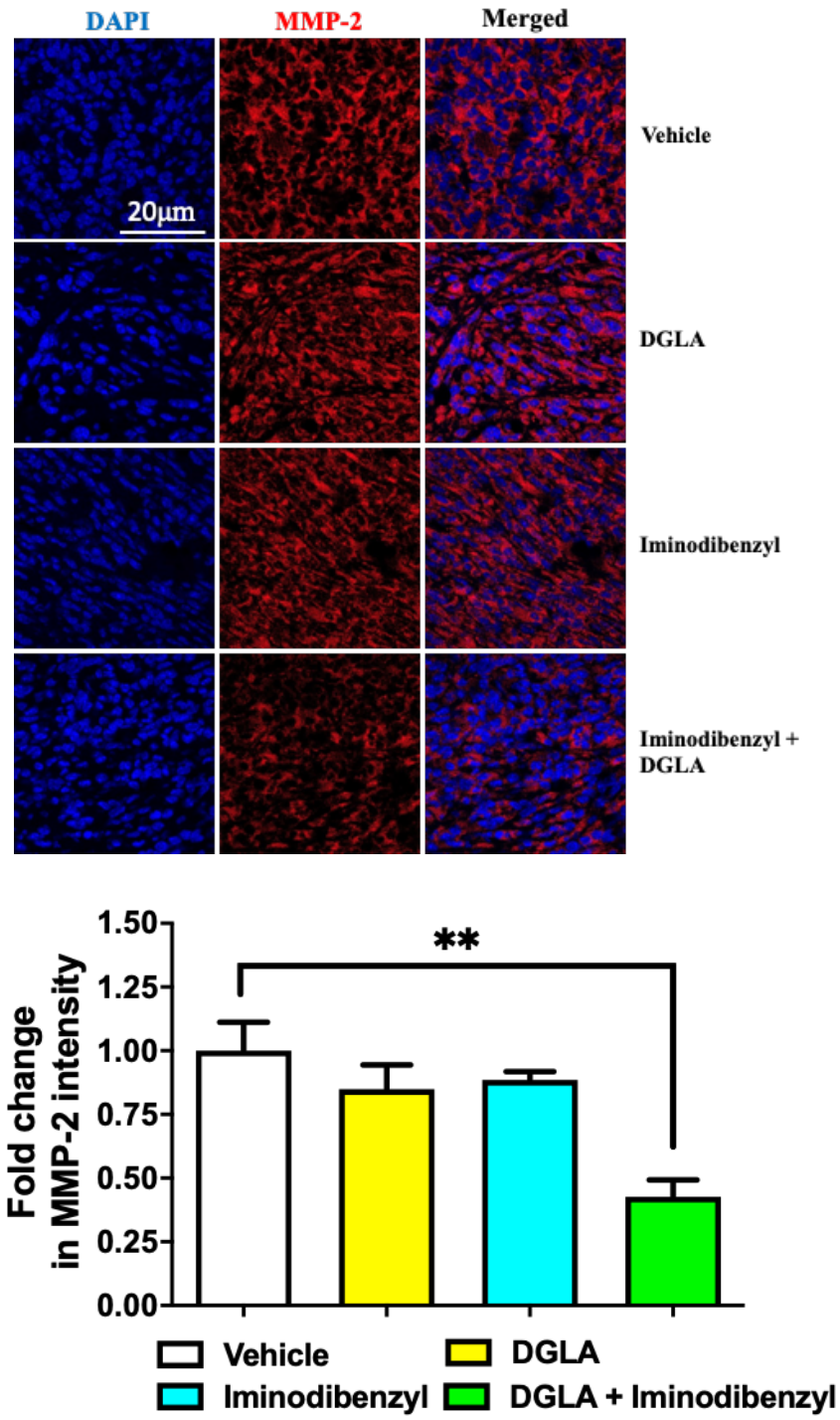

Figure 44. Qualitative and quantitative immunofluorescence analysis of MMP-2 protein expression in tumors. Representative images for MMP-2 expression in tumor tissues. MMP-2 was stained in red; cell nuclei were counter stained with DAPI in blue. Mean intensity of MMP-2 in each sample was quantified as an index of its expression level in tumor tissue. Data is represented as Mean ± SEM from three tumors. ***P<0.01 vs.* Vehicle.

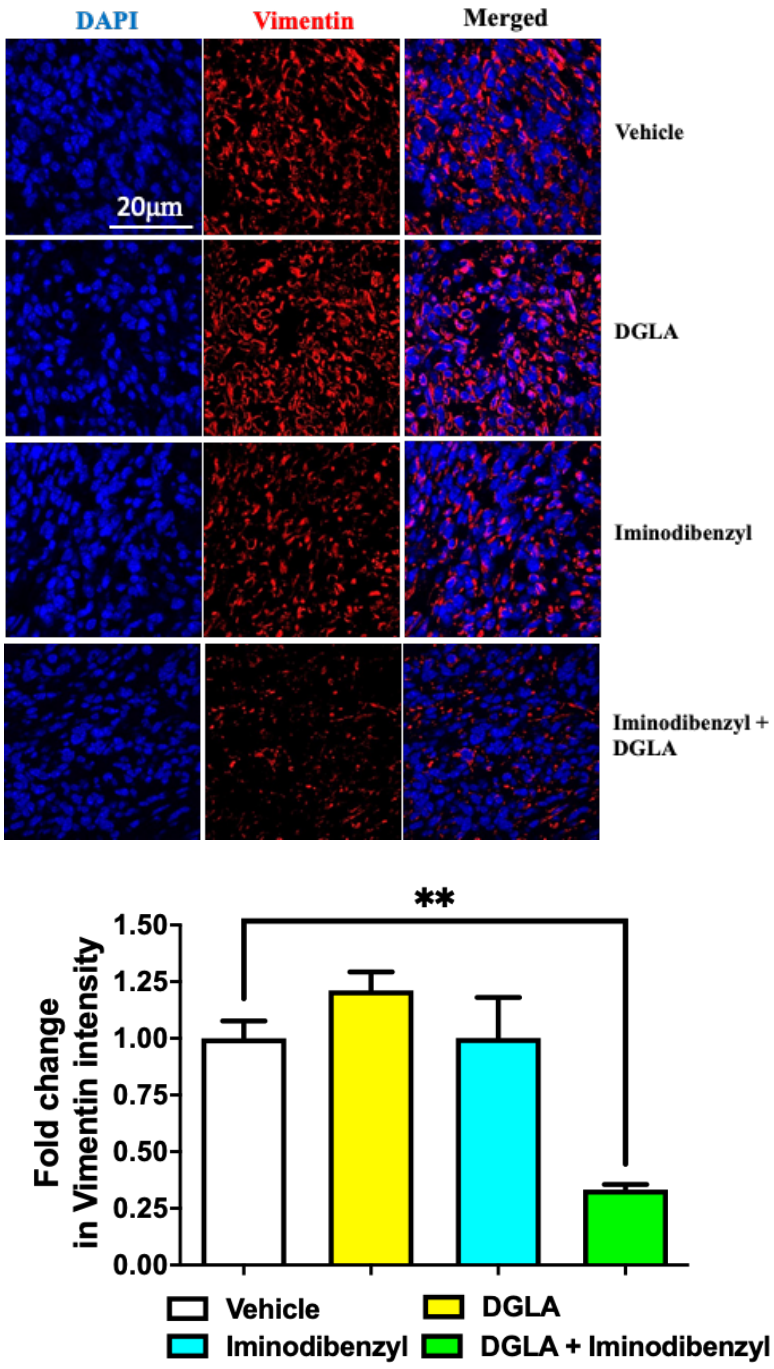

Figure 45. Qualitative and quantitative immunofluorescence analysis of EMT marker Vimentin protein expression in tumors. Representative images for Vimentin expression in tumor tissues. Vimentin was stained in red; cell nuclei were counter stained with DAPI in blue. Mean intensity of Vimentin in each sample was quantified as an index of its expression level in tumor tissue. Data is represented as Mean ± SEM from three tumors. ***P<0.01 vs.* Vehicle.

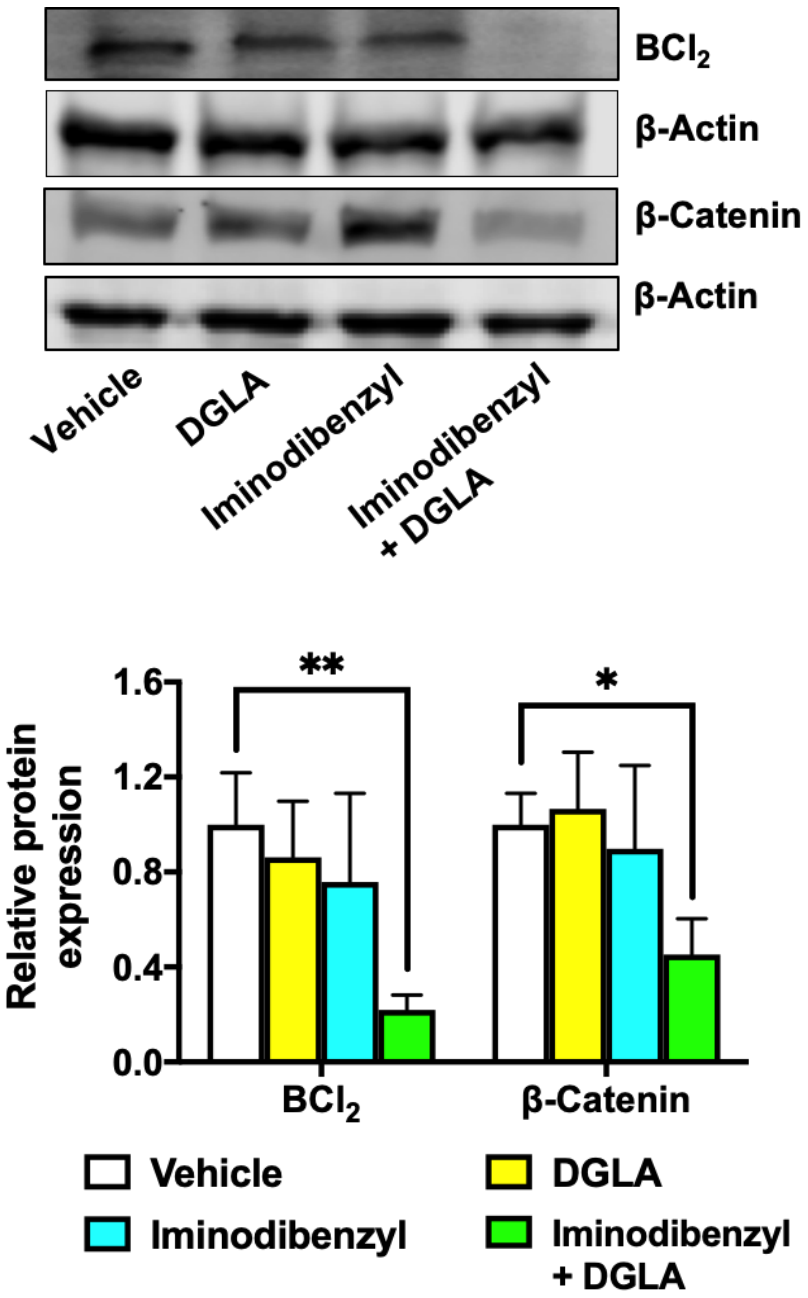

Figure 46. Relative BCl_2 and β-Catenin level determination from tumor samples. Western blot analysis and densitometry analysis of BCl_2 and β-Catenin in breast tumor tissue. The protein expression level in the Vehicle was normalized to 1, β-Actin serves as a loading control. Data represent as a mean ± SEM with at least three separate experiments. $^{**}P<0.01$ and $^{*}P<0.05$ *vs.* Vehicle.

To find the upstream marker, we also analyzed β-Catenin level. On analysis, we found a significant reduction in β-Catenin level in tumor samples extracted from animals treated with

Iminodibenzyl and DGLA combination (Figure 46, *P<0.05*), while DGLA or Iminodibenzyl administration did not exert any *in vivo* effect on β-Catenin level (Figure 46).

5.2. Pharmacokinetic profile of Iminodibenzyl

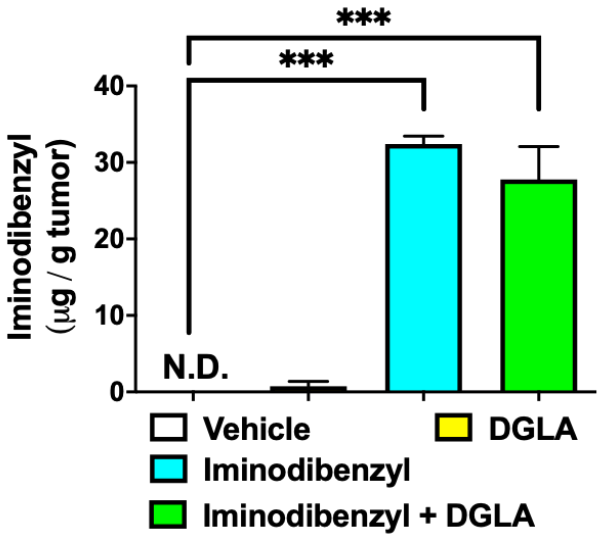

Figure 47. Iminodibenzyl quantification in the tumor samples by LC/MS. The tumor samples were subjected to liquid-liquid extraction using organic solvent. The extracted Iminodibenzyl was quantified by using LC/MS approach. Data represent as a mean ± SEM from tumors extracted from three animals in each group. ****P<0.001 vs.* Vehicle. N.D. = Not detectable.

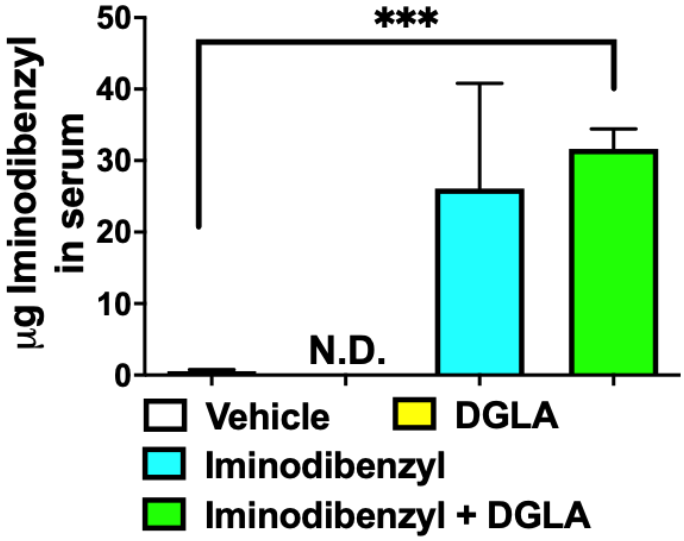

Figure 48. Iminodibenzyl quantification in the serum by LC/MS. Iminodibenzyl was extracted from the serum and quantified by using LC/MS approach. Data represent as a mean ± SEM from serum separated from blood obtained from three animals in each group. ****P<0.001 vs.* Vehicle. N.D. = Not detectable.

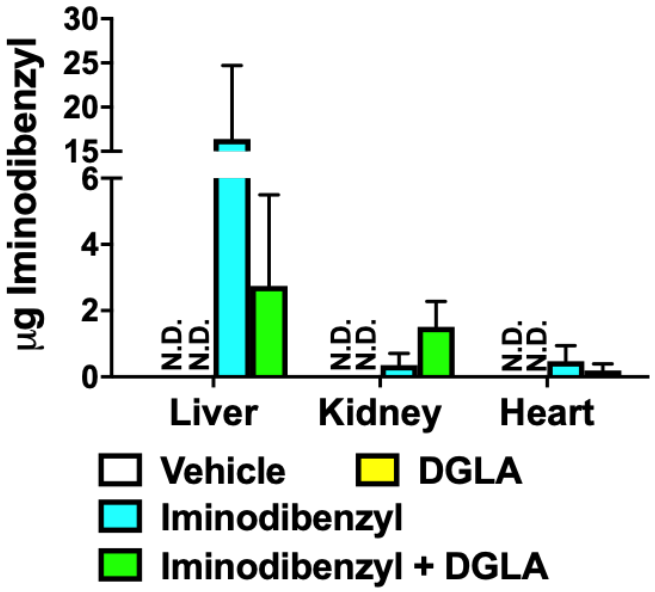

Figure 49. Iminodibenzyl quantification in different organs by LC/MS. Iminodibenzyl was extracted from the liver, kidney, and heart from animals and quantified by using LC/MS approach. Data represent as a mean ± SEM from different organs from three different animals from each treatment group. N.D. = Not detectable.

To explore the possible pharmacokinetic profile of Iminodibenzyl, we collected blood, vital organs, and tumor during animal euthanasia. The serum was separated from the blood after a few hours of blood collection. In order to determine the concentration of Iminodibenzyl at the target site, in systemic circulation, and in various organs, the Iminodibenzyl was extracted first by using liquid-liquid extraction method using ethanol and then LC/MS analysis was done to quantify the Iminodibenzyl. On analysis, it was found that approximately 8-9% of the administered drug reached to the site of action, tumor (Figure 47) and approximately 6-7% of the Iminodibenzyl was found in systemic circulation (Figure 48). We also found significantly high quantity of Iminodibenzyl in the liver and kidney, which suggested the accumulation of Iminodibenzyl in the liver and kidney over a period of treatment (Figure 49).

5.3. Limitations

In animal study, due to significantly less solubility of the Iminodibenzyl in majority of the solvent, we have used DMSO as a solvent. However, in our future *in vivo* study we are planning to use corn oil or sesame oil as a vehicle to dissolve Iminodibenzyl to divert DGLA metabolism and additionally to avoid any DMSO related toxic effects. During apoptosis many molecular changes occurs including modulation of cleaved caspase-3. In our *in vitro* analysis, we measured the relative change in cleaved caspase-3 level in 4T1 cells after various treatments, however, due to technical limitations, we could not measure the changes in cleaved caspase-3 level in tumor developed from 4T1 cells.

5.4. Conclusion and discussion

In this chapter, we analyzed the *in vivo* efficiency of Iminodibenzyl to divert DGLA metabolism from pro-cancer pathway to anti-cancer pathway by COX-2 induced peroxidation by performing orthotopic breast cancer model developed by mammary fat pad transplantation of 4T1 cancer cells, which caused significant reduction in tumor size.

In the proof of concept study done by delivering 3WJ-D5D siRNA nanoparticle and DGLA in an orthotopic breast cancer model, we have seen significant reduction in tumor size by activation of alternate metabolism pathway of DGLA resulting in accumulation of DGLA in tumor cells, which consequently metabolized to 8-HOA by COX-2 in tumor cells causing tumor shrinking[57]. Similarly, here in this chapter, we have observed that Iminodibenzyl was able to inhibit the administered DGLA metabolism resulting in accumulation of DGLA in tumor of the animal administered combination (Iminodibenzyl and DGLA) and the accumulated DGLA was further metabolized to 8-HOA. We also observed increased DGLA/AA ratio in the animals' provided combination, which was due to inhibition of DGLA metabolism and hence less production of AA.

Notable, increased AA was observed in tumors from animals provided DGLA as a supplement, which was predicted to be due to COX-2 catalyzed DGLA peroxidation to produce more AA. These group chromatographic analysis provided comprehensive evidence about the *in vivo* COX-2 paradigm shift exerted by Iminodibenzyl in breast cancer cells.

From our *in vitro* studies (chapter 5) and the previously published study[57], we have found that the D5D inhibition led produced 8-HOA activate caspase dependent death pathway and reduced the EMT markers. Similarly, from this chapter, we have noted that administration of Iminodibenzyl and DGLA caused caspase dependent death pathway activation and significant reduction in EMT markers, which might be a possible reason behind shrunken tumor and a lesser number of metastatic nodules. Additionally, in line with the *in vitro* findings from chapter 5, we observed significantly reduced HDAC activity and β-Catenin level in the tumors from combination provided treatment.

Interestingly, we also observed moderate reduction in tumor size in animals provided Iminodibenzyl alone as a treatment, which might be explained from moderately reduced HDAC activity in the Iminodibenzyl treated animals. Additionally, others have also reported reduction in HDAC activity by Iminodibenzyl or from structurally similar compounds[93,130,131]. β-catenin is an appealing target due to its ability to abolish cancer relapse. Here, we have perceived that Iminodibenzyl and DGLA combination caused downregulation of β-catenin, which could be another possible mechanism leading to breast cancer cell apoptosis and reduced cell proliferation leading to reduced tumor growth by Iminodibenzyl and DGLA combination treatment. The downregulated β-catenin also has an inhibitory role in EMT resulting in less metastasis of tumor cells from the site of inoculation to the lungs in the orthotopic tumor model.

In a summary, this chapter provided evidence about the in vivo efficiency of Iminodibenzyl to exhibit the COX-2 paradigm shift to exhibit tumor growth inhibition. From an orthotopic breast tumor model, it was evident that combination treatment with Iminodibenzyl and DGLA brought out a significantly high level of 8-HOA, which further downregulated HDAC activity causing caspase dependent apoptosis pathway activation. The produced 8-HOA (from Iminodibenzyl catalyzed DGLA metabolism inhibition and simultaneous COX-2 induced peroxidation) also has dampening effect on β-catenin level, which might be another possible mode of action for observed reduced tumor size.

6. SUMMARY, LIMITATIONS AND FUTURE DIRECTIONS

6.1. Summary

Breast cancer is one of most commonly occurring cancer in female population in world. There are many risk factors responsible for breast cancer development, out of which consumption of ω-6 polyunsaturated fatty acid (ω-6 PUFAs) rich diet is one of them, which has increased by 30-fold in last few years. Additionally, many molecular changes occur during cancer development, COX modulation is one of them. There are multiple clinical studies available, which have reported COX-2 overexpression in various stages of breast cancers. Moreover, COX-2 also has a vital role in ω-6 PUFAs metabolism. Downstream ω-6 PUFAs like DGLA on metabolism by D5D produces AA, which further on peroxidation by COX-2 produce precancerous PGE_2. The produced PGE_2 activate various pathways leading to cancer cell proliferation, metastasis, and resistance to apoptosis. Hence, by considering the role of COX-2 in production of precancerous prostaglandins, COX-2 inhibition seemed to be an ideal strategy to inhibit the cancer progression, which provided inconclusive findings in clinical settings. Contrary, the use of selective and non-selective inhibitor resulted in severe cardiovascular adverse events, which resulted in clinical subjects' death. Hence by considering the risk associated with the use of COX-2 inhibitors, it is no longer being used for cancer management.

Recently, we have come up with the novel strategy in cancer therapeutics, where instead of inhibiting we are exploiting overexpressed COX-2 to metabolize upstream ω-6 PUFAs, DGLA, after inhibiting the D5D enzyme to an anti-cancer metabolite 8-HOA. Since we are using COX-2 instead of inhibiting to achieve cancer inhibition, it is being known as COX-2 paradigm shift approach. Previously, we have used D5D siRNA/shRNA to inhibit the D5D enzyme, which resulted in diversion of DGLA metabolism to an 8-HOA, which has an anti-cancer activity.

However, the use of siRNA and shRNA is restricted due to physiological endonucleases mediated degradation and inability to cross the cell membrane, which led to difficulty in executing the paradigm shift approach in a physiological environment. To overcome the limitations associated with RNAi therapy, we identified the D5D activity inhibitor Iminodibenzyl and hypothesized that administration of Iminodibenzyl would shift the DGLA metabolism producing 8-HOA, which would produce anti-cancer activity against breast cancer cells. In *in vitro* experiment, when 4T1 and MDA-MB-231 cells were treated with Iminodibenzyl and DGLA, significant reduction in survival fraction, cell proliferation, and increased apoptosis was observed. On elucidating molecular mechanism, it was found that Iminodibenzyl and DGLA combination caused significant reduction in HDAC activity resulting in activation of caspase dependent death pathway as validated by Z-VAD-FMK pretreatment. Additionally, significant reduction in cancer cell migration was also noted after the combination treatment, which might be due to reduced lamellipodia, filopodia, and EMT markers. To validate physiological efficacy of Iminodibenzyl to execute a paradigm shift of COX-2 approach, orthotopic breast cancer model was developed, and animals were provided Vehicle, DGLA, Iminodibenzyl, and combination of Iminodibenzyl and DGLA as a treatment. At the end of treatment period, significant reduction in tumor size was observed in group of animals received combination treatment. Additionally, significantly less number of metastatic lung nodules were observed in group of animals provided combination treatment. Based on the immunohistochemistry study and Western analysis, activation of caspases, downregulation of HDAC activity and EMT markers were observed, which might have produced shrunken tumors and less number of nodules. Additionally, reduced β-catenin was observed in both in vitro and in vivo studies, which could be an additional mechanism behind reduced cancer growth.

6.2. Future directions

6.2.1. Screening more D5D activity inhibitors

In the present study, we have used Iminodibenzyl to inhibit D5D activity and brought out anti-cancer effect against breast cancer. Iminodibenzyl is a building block of many antipsychotics[94]. Hence, here based on the observed therapeutic efficacy after Iminodibenzyl and DGLA administration, in our future studies, a different structural analog of Iminodibenzyl will be prepared by attaching various functional groups and comparative analysis will be done to identify the potent inhibitor. Additionally, there are few Iminodibenzyl analogs such as trimethoprim, clomipramine, etc. are available in the market as antipsychotic. We are also planning to analyze the D5D inhibitory potential of the compound by using rat liver microsome system. Additionally, recently a new D5D inhibitor compound 326 (Takeda Pharmaceuticals) was developed, which is orally available, potent selective D5D inhibitor[132]. In our near future study, we will explore compound 326 as a potential candidate for D5D activity inhibitor to achieve COX-2 paradigm shift in cancer.

6.2.2. Combination with other chemotherapeutic agents to improve therapeutic effect

Raising prevalence in drug resistant cancer cases is a major concern in cancer therapeutics[58,60,133]. There are multiple reasons behind resistance development, out of which drug efflux, DNA damage repair, cell death inhibition, epigenetics, drug inactivation, and drug target alteration are few of them[134]. In this study in chapter 4 and 5, we have made an attempt to explore the possible molecular mechanism by identifying involvement of HDAC activity, caspase dependent death pathway, and catenin pathway. There are multiple evidences available depicting role of a therapeutic moiety to overcome drug resistance by inhibiting the catenin activity[135,136]. Based on available reports and observed findings, we will incorporate Iminodibenzyl with other

chemotherapeutic modalities such as trastuzumab, 5-FU, or gemcitabine can be combined with multiple modalities, which have failed due to cancer resistance[137-139]. Additionally, Iminodibenzyl can inhibit the HDAC activity[93] and it has been found that HDAC inhibitors can synergistically increase the activity of other chemotherapeutic agents[140,141]. Hence, in our future studies, we will combine Iminodibenzyl based treatment strategy to other chemotherapeutic agents and evaluate the additive or synergistic effect on cancer.

6.2.3. Determination of anti-metastatic potential after Iminodibenzyl and DGLA treatment

Metastasis in breast cancer is a leading cause of death in breast cancer patients. Metastasis is defined as a condition in which cancer cells have spread from breast to the distant organs such as bones, lung, liver, and/or brain[142]. In our study, we have attempted to determine the effect of treatment on breast cancer migration and findings from chapter 3 and 4 suggested reduction in cancer cell migration and EMT markers. Additionally, to analyze *in vivo* anti-metastatic effect, we also performed the orthotopic breast cancer model by inoculating breast cancer cells in mammary fat pad and found significant reduction in lung metastatic nodules after providing combination treatment in comparison to vehicle treated group. However, to conclude the anti-metastatic effect, we are also required to analyze the effect in an another orthotopic breast cancer model developed by delivering cancer cells through i.v. route[143]. Hence, in our future study, we will develop an orthotopic model by implanting cancer cells through tail vein injection and animals will be provided simultaneous treatment with Iminodibenzyl and DGLA as per the protocol.

6.2.4. Develop targeted drug delivery approach to increase bioavailability

Cancer therapy resistance is a major barrier leading to chemotherapy failure. There are multiple reasons responsible for chemotherapy failure, including oxygen deficient environment known as hypoxia[144]. Additionally, as per our pharmacokinetic data (chapter 5), only 8-9% of the

administered drug was available at the site of action and 6-7% was available in the systemic circulation. Hence, to deliver high quantity of administered drug to the tumor site and into the hypoxic region, we will develop the tumor cell surface protein targeted nanoparticles enclosing Iminodibenzyl and analyze its cancer growth inhibitory effect in 2D and 3D cell culture as well as in *in vivo*. In this study, we are planning to incorporate P-gp or EpCAM aptamer to the targeting protein and Iminodibenzyl will be encapsulated in the nanoparticle. After optimizing the encapsulation efficiency, and validating the targeting and release properties of nanoparticle, we will perform an in vivo efficacy study by developing orthotopic breast cancer model by using 4T1 or MDA-MB-231 cells.

REFERENCES

1 Society, A. C. <https://www.cancer.org/content/dam/cancer-org/research/cancer-facts-and-statistics/breast-cancer-facts-and-figures/breast-cancer-facts-and-figures-2019-2020.pdf> (2020).

2 Siegel, R. L., Miller, K. D., Fuchs, H. E. & Jemal, A. Cancer Statistics, 2021. *CA Cancer J Clin* **71**, 7-33, doi:10.3322/caac.21654 (2021).

3 Bartsch, H., Nair, J. & Owen, R. W. Dietary polyunsaturated fatty acids and cancers of the breast and colorectum: emerging evidence for their role as risk modifiers. *Carcinogenesis* **20**, 2209-2218, doi:10.1093/carcin/20.12.2209 (1999).

4 Khankari, N. K. *et al.* Polyunsaturated fatty acid interactions and breast cancer incidence: a population-based case-control study on Long Island, New York. *Ann Epidemiol* **25**, 929-935, doi:10.1016/j.annepidem.2015.09.003 (2015).

5 Nguyen, N. M. *et al.* Maternal intake of high n-6 polyunsaturated fatty acid diet during pregnancy causes transgenerational increase in mammary cancer risk in mice. *Breast Cancer Research* **19**, 77, doi:10.1186/s13058-017-0866-x (2017).

6 Shahidi, F. & Ambigaipalan, P. Omega-3 Polyunsaturated Fatty Acids and Their Health Benefits. *Annu Rev Food Sci Technol* **9**, 345-381, doi:10.1146/annurev-food-111317-095850 (2018).

7 Gammone, M. A., Riccioni, G., Parrinello, G. & D'Orazio, N. Omega-3 Polyunsaturated Fatty Acids: Benefits and Endpoints in Sport. *Nutrients* **11**, doi:10.3390/nu11010046 (2018).

8 Swanson, D., Block, R. & Mousa, S. A. Omega-3 fatty acids EPA and DHA: health benefits throughout life. *Adv Nutr* **3**, 1-7, doi:10.3945/an.111.000893 (2012).

9 Weylandt, K. H. *et al.* Omega-3 Polyunsaturated Fatty Acids: The Way Forward in Times of Mixed Evidence. *BioMed Research International* **2015**, 143109, doi:10.1155/2015/143109 (2015).

10 Blasbalg, T. L., Hibbeln, J. R., Ramsden, C. E., Majchrzak, S. F. & Rawlings, R. R. Changes in consumption of omega-3 and omega-6 fatty acids in the United States during the 20th century. *Am J Clin Nutr* **93**, 950-962, doi:10.3945/ajcn.110.006643 (2011).

11 Simopoulos, A. P. An Increase in the Omega-6/Omega-3 Fatty Acid Ratio Increases the Risk for Obesity. *Nutrients* **8**, 128, doi:10.3390/nu8030128 (2016).

12 Hosseinkhani, S. *et al.* Association of circulating omega 3, 6 and 9 fatty acids with gestational diabetes mellitus: a systematic review. *BMC Endocrine Disorders* **21**, 120, doi:10.1186/s12902-021-00783-w (2021).

13 Mazhar, D., Ang, R. & Waxman, J. COX inhibitors and breast cancer. *Br J Cancer* **94**, 346-350, doi:10.1038/sj.bjc.6602942 (2006).

14 Miglietta, A. *et al.* COX-2 expression in human breast carcinomas: correlation with clinicopathological features and prognostic molecular markers. *Expert Opinion on Therapeutic Targets* **14**, 655-664, doi:10.1517/14728222.2010.486792 (2010).

15 Stasinopoulos, I., Shah, T., Penet, M.-F., Krishnamachary, B. & Bhujwalla, Z. COX-2 in cancer: Gordian knot or Achilles heel? *Frontiers in Pharmacology* **4**, doi:10.3389/fphar.2013.00034 (2013).

16 Singh, B. *et al.* COX-2 involvement in breast cancer metastasis to bone. *Oncogene* **26**, 3789-3796, doi:10.1038/sj.onc.1210154 (2007).

17 Harris, R. E., Casto, B. C. & Harris, Z. M. Cyclooxygenase-2 and the inflammogenesis of breast cancer. *World J Clin Oncol* **5**, 677-692, doi:10.5306/wjco.v5.i4.677 (2014).

18 Half, E. *et al.* Cyclooxygenase-2 expression in human breast cancers and adjacent ductal carcinoma in situ. *Cancer Res* **62**, 1676-1681 (2002).

19 Ranger, G. S., Thomas, V., Jewell, A. & Mokbel, K. Elevated cyclooxygenase-2 expression correlates with distant metastases in breast cancer. *Anticancer Res* **24**, 2349-2351 (2004).

20 Hoellen, F. *et al.* Impact of Cyclooxygenase-2 in Breast Cancer. *Anticancer Research* **31**, 4359 (2011).

21 Akasaka, H. & Ruan, K. H. Identification of the two-phase mechanism of arachidonic acid regulating inflammatory prostaglandin E2 biosynthesis by targeting COX-2 and mPGES-1. *Arch Biochem Biophys* **603**, 29-37, doi:10.1016/j.abb.2016.04.011 (2016).

22 Ristimäki, A. *et al.* Prognostic significance of elevated cyclooxygenase-2 expression in breast cancer. *Cancer Res* **62**, 632-635 (2002).

23 Arun, B. & Goss, P. The role of COX-2 inhibition in breast cancer treatment and prevention. *Semin Oncol* **31**, 22-29, doi:10.1053/j.seminoncol.2004.03.042 (2004).

24 Wang, D., Mann, J. R. & Dubois, R. N. The Role of Prostaglandins and Other Eicosanoids in the Gastrointestinal Tract. *Gastroenterology* **128**, 1445-1461, doi:https://doi.org/10.1053/j.gastro.2004.09.080 (2005).

25 Wang, Q. *et al.* COX-2 induces apoptosis-resistance in hepatocellular carcinoma cells via the HIF-1α/PKM2 pathway. *Int J Mol Med* **43**, 475-488, doi:10.3892/ijmm.2018.3936 (2019).

26 Totzke, G., Schulze-Osthoff, K. & Jänicke, R. U. Cyclooxygenase-2 (COX-2) inhibitors sensitize tumor cells specifically to death receptor-induced apoptosis independently of COX-2 inhibition. *Oncogene* **22**, 8021-8030, doi:10.1038/sj.onc.1206837 (2003).

27 Sobolewski, C., Cerella, C., Dicato, M., Ghibelli, L. & Diederich, M. The role of cyclooxygenase-2 in cell proliferation and cell death in human malignancies. *Int J Cell Biol* **2010**, 215158, doi:10.1155/2010/215158 (2010).

28 Tong, X. & Pelling, J. C. Targeting the PI3K/Akt/mTOR axis by apigenin for cancer prevention. *Anticancer Agents Med Chem* **13**, 971-978, doi:10.2174/18715206113139990119 (2013).

29 Lim, J. W., Kim, H. & Kim, K. H. Nuclear factor-kappaB regulates cyclooxygenase-2 expression and cell proliferation in human gastric cancer cells. *Lab Invest* **81**, 349-360, doi:10.1038/labinvest.3780243 (2001).

30 Hendrickx, N. *et al.* Up-regulation of cyclooxygenase-2 and apoptosis resistance by p38 MAPK in hypericin-mediated photodynamic therapy of human cancer cells. *J Biol Chem* **278**, 52231-52239, doi:10.1074/jbc.M307591200 (2003).

31 Bresalier, R. S. *et al.* Cardiovascular events associated with rofecoxib in a colorectal adenoma chemoprevention trial. *N Engl J Med* **352**, 1092-1102, doi:10.1056/NEJMoa050493 (2005).

32 Howe, L. R. *et al.* Celecoxib, a selective cyclooxygenase 2 inhibitor, protects against human epidermal growth factor receptor 2 (HER-2)/neu-induced breast cancer. *Cancer Res* **62**, 5405-5407 (2002).

33 Dang, C. T. *et al.* Phase II study of celecoxib and trastuzumab in metastatic breast cancer patients who have progressed after prior trastuzumab-based treatments. *Clin Cancer Res* **10**, 4062-4067, doi:10.1158/1078-0432.ccr-03-0463 (2004).

34 Martin, L. A. *et al.* Pre-surgical study of the biological effects of the selective cyclo-oxygenase-2 inhibitor celecoxib in patients with primary breast cancer. *Breast Cancer Res Treat* **123**, 829-836, doi:10.1007/s10549-010-1100-z (2010).

35 De Vecchis, R. *et al.* Cardiovascular risk associated with celecoxib or etoricoxib: a meta-analysis of randomized controlled trials which adopted comparison with placebo or naproxen. *Minerva Cardioangiol* **62**, 437-448 (2014).

36 FitzGerald, G. A. Coxibs and Cardiovascular Disease. *New England Journal of Medicine* **351**, 1709-1711, doi:10.1056/NEJMp048288 , note = PMID: 15470192 (2004).

37 *NIH Halts Use Of COX-2 Inhibitor In Large Cancer Prevention Trial*, <https://www.sciencedaily.com/releases/2004/12/041219115114.htm> (2004).

38 D'Eliseo, D. & Velotti, F. Omega-3 Fatty Acids and Cancer Cell Cytotoxicity: Implications for Multi-Targeted Cancer Therapy. *J Clin Med* **5**, doi:10.3390/jcm5020015 (2016).

39 Freitas, R. D. S. & Campos, M. M. Protective Effects of Omega-3 Fatty Acids in Cancer-Related Complications. *Nutrients* **11**, doi:10.3390/nu11050945 (2019).

40 Fabian, C. J., Kimler, B. F. & Hursting, S. D. Omega-3 fatty acids for breast cancer prevention and survivorship. *Breast Cancer Research* **17**, 62, doi:10.1186/s13058-015-0571-6 (2015).

41 Kelavkar, U. P. *et al.* Prostate tumor growth and recurrence can be modulated by the omega-6:omega-3 ratio in diet: athymic mouse xenograft model simulating radical prostatectomy. *Neoplasia* **8**, 112-124, doi:10.1593/neo.05637 (2006).

42 Apte, S. A., Cavazos, D. A., Whelan, K. A. & Degraffenried, L. A. A low dietary ratio of omega-6 to omega-3 Fatty acids may delay progression of prostate cancer. *Nutr Cancer* **65**, 556-562, doi:10.1080/01635581.2013.775316 (2013).

43 Arem, H. *et al.* Omega-3 and omega-6 fatty acid intakes and endometrial cancer risk in a population-based case-control study. *Eur J Nutr* **52**, 1251-1260, doi:10.1007/s00394-012-0436-z (2013).

44 Azrad, M., Turgeon, C. & Demark-Wahnefried, W. Current evidence linking polyunsaturated Fatty acids with cancer risk and progression. *Front Oncol* **3**, 224, doi:10.3389/fonc.2013.00224 (2013).

45 Bagga, D. *et al.* Dietary Modulation of Omega-3/Omega-6 Polyunsaturated Fatty Acid Ratios in Patients With Breast Cancer. *Journal of the National Cancer Institute* **Volume 89**, 1123–1131, doi:https://doi.org/10.1093/jnci/89.15.1123 (1997).

46 Draycott, S. A. V., Elmes, M. J., Muhlhausler, B. S. & Langley-Evans, S. Omega-6:Omega-3 Fatty Acid Ratio and Total Fat Content of the Maternal Diet Alter Offspring Growth and Fat Deposition in the Rat. *Nutrients* **12**, doi:10.3390/nu12092505 (2020).

47 Xu, Y. & Qian, S. Y. Anti-cancer activities of ω-6 polyunsaturated fatty acids. *Biomed J* **37**, 112-119, doi:10.4103/2319-4170.131378 (2014).

48 Wang, X., Lin, H. & Gu, Y. Multiple roles of dihomo-γ-linolenic acid against proliferation diseases.

49 Xiao, Y. *et al.* Characterization of free radicals formed from COX-catalyzed DGLA peroxidation. *Free Radic Biol Med* **50**, 1163-1170, doi:10.1016/j.freeradbiomed.2011.02.001 (2011).

50 Xu, Y. *et al.* Dihomo-γ-linolenic acid inhibits xenograft tumor growth in mice bearing shRNA-transfected HCA-7 cells targeting delta-5-desaturase. *BMC Cancer* **18**, 1268, doi:10.1186/s12885-018-5185-9 (2018).

51 Xu, Y. *et al.* Knockdown delta-5-desaturase in breast cancer cells that overexpress COX-2 results in inhibition of growth, migration and invasion via a dihomo-γ-linolenic acid peroxidation dependent mechanism. *BMC Cancer* **18**, 330, doi:10.1186/s12885-018-4250-8 (2018).

52 Yang, X. *et al.* Knockdown delta-5-desaturase promotes the formation of a novel free radical byproduct from COX-catalyzed ω-6 peroxidation to induce apoptosis and sensitize pancreatic cancer cells to chemotherapy drugs. *Free Radic Biol Med* **97**, 342-350, doi:10.1016/j.freeradbiomed.2016.06.028 (2016).

53 Xu, Y. *et al.* Knockdown of delta-5-desaturase promotes the anti-cancer activity of dihomo-γ-linolenic acid and enhances the efficacy of chemotherapy in colon cancer cells expressing COX-2. *Free Radic Biol Med* **96**, 67-77, doi:10.1016/j.freeradbiomed.2016.04.016 (2016).

54 Xu, Y. *et al.* Knockdown delta-5-desaturase in breast cancer cells that overexpress COX-2 results in inhibition of growth, migration and invasion via a dihomo-γ-linolenic acid peroxidation dependent mechanism. *BMC cancer* **18**, 330-330, doi:10.1186/s12885-018-4250-8 (2018).

55 Yang, X., Xu, Y., Gao, D., Yang, L. & Qian, S. Y. Dihomo-γ-linolenic acid inhibits growth of xenograft tumors in mice bearing human pancreatic cancer cells (BxPC-3) transfected with delta-5-desaturase shRNA. *Redox biology* **20**, 236-246, doi:10.1016/j.redox.2018.10.001 (2019).

56 Xu, Y. *et al.* Knockdown delta-5-desaturase in breast cancer cells that overexpress COX-2 results in inhibition of growth, migration and invasion via a dihomo-γ-linolenic acid peroxidation dependent mechanism. *BMC Cancer* **18**, 330, doi:10.1186/s12885-018-4250-8 (2018).

57 Shah, H. *et al.* Growth inhibitory and anti-metastatic activity of epithelial cell adhesion molecule targeted three-way junctional delta-5-desaturase siRNA nanoparticle for breast cancer therapy. *Nanomedicine* **30**, 102298, doi:10.1016/j.nano.2020.102298 (2020).

58 Vasan, N., Baselga, J. & Hyman, D. M. A view on drug resistance in cancer. *Nature* **575**, 299-309, doi:10.1038/s41586-019-1730-1 (2019).

59 Mansoori, B., Mohammadi, A., Davudian, S., Shirjang, S. & Baradaran, B. The Different Mechanisms of Cancer Drug Resistance: A Brief Review. *Adv Pharm Bull* **7**, 339-348, doi:10.15171/apb.2017.041 (2017).

60 Housman, G. *et al.* Drug resistance in cancer: an overview. *Cancers (Basel)* **6**, 1769-1792, doi:10.3390/cancers6031769 (2014).

61 Reischl, D. & Zimmer, A. Drug delivery of siRNA therapeutics: potentials and limits of nanosystems. *Nanomedicine: Nanotechnology, Biology and Medicine* **5**, 8-20, doi:https://doi.org/10.1016/j.nano.2008.06.001 (2009).

62 Fujiyama-Fujiwara, Y., Umeda, R. & Igarashi, O. Effects of sesamin and curcumin on delta 5-desaturation and chain elongation of polyunsaturated fatty acid metabolism in primary cultured rat hepatocytes. *J Nutr Sci Vitaminol (Tokyo)* **38**, 353-363, doi:10.3177/jnsv.38.353 (1992).

63 Qian Yue (Steven), Z. P., Yan Changhui. Compound for inhibition of delta-5-desaturase (d5d) and treatment of cancer and inflammation. United States patent (2017).

64 Obukowicz, M. G. *et al.* Identification and characterization of a novel delta6/delta5 fatty acid desaturase inhibitor as a potential anti-inflammatory agent. *Biochem Pharmacol* **55**, 1045-1058, doi:10.1016/s0006-2952(97)00665-5 (1998).

65 Shimizu, S. *et al.* Sesamin is a potent and specific inhibitor of delta 5 desaturase in polyunsaturated fatty acid biosynthesis. *Lipids* **26**, 512-516, doi:10.1007/bf02536595 (1991).

66 Setoguchi, M., Sakamori, M., Takehara, S. & Fukuda, T. Effects of iminodibenzyl antipsychotic drugs on cerebral dopamine and α-adrenergic receptors. *European Journal of Pharmacology* **112**, 313-322, doi:https://doi.org/10.1016/0014-2999(85)90776-9 (1985).

67 van Meerloo, J., Kaspers, G. J. & Cloos, J. Cell sensitivity assays: the MTT assay. *Methods Mol Biol* **731**, 237-245, doi:10.1007/978-1-61779-080-5_20 (2011).

68 Franken, N. A. P., Rodermond, H. M., Stap, J., Haveman, J. & van Bree, C. Clonogenic assay of cells in vitro. *Nature Protocols* **1**, 2315-2319, doi:10.1038/nprot.2006.339 (2006).

69 Rieger, A. M., Nelson, K. L., Konowalchuk, J. D. & Barreda, D. R. Modified annexin V/propidium iodide apoptosis assay for accurate assessment of cell death. *J Vis Exp*, doi:10.3791/2597 (2011).

70 Logue, S. E., Elgendy, M. & Martin, S. J. Expression, purification and use of recombinant annexin V for the detection of apoptotic cells. *Nature Protocols* **4**, 1383-1395, doi:10.1038/nprot.2009.143 (2009).

71 Quehenberger, O., Armando, A., Dumlao, D., Stephens, D. L. & Dennis, E. A. Lipidomics analysis of essential fatty acids in macrophages. *Prostaglandins Leukot Essent Fatty Acids* **79**, 123-129, doi:10.1016/j.plefa.2008.09.021 (2008).

72 Pang, L. *et al.* EpCAM-Targeted 3WJ RNA Nanoparticle Harboring Delta-5-Desaturase siRNA Inhibited Lung Tumor Formation via DGLA Peroxidation. *Molecular Therapy - Nucleic Acids* **22**, 222-235, doi:https://doi.org/10.1016/j.omtn.2020.08.024 (2020).

73 Pillar, N., Polsky, A. L., Weissglas-Volkov, D. & Shomron, N. Comparison of breast cancer metastasis models reveals a possible mechanism of tumor aggressiveness. *Cell Death & Disease* **9**, 1040, doi:10.1038/s41419-018-1094-8 (2018).

74 Zhang, Y. *et al.* Establishment of a murine breast tumor model by subcutaneous or orthotopic implantation. *Oncol Lett* **15**, 6233-6240, doi:10.3892/ol.2018.8113 (2018).

75 Guo, W., Zhang, S. & Liu, S. Establishment of a novel orthotopic model of breast cancer metastasis to the lung. *Oncol Rep* **33**, 2992-2998, doi:10.3892/or.2015.3927 (2015).

76 Paschall, A. V. & Liu, K. An Orthotopic Mouse Model of Spontaneous Breast Cancer Metastasis. *J Vis Exp*, doi:10.3791/54040 (2016).

77 Džodić, P. L., ivanovi, L. J., Proti, A. D., Zeevi, M. L. & Joci, B. M. Determination of Carbamazepine and Its Impurities Iminostilbene and Iminodibenzyl in Solid Dosage Form by Column High-Performance Liquid Chromatography. *Journal of AOAC INTERNATIONAL* **93**, 1059-1068, doi:10.1093/jaoac/93.4.1059 (2010).

78 Kuehl, F. A., Jr. & Egan, R. W. Prostaglandins, arachidonic acid, and inflammation. *Science* **210**, 978-984, doi:10.1126/science.6254151 (1980).

79 Nakanishi, M. & Rosenberg, D. W. Multifaceted roles of PGE2 in inflammation and cancer. *Semin Immunopathol* **35**, 123-137, doi:10.1007/s00281-012-0342-8 (2013).

80 Wang, J., Lu, Z., Wientjes, M. G. & Au, J. L. Delivery of siRNA therapeutics: barriers and carriers. *Aaps j* **12**, 492-503, doi:10.1208/s12248-010-9210-4 (2010).

81 Qian Yue (Steven), Z. P., Yan Changhui. Compound for inhibition of delta-5-desaturase (d5d) and treatment of cancer and inflammation. United States patent (2017/09/01).

82 Xu, Y., Qi, J., Yang, X., Wu, E. & Qian, S. Y. Free radical derivatives formed from cyclooxygenase-catalyzed dihomo-γ-linolenic acid peroxidation can attenuate colon cancer cell growth and enhance 5-fluorouracil's cytotoxicity. *Redox Biol* **2**, 610-618, doi:10.1016/j.redox.2014.01.022 (2014).

83 Chen, E. P. & Smyth, E. M. COX-2 and PGE2-dependent immunomodulation in breast cancer. *Prostaglandins Other Lipid Mediat* **96**, 14-20, doi:10.1016/j.prostaglandins.2011.08.005 (2011).

84 Greenhough, A. *et al.* The COX-2/PGE 2 pathway: key roles in the hallmarks of cancer and adaptation to the tumour microenvironment. *Carcinogenesis* **30**, 377-386, doi:10.1093/carcin/bgp014 (2009).

85 Falandry, C. *et al.* Celecoxib and exemestane versus placebo and exemestane in postmenopausal metastatic breast cancer patients: a double-blind phase III GINECO study. *Breast Cancer Res Treat* **116**, 501-508, doi:10.1007/s10549-008-0229-5 (2009).

86 Pang, L. *et al.* EpCAM-Targeted 3WJ RNA Nanoparticle Harboring Delta-5-Desaturase siRNA Inhibited Lung Tumor Formation via DGLA Peroxidation. *Mol Ther Nucleic Acids* **22**, 222-235, doi:10.1016/j.omtn.2020.08.024 (2020).

87 Ge, H. *et al.* Gamma-linolenic acid induces apoptosis and lipid peroxidation in human chronic myelogenous leukemia K562 cells. *Cell Biol Int* **33**, 402-410, doi:10.1016/j.cellbi.2009.01.014 (2009).

88 Lu, X., Yu, H., Ma, Q., Shen, S. & Das, U. N. Linoleic acid suppresses colorectal cancer cell growth by inducing oxidant stress and mitochondrial dysfunction. *Lipids Health Dis* **9**, 106, doi:10.1186/1476-511x-9-106 (2010).

89 Wallace, J. L. Recent advances in gastric ulcer therapeutics. *Current Opinion in Pharmacology* **5**, 573-577, doi:https://doi.org/10.1016/j.coph.2005.06.004 (2005).

90 Xu, L., Zhang, L., Yi, Y., Kang, H.-K. & Datta, S. K. Human lupus T cells resist inactivation and escape death by upregulating COX-2. *Nature Medicine* **10**, 411-415, doi:10.1038/nm1005 (2004).

91 Glover, J. A., Hughes, C. M., Cantwell, M. M. & Murray, L. J. A systematic review to establish the frequency of cyclooxygenase-2 expression in normal breast epithelium, ductal carcinoma in situ, microinvasive carcinoma of the breast and invasive breast cancer. *British Journal of Cancer* **105**, 13-17, doi:10.1038/bjc.2011.204 (2011).

92 Steinbach, G. *et al.* The effect of celecoxib, a cyclooxygenase-2 inhibitor, in familial adenomatous polyposis. *N Engl J Med* **342**, 1946-1952, doi:10.1056/nejm200006293422603 (2000).

93 Pang, L., Shah, H., Qian, S. & Sathish, V. Iminodibenzyl redirected cyclooxygenase-2 catalyzed dihomo-γ-linolenic acid peroxidation pattern in lung cancer. *Free Radic Biol Med* **172**, 167-180, doi:10.1016/j.freeradbiomed.2021.06.004 (2021).

94 Setoguchi, M., Sakamori, M., Takehara, S. & Fukuda, T. Effects of iminodibenzyl antipsychotic drugs on cerebral dopamine and alpha-adrenergic receptors. *Eur J Pharmacol* **112**, 313-322, doi:10.1016/0014-2999(85)90776-9 (1985).

95 Czabotar, P. E., Lessene, G., Strasser, A. & Adams, J. M. Control of apoptosis by the BCL-2 protein family: implications for physiology and therapy. *Nature Reviews Molecular Cell Biology* **15**, 49-63, doi:10.1038/nrm3722 (2014).

96 Zhang, J. & Zhong, Q. Histone deacetylase inhibitors and cell death. *Cell Mol Life Sci* **71**, 3885-3901, doi:10.1007/s00018-014-1656-6 (2014).

97 Vicente-Manzanares, M. & Horwitz, A. R. in *Cell Migration: Developmental Methods and Protocols* (eds Claire M. Wells & Maddy Parsons) 1-24 (Humana Press, 2011).

98 Zhao, X. & Guan, J. L. Focal adhesion kinase and its signaling pathways in cell migration and angiogenesis. *Adv Drug Deliv Rev* **63**, 610-615, doi:10.1016/j.addr.2010.11.001 (2011).

99 Parsons, J. T., Horwitz, A. R. & Schwartz, M. A. Cell adhesion: integrating cytoskeletal dynamics and cellular tension. *Nature Reviews Molecular Cell Biology* **11**, 633-643, doi:10.1038/nrm2957 (2010).

100 McLean, G. W. *et al.* The role of focal-adhesion kinase in cancer — a new therapeutic opportunity. *Nature Reviews Cancer* **5**, 505-515, doi:10.1038/nrc1647 (2005).

101 Franco, S. J. & Huttenlocher, A. Regulating cell migration: calpains make the cut. *J Cell Sci* **118**, 3829-3838, doi:10.1242/jcs.02562 (2005).

102 Deakin, N. O. & Turner, C. E. Paxillin comes of age. *Journal of Cell Science* **121**, 2435-2444, doi:10.1242/jcs.018044 (2008).

103 Zhang, W., Huang, Y., Wu, Y. & Gunst, S. J. A novel role for RhoA GTPase in the regulation of airway smooth muscle contraction. *Can J Physiol Pharmacol* **93**, 129-136, doi:10.1139/cjpp-2014-0388 (2015).

104 Carisey, A. *et al.* Vinculin Regulates the Recruitment and Release of Core Focal Adhesion Proteins in a Force-Dependent Manner. *Current Biology* **23**, 271-281, doi:https://doi.org/10.1016/j.cub.2013.01.009 (2013).

105 Zalewska, T. *et al.* Imipramine administration induces changes in the phosphorylation of FAK and PYK2 and modulates signaling pathways related to their activity. *Biochim Biophys Acta* **1860**, 424-433, doi:10.1016/j.bbagen.2015.11.008 (2016).

106 Benson, C. S., Babu, S. D., Radhakrishna, S., Selvamurugan, N. & Ravi Sankar, B. Expression of matrix metalloproteinases in human breast cancer tissues. *Dis Markers* **34**, 395-405, doi:10.3233/dma-130986 (2013).

107 Duffy, M. J., Maguire, T. M., Hill, A., McDermott, E. & O'Higgins, N. Metalloproteinases: role in breast carcinogenesis, invasion and metastasis. *Breast Cancer Research* **2**, 252, doi:10.1186/bcr65 (2000).

108 Wang, Y. & Zhou, B. P. Epithelial-mesenchymal transition in breast cancer progression and metastasis. *Chin J Cancer* **30**, 603-611, doi:10.5732/cjc.011.10226 (2011).

109 Wang, Z. *et al.* Clinical implications of β-catenin protein expression in breast cancer. *Int J Clin Exp Pathol* **8**, 14989-14994 (2015).

110 Li, S., Li, S., Sun, Y. & Li, L. The expression of β-catenin in different subtypes of breast cancer and its clinical significance. *Tumor Biology* **35**, 7693-7698, doi:10.1007/s13277-014-1975-0 (2014).

111 Miyahisa, I. *et al.* T-3364366 Targets the Desaturase Domain of Delta-5 Desaturase with Nanomolar Potency and a Multihour Residence Time. *ACS Med Chem Lett* **7**, 868-872, doi:10.1021/acsmedchemlett.6b00241 (2016).

112 Liu, C. *et al.* Control of β-Catenin Phosphorylation/Degradation by a Dual-Kinase Mechanism. *Cell* **108**, 837-847, doi:10.1016/S0092-8674(02)00685-2 (2002).

113 Tzifi, F. *et al.* The Role of BCL2 Family of Apoptosis Regulator Proteins in Acute and Chronic Leukemias. *Advances in Hematology* **2012**, 524308, doi:10.1155/2012/524308 (2012).

114 Campbell, K. J. & Tait, S. W. G. Targeting BCL-2 regulated apoptosis in cancer. *Open Biol* **8**, doi:10.1098/rsob.180002 (2018).

115 Tsujimoto, Y. Role of Bcl-2 family proteins in apoptosis: apoptosomes or mitochondria? *Genes to Cells* **3**, 697-707, doi:https://doi.org/10.1046/j.1365-2443.1998.00223.x (1998).

116 Feng, D. *et al.* Targeting of histone deacetylases to reactivate tumour suppressor genes and its therapeutic potential in a human cervical cancer xenograft model. *PLoS One* **8**, e80657, doi:10.1371/journal.pone.0080657 (2013).

117 Maziveyi, M. & Alahari, S. K. Cell matrix adhesions in cancer: The proteins that form the glue. *Oncotarget* **8**, 48471-48487, doi:10.18632/oncotarget.17265 (2017).

118 Chen, S. *et al.* Actin Cytoskeleton and Focal Adhesions Regulate the Biased Migration of Breast Cancer Cells on Nanoscale Asymmetric Sawteeth. *ACS Nano* **13**, 1454-1468, doi:10.1021/acsnano.8b07140 (2019).

119 Alblazi, K. M. & Siar, C. H. Cellular protrusions--lamellipodia, filopodia, invadopodia and podosomes--and their roles in progression of orofacial tumours: current understanding. *Asian Pac J Cancer Prev* **16**, 2187-2191, doi:10.7314/apjcp.2015.16.6.2187 (2015).

120 Ribatti, D., Tamma, R. & Annese, T. Epithelial-Mesenchymal Transition in Cancer: A Historical Overview. *Transl Oncol* **13**, 100773, doi:10.1016/j.tranon.2020.100773 (2020).

121 Wang, Y., Shi, J., Chai, K., Ying, X. & Zhou, B. P. The Role of Snail in EMT and Tumorigenesis. *Curr Cancer Drug Targets* **13**, 963-972, doi:10.2174/15680096113136660102 (2013).

122 Zhang, Y. & Wang, X. Targeting the Wnt/β-catenin signaling pathway in cancer. *Journal of Hematology & Oncology* **13**, 165, doi:10.1186/s13045-020-00990-3 (2020).

123 Jang, G.-B. *et al.* Blockade of Wnt/β-catenin signaling suppresses breast cancer metastasis by inhibiting CSC-like phenotype. *Scientific reports* **5**, 12465-12465, doi:10.1038/srep12465 (2015).

124 Cai, J. *et al.* MicroRNA-374a activates Wnt/β-catenin signaling to promote breast cancer metastasis. *The Journal of Clinical Investigation* **123**, 566-579, doi:10.1172/JCI65871 (2013).

125 Fani, S. *et al.* Monobenzyltin Complex C1 Induces Apoptosis in MCF-7 Breast Cancer Cells through the Intrinsic Signaling Pathway and through the Targeting of MCF-7-Derived Breast Cancer Stem Cells via the Wnt/β-Catenin Signaling Pathway. *PLoS One* **11**, e0160836, doi:10.1371/journal.pone.0160836 (2016).

126 Chen, S. *et al.* Wnt-1 signaling inhibits apoptosis by activating beta-catenin/T cell factor-mediated transcription. *The Journal of cell biology* **152**, 87-96, doi:10.1083/jcb.152.1.87 (2001).

127 Cheltsov, A. *et al.* Allosteric inhibitor of β-catenin selectively targets oncogenic Wnt signaling in colon cancer. *Sci Rep* **10**, 8096, doi:10.1038/s41598-020-60784-y (2020).

128 Schrörs, B. *et al.* Multi-Omics Characterization of the 4T1 Murine Mammary Gland Tumor Model. *Frontiers in Oncology* **10**, doi:10.3389/fonc.2020.01195 (2020).

129 Sun, X. *et al.* Anti-cancer effects of fisetin on mammary carcinoma cells via regulation of the PI3K/Akt/mTOR pathway: In vitro and in vivo studies. *Int J Mol Med* **42**, 811-820, doi:10.3892/ijmm.2018.3654 (2018).

130 Göttlicher, M. *et al.* Valproic acid defines a novel class of HDAC inhibitors inducing differentiation of transformed cells. *The EMBO Journal* **20**, 6969-6978, doi:https://doi.org/10.1093/emboj/20.24.6969 (2001).

131 Stettner, M. *et al.* Long-term antiepileptic treatment with histone deacetylase inhibitors may reduce the risk of prostate cancer. *European Journal of Cancer Prevention* **21**, 55-64, doi:10.1097/CEJ.0b013e32834a7e6f (2012).

132 Takagahara, S. *et al.* A novel orally available delta-5 desaturase inhibitor prevents atherosclerotic lesions accompanied with changes of fatty acid composition and eicosanoid production in ApoE knockout mice. *Journal of Pharmacology and Experimental Therapeutics*, jpet.119.259846, doi:10.1124/jpet.119.259846 (2019).

133 Nikolaou, M., Pavlopoulou, A., Georgakilas, A. G. & Kyrodimos, E. The challenge of drug resistance in cancer treatment: a current overview. *Clinical & Experimental Metastasis* **35**, 309-318, doi:10.1007/s10585-018-9903-0 (2018).

134 Zanoaga, O. *et al.* Implications of dietary ω-3 and ω-6 polyunsaturated fatty acids in breast cancer. *Exp Ther Med* **15**, 1167-1176, doi:10.3892/etm.2017.5515 (2018).

135 Liu, L. *et al.* Inhibition of Wnt/β-catenin pathway reverses multi-drug resistance and EMT in Oct4+/Nanog+ NSCLC cells. *Biomedicine & Pharmacotherapy* **127**, 110225, doi:https://doi.org/10.1016/j.biopha.2020.110225 (2020).

136 Cui, J., Jiang, W., Wang, S., Wang, L. & Xie, K. Role of Wnt/β-catenin signaling in drug resistance of pancreatic cancer. *Curr Pharm Des* **18**, 2464-2471, doi:10.2174/13816128112092464 (2012).

137 Takahashi, K. *et al.* Establishment of a 5-fluorouracil-resistant triple-negative breast cancer cell line. *Int J Oncol* **43**, 1985-1991, doi:10.3892/ijo.2013.2135 (2013).

138 Yang, X. L., Lin, F. J., Guo, Y. J., Shao, Z. M. & Ou, Z. L. Gemcitabine resistance in breast cancer cells regulated by PI3K/AKT-mediated cellular proliferation exerts negative feedback via the MEK/MAPK and mTOR pathways. *Onco Targets Ther* **7**, 1033-1042, doi:10.2147/ott.s63145 (2014).

139 Pohlmann, P. R., Mayer, I. A. & Mernaugh, R. Resistance to Trastuzumab in Breast Cancer. *Clin Cancer Res* **15**, 7479-7491, doi:10.1158/1078-0432.ccr-09-0636 (2009).

140 Kalac, M. *et al.* HDAC inhibitors and decitabine are highly synergistic and associated with unique gene-expression and epigenetic profiles in models of DLBCL. *Blood* **118**, 5506-5516, doi:10.1182/blood-2011-02-336891 (2011).

141 Chen, C. H. *et al.* Synergistic interaction between the HDAC inhibitor, MPT0E028, and sorafenib in liver cancer cells in vitro and in vivo. *Clin Cancer Res* **20**, 1274-1287, doi:10.1158/1078-0432.ccr-12-3909 (2014).

142 Jin, X. & Mu, P. Targeting Breast Cancer Metastasis. *Breast Cancer (Auckl)* **9**, 23-34, doi:10.4137/bcbcr.s25460 (2015).

143 Yang, S., Zhang, J. J. & Huang, X. Y. Mouse models for tumor metastasis. *Methods Mol Biol* **928**, 221-228, doi:10.1007/978-1-62703-008-3_17 (2012).

144 Minassian, L. M., Cotechini, T., Huitema, E. & Graham, C. H. Hypoxia-Induced Resistance to Chemotherapy in Cancer. *Adv Exp Med Biol* **1136**, 123-139, doi:10.1007/978-3-030-12734-3_9 (2019).